FINAL REPORT

MONITORING AND ASSESSMENT OF MOUNTAIN ECOSYSTEM AND SERVICES IN NORTH-WEST HIMALAYA (PHASE-II): MONITORING AND MODELING OF HYDROLOGICAL PROCESSES IN GLACIATED AND NON-GLACIATED WATERSHEDS OF NORTH-WEST HIMALAYA

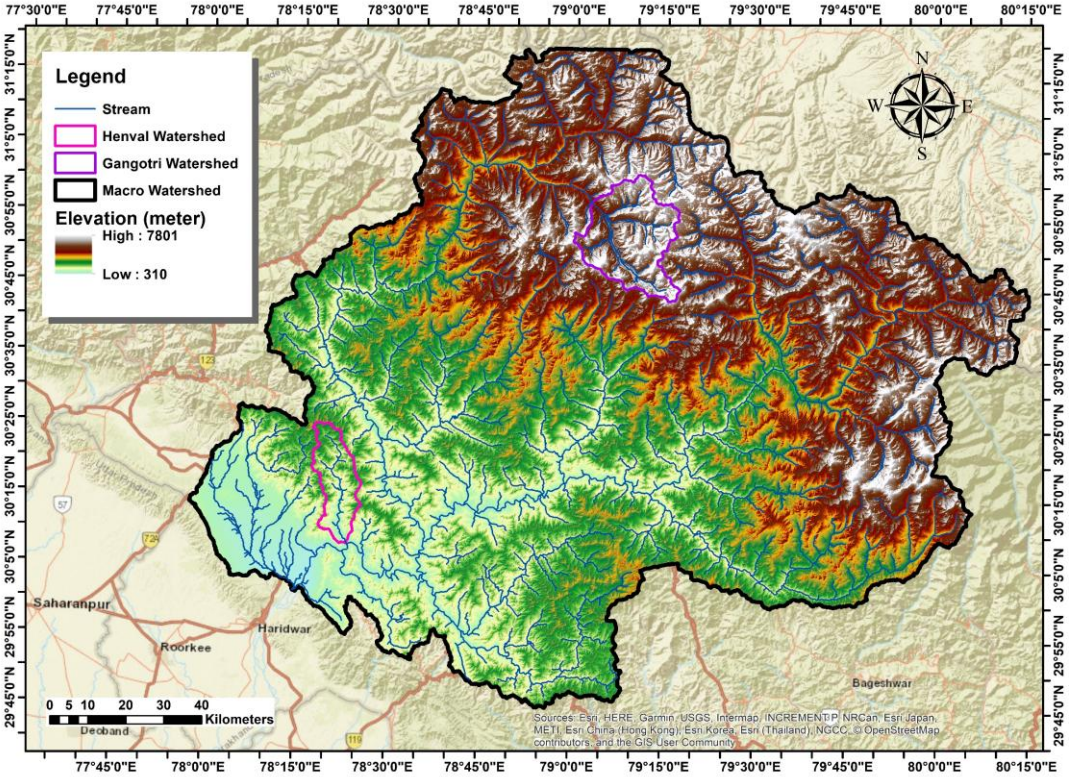

WATER RESOURCES SYSTEMS DIVISION

NATIONAL INSTITUTE OF HYDROLOGY

ROORKEE- 247 667, UTTRAKHAND, INDIA

March 2025

STUDY TEAM

Director	:	Dr M. K. Goel
Head	:	Dr. A. R. Senthil Kumar, Scientist 'G'
Investigators	:	Dr Manish K. Nema, Scientist 'E' (PI)
		Dr P. K. Mishra, Scientist 'D'
		Dr Pravin R. Patil, Scientist 'C'
		Er. Moncy S Akkara, JRF

TABLE OF CONTENTS

LIST OF FIGURES

LIST OF TABLES

ABSTRACT

This study aims to develop a deeper understanding of the hydrological responses from glaciated and non-glaciated regions of the North West Himalayas. The study is a part of the joint collaborative research project lead by IIRS, Dehradun and funded by ISRO, DoS and also the second phase of the project. In the first phase of the project, the Hydro-meteorological instrumental monitoring setup was designed and established in the watersheds in Himachal Pradesh and Uttarakhand.

The primary objective of the project was to establish instrumented experimental watersheds at different altitudes of North West Himalayas. The field observatory is intended to measure various hydrological and meteorological variables of the respective catchments located in the North West Himalayas. The experimental catchment at Henval has been established with the installations of up-listed instruments and sensors. The second objective of the project was to improve monitoring and estimates of various hydrological processes and parameters of high-altitude watersheds using RS-GIS viz. surface water, sediment load, snow cover, snowpack properties, glacier dynamics and runoff/melt.

To find an effective solution for the discrepancies in the rain gauge measurements of the Henval catchment after 2019, different satellite rainfall estimates were compared with the rain gauge measurements for the same region. The comparison study included different satellite rainfall products at varying spatial and temporal scales viz. GPM, NASA Power, CHIRPS, IMDAA. Overall, the NASA Power dataset has been identified as the better-performing dataset on a daily scale, with NSE and R2 values of 0.45 each whereas the CHIRPS dataset performed the best on a monthly scale with NSE and R2 values of 0.93 each. The consistent performance by NASA Power in the individual years and overall time period under consideration were found satisfactory to be identified as the better alternative to in-situ temperature measurements in Gangotri watershed.

The study applied the SPHY (Spatial Processes in Hydrology) model to simulate hydrological processes in a glaciated and non-glaciated watershed within the Upper Ganga Basin over a 14-year period (2010–2023). The model was calibrated and validated using observed hydrometeorological data and demonstrated robust performance in simulating key hydrological components—surface runoff, snowmelt runoff, glacier melt runoff, lateral flow, baseflow, and evapotranspiration—under complex Himalayan terrain. The SPHY model also proved adaptable for application across similar catchments in the northwestern Himalayas. Its

integration with geospatial tools and satellite-derived datasets further enhances its utility for hydrological assessment in data-limited regions.

The water balance of the watershed was established with glacio-hydrological modeling of the Henval and Gangotri watersheds using SPHY model to fulfil the third objective of studying the response of glaciers on the hydrology of high-altitude watersheds through on-field observations and modelling approach and further upscaling to basin level through hydro-glaciological modelling. Given the critical dependence of Himalayan hydrology on temperature and precipitation, particularly in light of climate change, SPHY provides a valuable platform for assessing watershed responses and informing water resource planning and adaptation strategies.

Chapter 1

1.0 INTRODUCTION

1.1 General

A watershed serves as a fundamental unit for studying hydrological processes and plays a central role in hydrology. Research in this area aims to understand how water interacts with soil, vegetation, topography, climate, and land management. Effective management of watersheds whether agricultural or forested requires insights into the connections between ecological and hydrological systems. While modeling is a key tool, field-based experimental hydrology continues to be essential, especially in studying surface, subsurface, and atmospheric water interactions.

Current watershed models face notable limitations. Many are based on simplified assumptions, such as linearity and uniformity, which do not reflect the complexity of real-world systems. Often, watersheds are treated as isolated units, focusing mainly on surface runoff at the outlet while neglecting subsurface dynamics. This narrow approach hinders the development of a comprehensive understanding of watershed behavior and the creation of more robust models. A shift toward broader, more integrated perspectives is needed to better capture hydrologic behavior across different regions and scales.

In mountainous regions like the Himalayas, local water sources such as springs and shallow seepage wells are crucial for daily use. However, human activities such as deforestation, overgrazing, soil erosion, and infrastructure development disrupt the natural infiltration capacity of the land. This results in excessive runoff during monsoons, leading to floods in lowlands and water shortages in upland villages. The complex terrain makes direct observation and data collection challenging, highlighting the importance of field-based studies for effective water resource planning and management.

Major river systems of North West Himalaya (NWH) mountain ecosystem are fed by snow and glacier melt during non-monsoon season. In the Himalayan mountains, “Naula” (1-2 m deep, approximately lined wells to get water from seepage) and "Dhara" (springs) are the primary sources of water for drinking and household consumption. Deforestation, grazing and trampling by livestock, erosion of top fertile soil, forest fires and development activities

(e.g. road-widening, mining, building construction, etc.) reduce the infiltration rate and sponge action of the land, which results in unchecked flow of water during the monsoon to cause sudden swelling of streams and rivers, so that there are floods in the foothills and even in the plains, and droughts in the villages located on the slope of the mountains. The difficulty in understanding the nature of hilly areas possesses severe limitations in ground observation. Field experimentation and information collection to understand various hydrological processes and planning activities for proper development and management of water resources are therefore necessary for NWH river basins.

Hydrological changes experienced by the Himalayan basins are very critical to the water security of the northern Indian plains due to the significant precipitation contributions from both SouthWest and NorthEast monsoon systems, rugged and steep mountainous topography, limited ground observations, weather extremes, variable hydrological processes such as glacier and snow melt (Rowan et al., 2017), large spatio-temporal and elevation based changes in hydro-meterological parameters (Simoni et. al.,2011) and even variable water demand and use patterns. Rising temperatures, changing glaciers and decreasing snow cover are indicators of the nature of the changing climate of the Himalayas in the recent past (Bhutiyani et al., 2007, 2010). While cryosphere components dictate the hydrology of the higher Himalayan region, the lesser Himalayan region experiences the highest precipitation across the Himalayan slopes and have considerable influence on the basin hydrology. However, the climate-hydrology linkages of this critical region are least known. The climate of the Himalayan slopes is dictated by the orographic forcing and strong linkages between the temperature distribution of the mountain slopes and atmospheric saturation conditions by summer/winter monsoon (Thayyen and Dimri, 2014). The impact of these processes on the present and future regional hydrology is a crucial question. Thorough understanding of the coupling between surface hydrologic systems and the overlying atmospheric system under orographic moisture flow is essential to address this question. Experimental watersheds with state-of-art instrumentation with a long-term research framework has been set up at different altitudes of NWH to gain insights on these issues. The research stations installed in the experimental watersheds is aimed to produce baseline data of weather and hydrology of the North West Himalayan mountains leading to a better understanding of climate-hydrology interaction under changing climate of the region. Since the Himalayan tributaries play an essential role in maintaining the hydrologic regime of the Ganges River; sustained research

from this experimental station will help in managing the water resources of Himalayan tributaries of Ganges River under the climate change scenario.

1.2 Background

Monitoring hydrological responses vis-à-vis available water is very important for better water resources management for various stake holders in North-West Himalaya (NWH). All the major rivers of this region are fed by contribution from snow and glacier melt during non-monsoon season. This area has unique hydrological system, due to significant precipitation contributions from both Southwest and Northeast monsoon systems, rugged and steep mountainous topography, sparse ground observations, weather extremes, variable hydrological processes such as snow-glacier melt runoff (Rowan et. al., 2017), large spatio-temporal and elevation-based changes in hydro-meteorological parameters (Simoni et. al., 2011) and variable water use/demand patterns. In addition to this, the changes in land surface and climatic inputs can also result in changes in various components of hydrological cycle such as infiltration, evapotranspiration, surface runoff and base flow (snow melt, glacier melt and ground water) of the major river systems of NWH mountain ecosystem. Therefore, it is essential to make accurate assessment, better understanding of various hydrological processes by using variety of ground and space-based observations, hydrological models for NWH and also quantify the impact of changing environment for further understanding of status of water resources in NWH River Basins.

In the first phase of this project, the detailed assessment of current and future water resources and hydrological cycle components was done for Beas basin. During the first phase of this project, it was realized that there is still a need for improving the understanding of the hydrological responses from glaciated and non-glaciated regions of the NWH. The improvements in the hydro-glaciological models can be achieved thorough assimilation of remote sensing and field observations of these glaciated and non-glaciated regions.

With this background, the second phase of this project has been formulated for monitoring the hydrological parameters and processes in these glaciated and non-glaciated regions. The main emphasis will be on establishment of experimental glaciated and non-glaciated watershed in different altitudinal regions of NWH, monitoring their hydrological response, parameterization of hydro-glaciological model and up-scaling of this model to a basin scale.

Two experimental watersheds were proposed in the North West Himalayan region- one in the lesser Himalaya and the other Gangotri basin in the upper Ganga basin, with a significant

focus on developing a predictive understanding of the glaciated and non-glaciated watersheds in NWH and ecosystems response to changes in climate. Monitoring and modelling of the hydrological parameters and processes in the glaciated and non-glaciated watersheds of the North-West Himalayas is the core activity. Annual and inter-annual variability of water balance components to be assessed through ground-based hydro-meteorological monitoring. Apart from orographic precipitation, convective precipitation also plays a vital role in governing the microclimatic conditions of a mountainous watershed. Snow and glacier melt also play a significant role in the case of a glaciated watershed. Energy balance is considered to be an essential component of forested watershed hydrology while mass balance is crucial in terms of glaciated hydrology. Based on the background above the study has been taken up for long-term monitoring with the following objectives:

1. Establishment of instrumented experimental watersheds at different altitudes of NWH.
2. To improve monitoring and estimates of various hydrological processes and parameters of high-altitude watersheds using RS-GIS. (Surface water, sediment load, snow cover, snow pack properties, glacier dynamics and runoff/melt)
3. To study the response of glaciers on hydrology of high-altitude watersheds through on-field observations and modeling approach and upscaling to basins level through hydro-glaciological modelling.

Chapter 2

2.0 STUDY AREA

2.1 General

A non-glaciated Himalayan watershed of Henval River and a glaciated mountainous watershed of Gangotri have been selected in the upper Ganga basin in the state of Uttarakhand for the study. The Henval watershed actually consists of paired sub-catchments. One of them is a forested catchment (undisturbed), and the other one is an agricultural watershed with anthropogenic interventions including a semi-urban habitat at Chamba (Uttarakhand). The geographical extent of the study area is from $30^0$17'N–$30^0$26'N latitude and $78^0$16'E–$78^0$25'E longitude. The area is a typical representative of a combination of lesser Himalayan hilly temperate climatic conditions with an average annual rainfall range of 1200-1800 mm. The Himalayan subtropical forests yield a belt of broad temperate leaf and mixed forest mainly comprising of pine forest. The total area under study is 254 km^2 approximately up to the confluence of river Ganga at Shivapuri with an elevation range of 362-2676 m. The stream in the forested sub-catchment is the source of drinking water for 87 nearby villages. This stream is being pumped 24x7 by the state authorities at its outlet at Dev Nagar for drinking water supply to the villages.

The glaciated watershed of Gangotri (Gangotri Glacier System) comprises of a cluster of many glaciers with the main Gangotri glacier as the trunk of the glacier system. The proglacial meltwater stream namely Bhagirathi River which emerges from the terminus of Gangotri glacier, is the major source of the river Ganga. The Gangotri glacier is located at a latitude of 30°57′ N and longitude of 79°03′ E with an elevation range of 4000-7000 m. The watershed covers a total area of 556 km^2 with a glacierized area of 286 km^2. The most striking feature of the system is a debris layer that covers most of the ablation zone with a varying thickness of a few millimeters to a few meters while large rocks are piled up to several meters in some locations. The location map of the watersheds within the Upper Ganga Basin is given in Fig. 2.1.

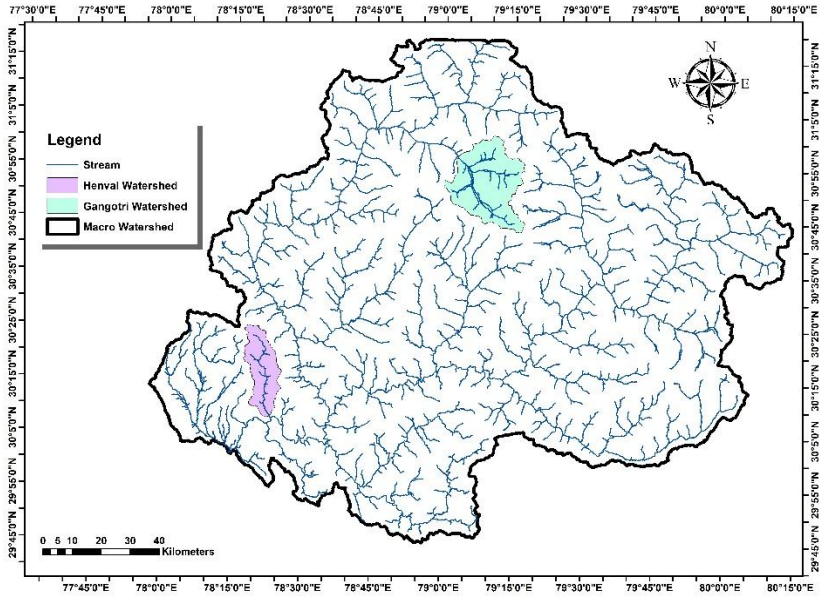

Fig. 2. 1 Location of the Henval and Gangotri watersheds within Upper Ganga Basin

2.2 Climate

The climate of the Henval watershed is generally humid and temperate, but observed variations are attributed to physiographic aspects such as altitude, aspect, slope, drainage condition, vegetation, etc. The valleys are hot in summer and cold in winter. The average temperature generally varies from 3°C to 30°C. The average yearly rainfall varies from 1200 to 1800 mm. About 70 to 80% of the rainfall occurs during June and September. The rainfall in the study area starts during May and lasts up to November. It was noticed that the uniformity of rainfall was pronounced from the end of June to mid-September, whereas during the other period, rainfall distribution was poor and erratic. The Gangotri watershed is characterized by snow precipitation along with occasional rain showers. Though the total seasonal rainfall exhibits huge variability every year with July and August months record maximum precipitation. The average temperature varies from -10 °C to 14.7 °C.

2.3 Digital Elevation Model

The project studies two watersheds- Henval which is a representative of the lesser Himalayas and Gangotri, a representative of the Greater Himalayas. To characterize the topographical features and delineate the catchment boundaries, Shuttle Radar Topographic Mission (SRTM) Digital Elevation Model (DEM) data of 30m spatial resolution has been used. The Henval watershed is characterized by very rugged topography, where the elevation ranges from 378 m to 2703 m above mean sea level whereas the Gangotri watershed is characterized

by the second biggest glacier in India with an elevation ranging from 3739 m to 7077 m. The elevation maps of both watersheds is given in Fig. 2.2.

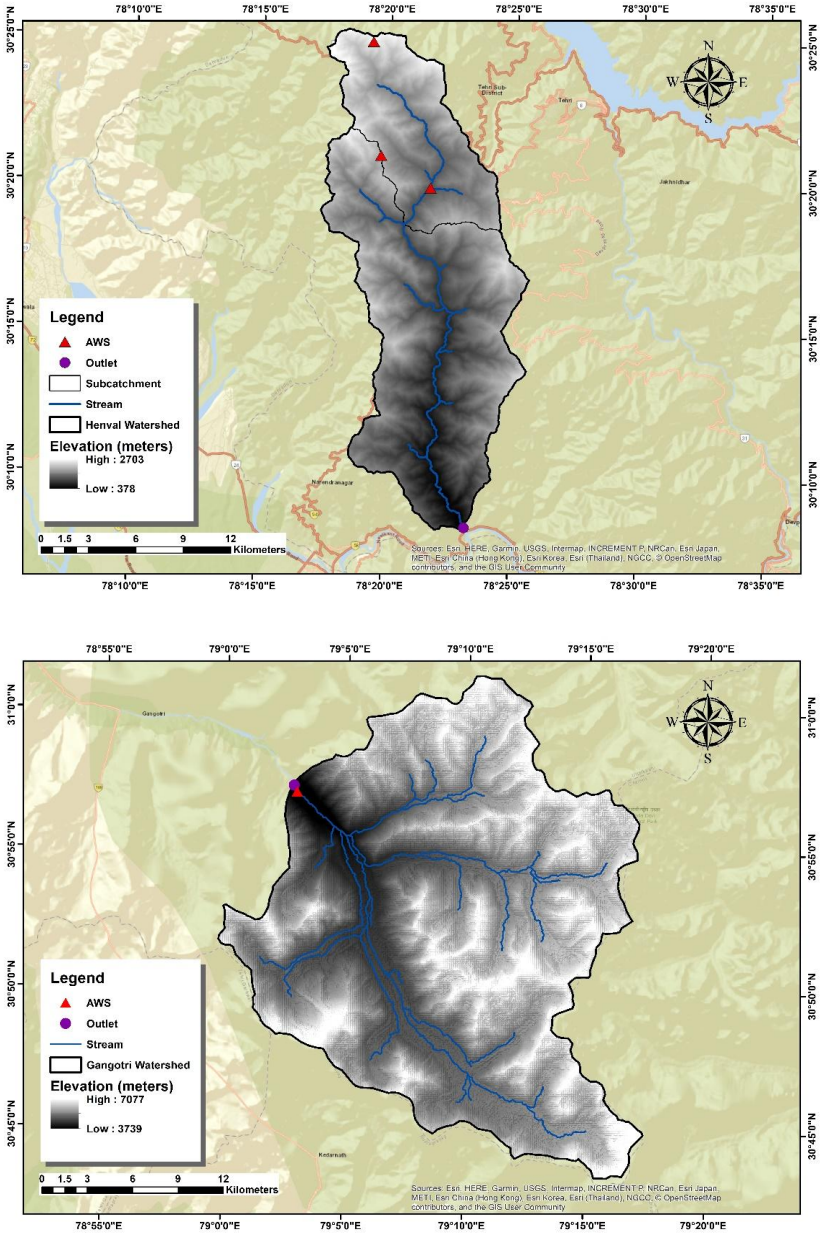

Fig. 2. 2 DEM of the study catchments

The slope maps of both watersheds are given in Fig. 2.3. Hypsometric analysis of the study catchments has also been done and presented in Fig. 2.4 and Table 2.1.

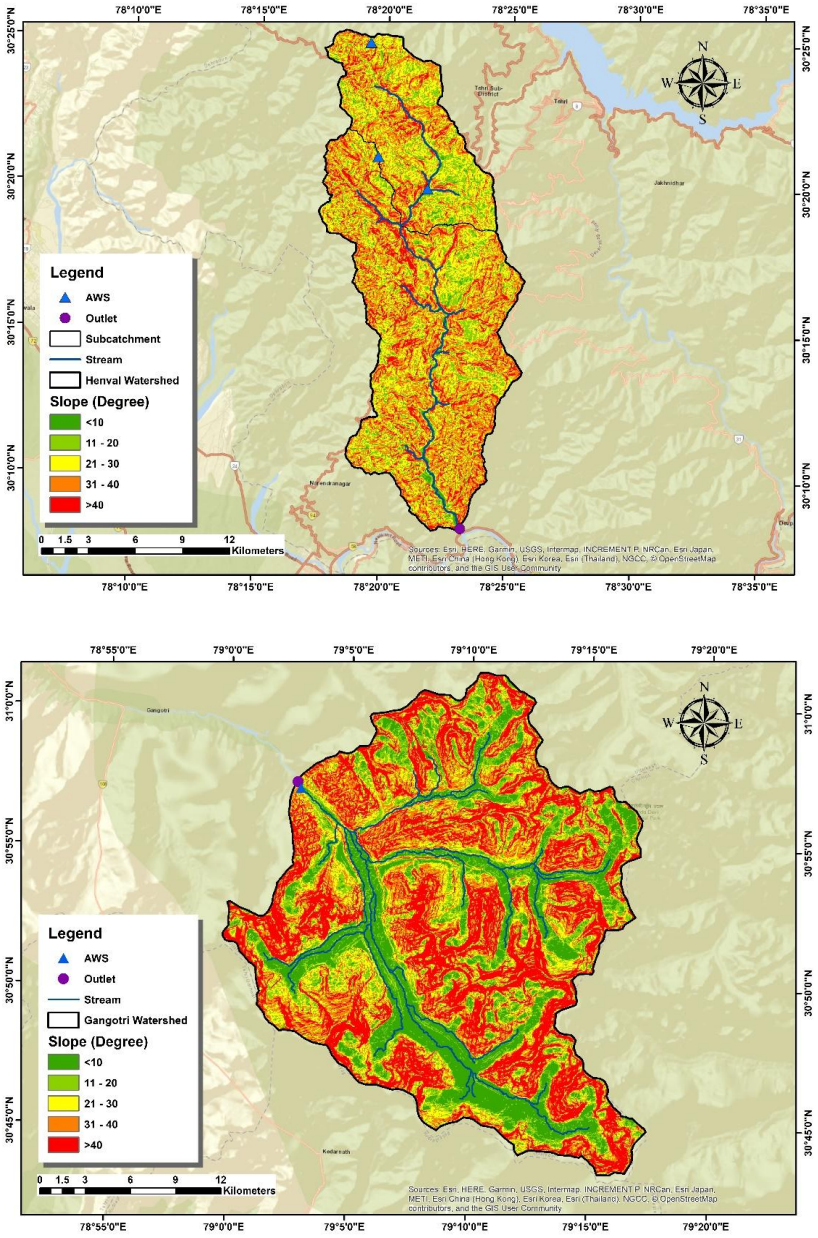

Fig. 2. 3 Slope Maps of the study catchments

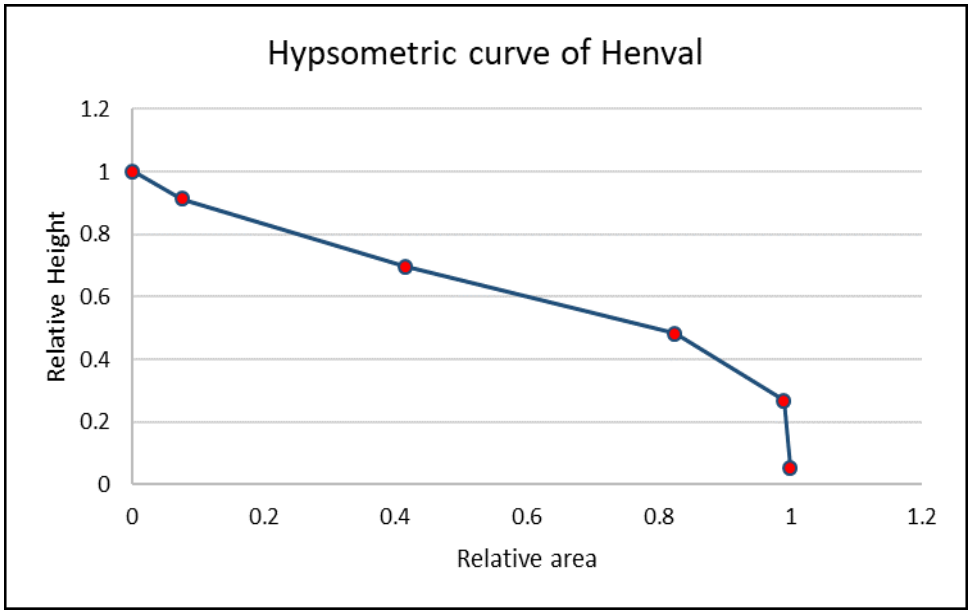

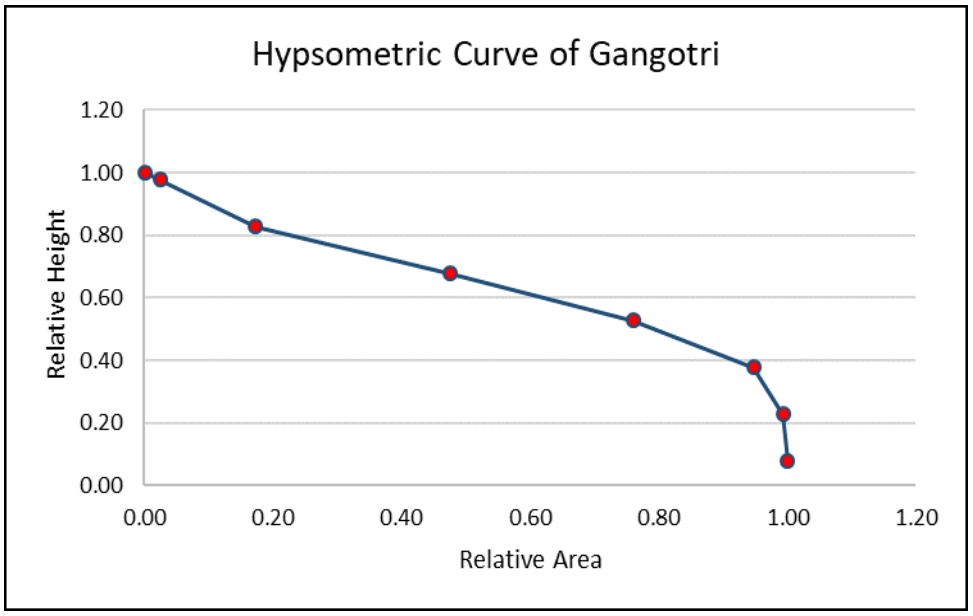

Fig. 2. 4 Hypsometry Curve of study catchments

Table 2. 1 Area under various percentage slope classes for the study catchments

Sl. No.	Slope (Degree)	Area under slope (%)	
		Henval	Gangotri
1	< 10	3.83	19.98
2	10 - 20	16.10	15.68
3	20 - 30	34.48	15.72
4	30 - 40	33.05	18.40
5	>40	12.53	30.22

2.4 Land Use land cover

The Henval watershed is a representative of the lesser Himalayas. The forest is the major land-cover feature of the Henval catchment. Henval catchment has other land use classes viz. as settlements, agricultural and fallow lands (the year 2022) that represent human interventions in the catchment. However, the representation of each of these classes are significantly less compared to the forest and range land. The Gangotri watershed represents the Greater Himalayas. Glacier and Snow is the major land cover feature of the watershed which is the second largest glacier in India. Vegetation is relatively sparse in the watershed and almost no human intervention. The land use land cover (LULC) maps of both catchments have been prepared based on the ESRI LULC product at a spatial resolution of 10 meters for the year 2022.

LULC map of Henval catchment (Fig. 2.5) shows six land cover types in 2022 i.e. trees (forest), rangeland (open forest), built area (human settlement), water, crops (agricultural land) and bare ground (barren land) among which only three land cover types are significant – forest, range land and built area. More than half of the watershed is forested (59%) followed by the open forest (37%). The human interventions in the catchment are very limited to 4% of the total area.

LULC map of Gangotri catchment (Fig. 2.6) for the same year is characterized by five land cover types viz. snow/ice (glacier), bare ground (barren land), rangeland (open forest), water and trees (forest) among which only three land cover types are significant – glaciers, bare ground and range land. Around half of the watershed is purely glaciated (48%). LULC statistics show bare land with very little to no vegetation in the entire year (42%) and 10% coverage with rangeland.

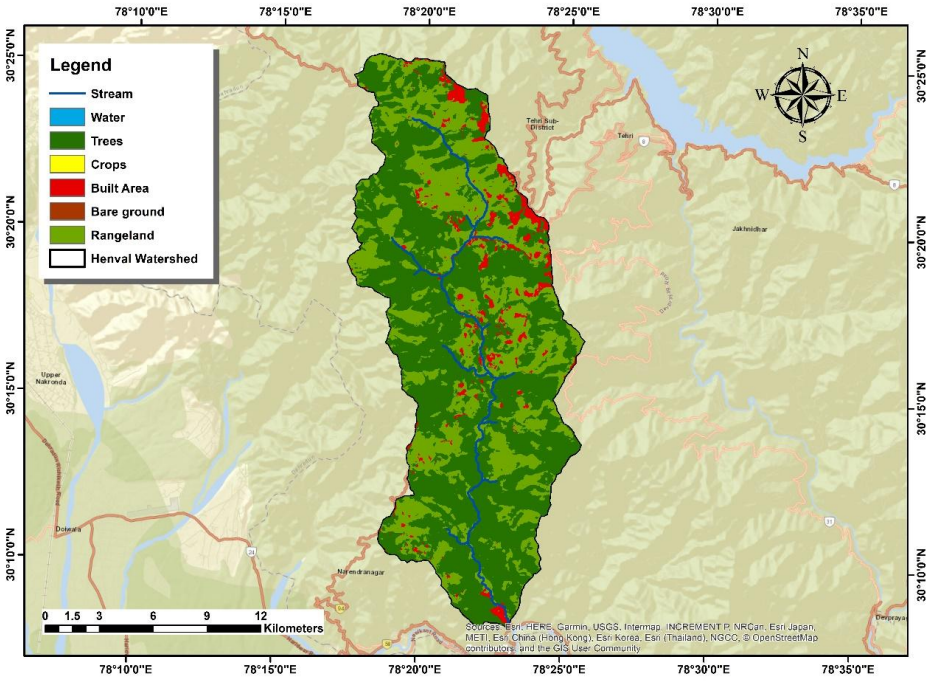

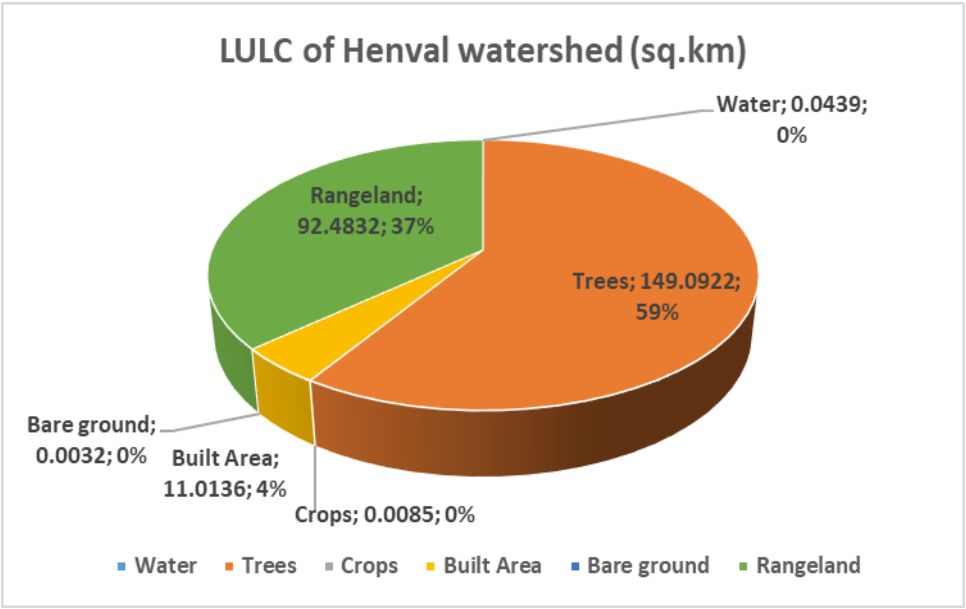

Fig. 2. 5 LULC of the Henval Catchment for the year 2022

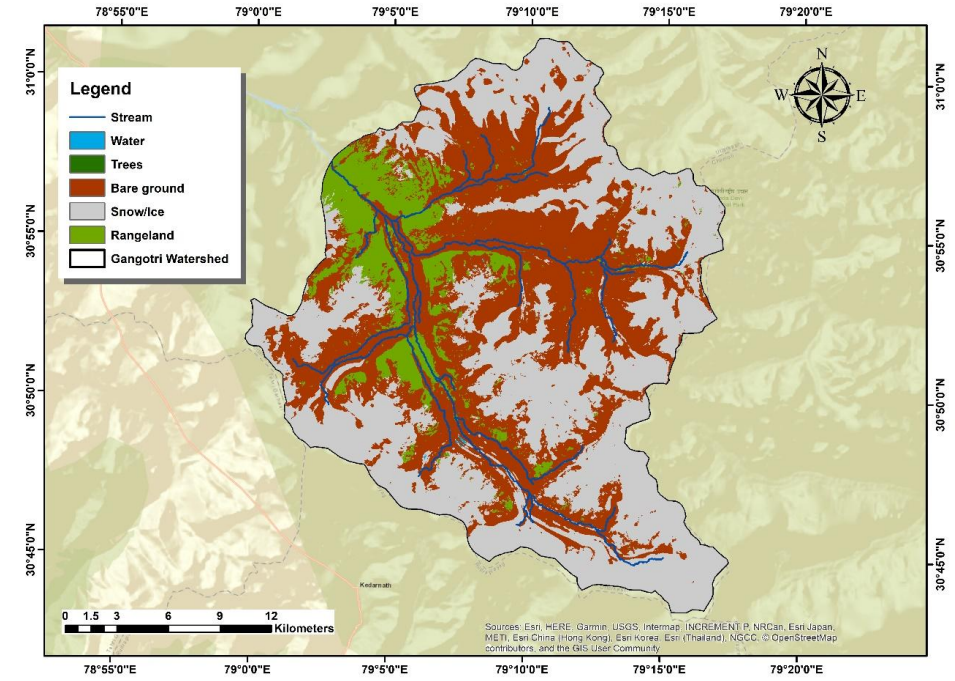

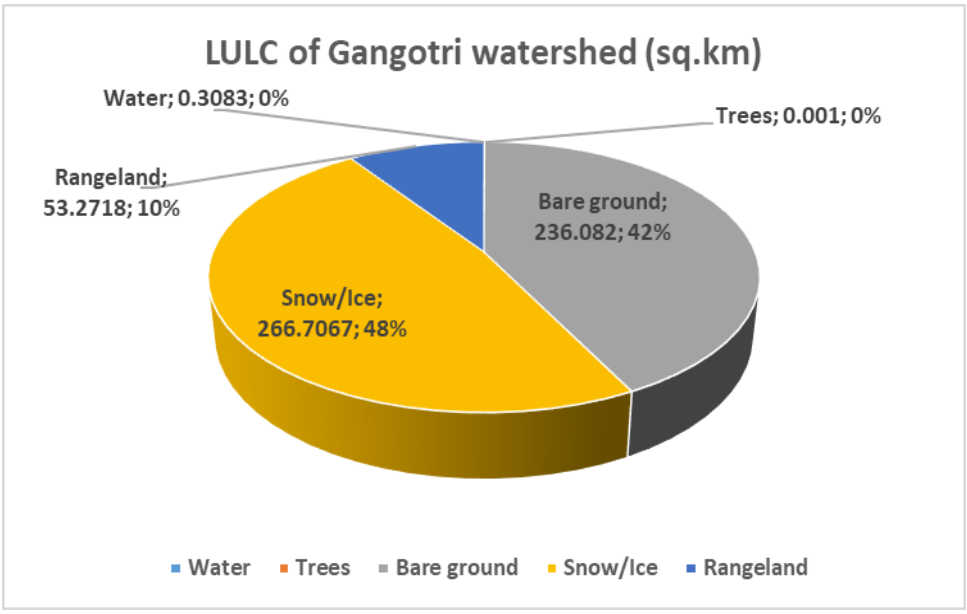

Fig. 2. 6 LULC of the Gangotri Catchment for the year 2022

Chapter 3

3.0 DATA AND INSTRUMENTATION

Among the three major objectives, the main emphasis is given to the establishment of experimental watersheds with extensive instrumentation in different altitudinal regions of NWH for monitoring the hydrological processes of glaciated and non-glaciated watersheds of Gangotri and Henval, respectively. Various hydro-meteorological datasets were generated for the study catchments to understand the hydrological and climatic processes and their interactions.

3.1 Gauging and Discharge Station

Discharge is an essential component and process of the hydrological cycle. The first weir at Henval is constructed just upstream of the pedestrian cross-over bridge near the pumping station of Uttarakhand Jal Sansthan (UJS) at Jijali-Devnagar. The length of the weir is 11m, the height is 1.0m (initially 0.7m), and the width of the crest is 0.5m. The weir at Henval was also provided with one staff gauge to measure the water level in upstream of the weir. Fig. 3.1 shows the weir at Henval.

Fig. 3. 1 Discharge weir at Henval

The second weir at Jijali stream of the non-glaciated Henval catchment has been constructed about 250m upstream of the confluence of Jijali and Henval. The dimensions of this weir are

11.5m X 0.7m X 0.5m. However, the requisite free-flow condition for the Jijali weir could not be created in that location due to the construction of a water intake structure just downstream of the weir by the Utharakhand Jal Sansthan (UJS). Hence, no observations are available from the Jijali weir. Submerged weir is shown in the Fig. 3.2

Fig. 3. 2 Discharge weir at Jijali

3.2 Automatic Water Level Recorder (AWLR)

An automatic radar type water level recorder with telemetric arrangement has been purchased and installed (Fig. 3.3) to monitor the water levels (head over the weir). Installation of AWLR is in the upstream of pedestrian cross-over bridge near the pumping station of Uttarakhand Jal Sansthan (UJS) at Jijali-Devnagar. AWLR is a fully computerized, digital and self-contained power source system, fitted with data logger and battery charging solar panel with rechargeable batteries with sealed waterproof enclosure for the data logger.

Fig. 3. 3 The digital water level recorder (DWLR) installed on the outlet of Henval stream at Jijali-Devnagar

3.3 Automatic Weather Station (AWS)

One automatic weather station (AWS) with soil parameters monitoring station has been installed in the forested catchment (Fig. 3.4) near village Nagani of Henval watershed at 1090 m a.s.l.. Initially, the data at an interval of 30 minutes were received at NIH servers through FTP from March 23rd, 2016 on a near real-time basis, but due to poor mobile network, it was shifted to email-based reporting. The data received since March 23rd, 2016, has been processed, analysed, and the results are presented in this report.

The various sensors, their make and accuracy and other installation details are given in Table 3.1.

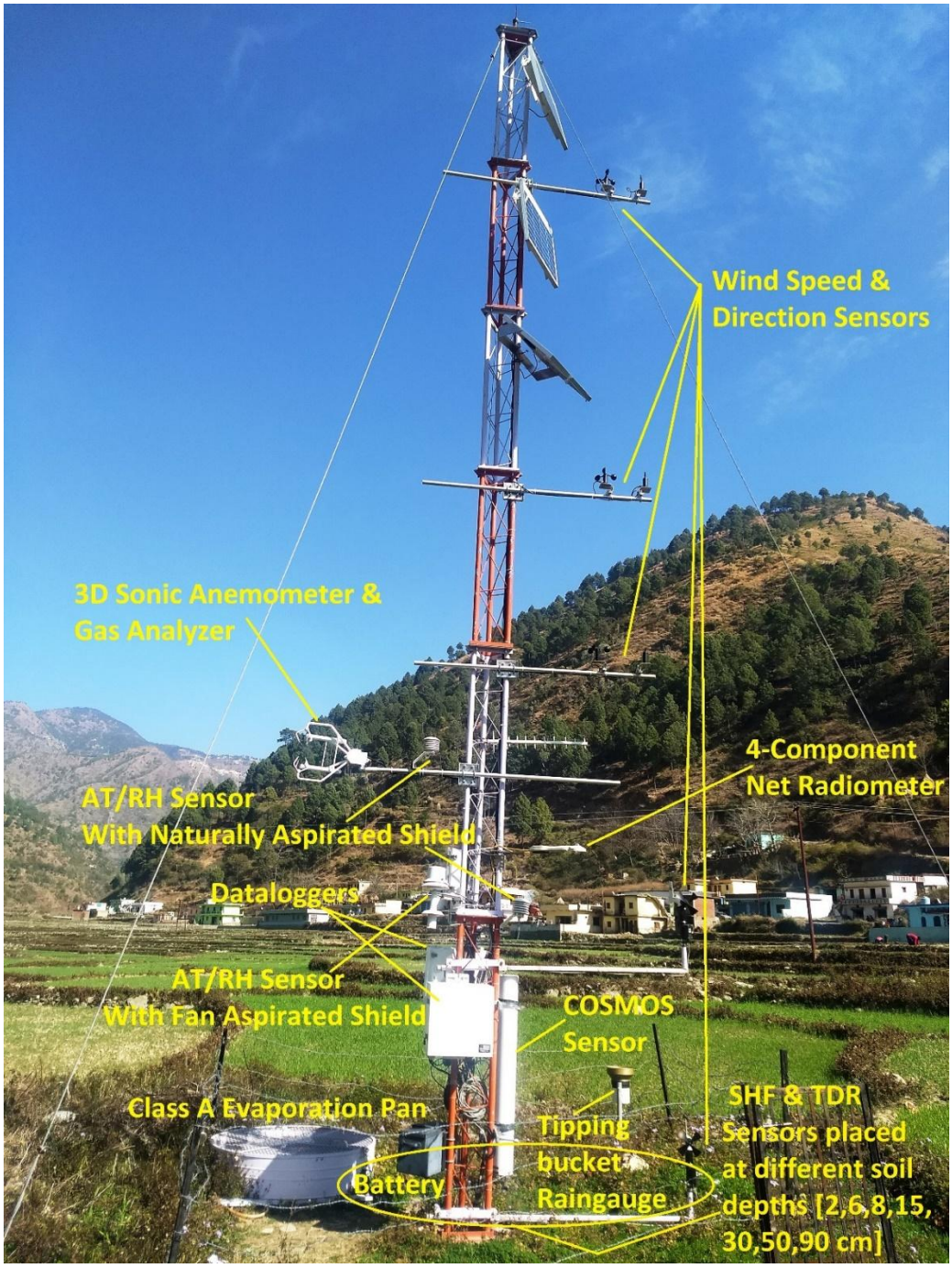

Fig. 3. 4 The automatic weather station (AWS) installed at Henval Catchment

Table 3. 1 Details of the sensors, their accuracy and installation information plugged in in the AWS and the soil Monitoring Station at Nagani of Henval watershed

Sensor	Symbol (Unit)	Make	Height/Depth (m)	Stated accuracy
Data loger		Campbell CR1000	NA	NA
AT/RH: Radiation Shield	Ta (^{0}C) RH (%)	Rotronics-HygroClip2	2.0m	±0.2^{0}C ±1.5% RH
Air temperature/Fan Aspirated	Ta (^{0}C)	Rotronics-HygroClip2	2.0m	±0.2^{0}C
Relative Humidity/ Fan Aspirated	RH (%)	Rotronics-HygroClip2	2.0m	±1.5% RH
Wind Speed	U (ms^{-1})	RM Young 05103-45	2.0, m	±0.3m/s
Wind Direction (WD2.0)	WD (^{0})	RM Young 05103-5	2.0 m	±0.3^0
Wind Speed (WS 63cm)	U (ms^{-1})	RM Young 05103-5	2.0m	±0.3m/s
Wind Direction (WD 63 cm)	WD (^{0})	RM Young 05103-5	2.0 m	±0.3^0
Four Component radiometer	(W m^{-2})	Kipp & Zonen (CNR4)	2.5 m	
Air pressure	hpa	Setra CS100 (500-1100hPa)		±0.3hpa
Rain Gauge	(m)	TE525MM	1.0	±1.0cm
Soil temperature (04 Nos.)	T (^{0}C)	107-L	2.0cm (L, R) 30 cm (L, R)	
Soil Moisture, Temp(TDR) Sensor (05 Nos.)		CS655	6.0 cm (L, R) 15 cm (Centre) 50 cm (Centre) 90 cm (Centre)	
Soil Heat flux plate (02 Nos)	(W m^{-2})	Hukseflux HFP01-L	8.0 cm (L, R)	

3.4 Eddy Flux Tower

Variables describing the turbulent transport such as three components of the 3-dimensional wind speed (u, v, w), sonic temperature (Ts), the concentration of the gas of interest, and water vapour serves the requirement of eddy covariance method for the computation of evapotranspiration. These measurements have to be fast to be able to compute the gas flux and are captured by an eddy covariance station. The term “fast” usually refers to devices capable of adequately measuring processes at about 10 Hz (10 times per second). The instrumentation consists of a **3-dimensional sonic anemometer** and an **open-path gas**

analyser. The gas analyser is usually positioned at or slightly below the sonic anemometer level. The vertical and horizontal separation between the anemometer and other instruments should be kept to a minimum, preferably not exceeding 15 to 20 cm.

3.4.1 Three-Dimensional Sonic Anemometer

A 3-dimensional sonic anemometer uses 3 pairs of transducers to measure the speed of sound for each pair. Three vector wind speed components are then computed, and the vertical wind speed component (w) is used for the eddy covariance calculations. The three main types of the physical arrangement of sonic anemometers most used in eddy covariance are:

1. Omni-directional design with u, v and w components measured in the same physical space by non-orthogonal off-axis pairs of transducers (e.g., not at 90° to each other),
2. Non-Omni directional c-clamp design with u, v and w components measured in the same physical space by non-orthogonal pairs of transducers,
3. C-clamp design with u, v and w components measured in the same or different physical spaces by orthogonal transducers, with w measured by a pair of vertically aligned transducers.

3.4.2 Gas Analyser

There are many different ways to measure gas content in the air. These may be based on chemical, electric, optical and other types of technology. However, not all of these measurements are suitable for eddy covariance. In the eddy covariance method, fast fluctuations in atmospheric gas concentration need to be sampled with high resolution at a frequency of about 10 Hz. Chemical sensors are usually too slow for such sampling, and electric sensors generally do not work well with the low concentrations of gases typically found in the atmosphere. Optical analysers, however, can be sufficiently fast for use in eddy covariance, depending on the performance of the specific instruments.

The flux tower arrangement installed at the site in Henval valley contains a 3-D sonic anemometer, i.e**. CSAT-3A** by Campbell scientific, for the measurements of the turbulent fluctuations of horizontal and vertical wind, and an open-path gas analyser, i.e. **EC 150** by Campbell scientific (Fig 3.5), specially designed for eddy-covariance carbon and water flux measurements. As a stand-alone analyser, it simultaneously measures absolute carbon-dioxide and water-vapour densities, air temperature, and barometric pressure.

Fig. 3. 5 The Eddy covariance sensor installed at Nagani AWS station

Chapter 4

4.0 BASIC ANALYSIS OF THE DATA

4.1 Preparation of Base Map

A base map for the study catchments has been prepared using India street map in ArcGIS (source: Esri, HERE, Garmin, USGS, Intermap, INCREMENT P, NRCan, Esri Japan, METI, Esri China (Hong Kong), Esri Korea, Esri (Thailand), NGCC, © OpenStreetMap contributors, and the GIS User Community) on scale 1:182745 for Henval and 1:190861 for Gangotri. The significant features such as the location of villages, roads, rivers, and spot heights are depicted on the map. Henval is the principal river that drains the Henval catchment which mainly flows from north to south whereas the Gangotri catchment drains from south-east to north-west direction to the Bhagirathi River which is the major source of the Ganga River. The prepared base maps are shown in Fig. 4.1 and Fig 4.2.

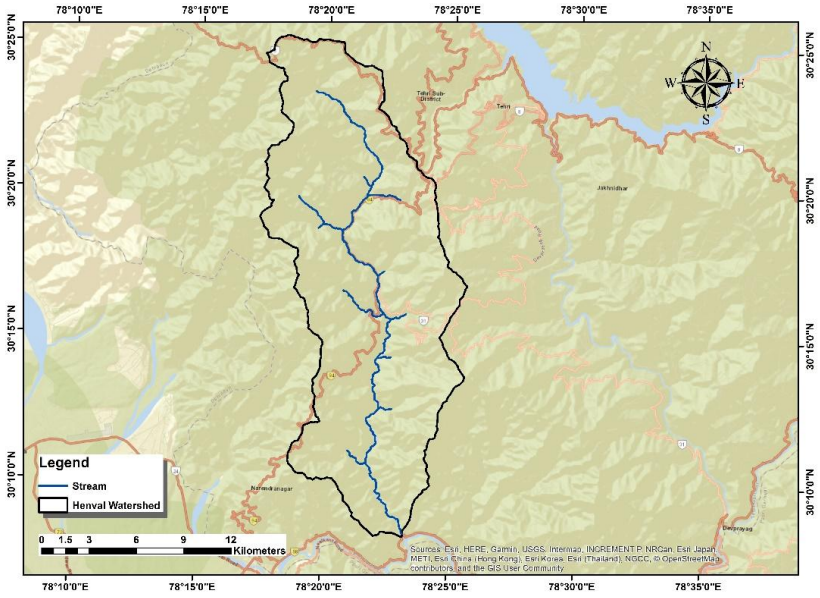

Fig. 4. 1 Base map of Henval catchment

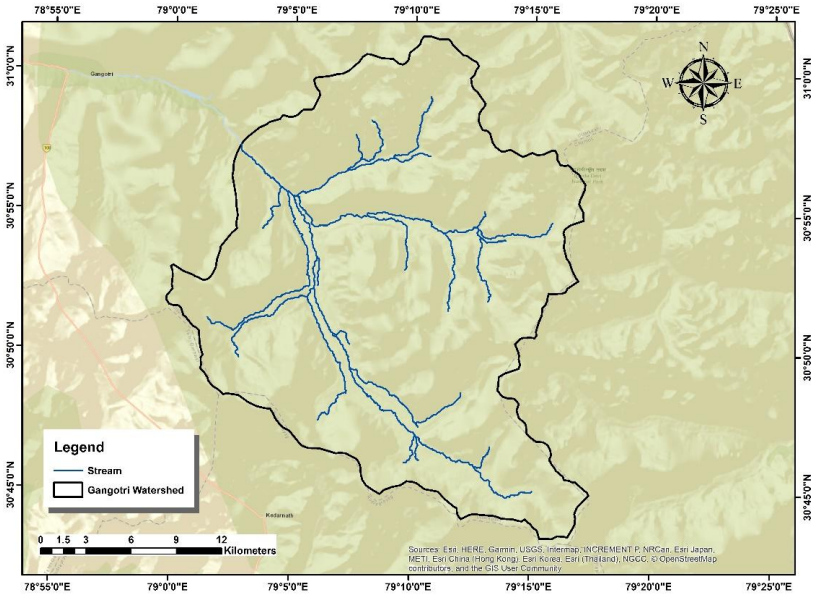

Fig. 4. 2 Base map of Gangotri catchment

4.2 Delineation of Sub-watersheds

Shuttle Radar Topographic Mission (SRTM) Digital Elevation Model (DEM) data of 30m resolution obtained from the website https:// search.earthdata.nasa.gov, has been used to represent topographical characteristics and delineate watersheds within the study catchments. The Henval catchment is characterized by very rugged topography, where the elevation ranges from 378 m to 2703 m (Fig. 4.3).

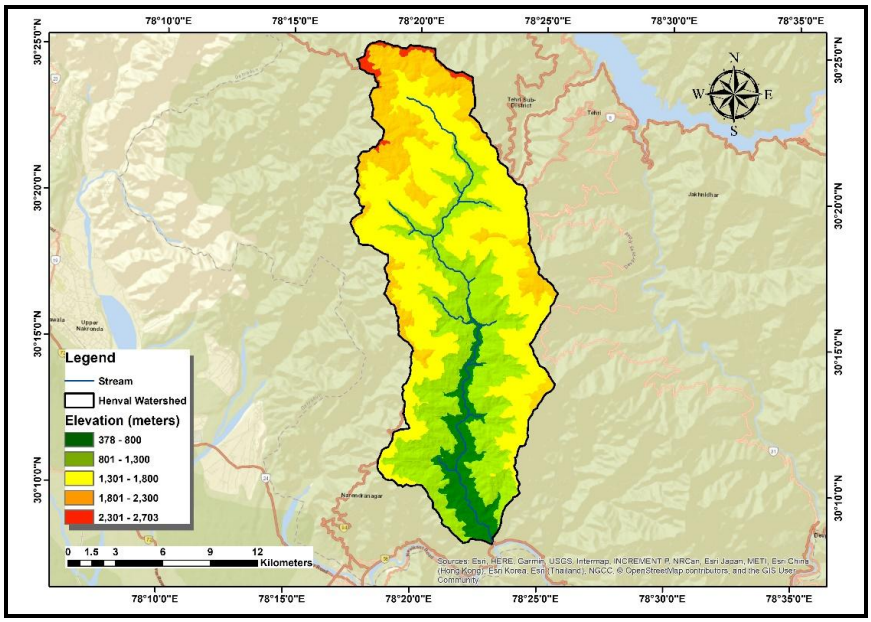

Fig. 4. 3 Map showing topographical characteristics within the Henval catchment

The Gangotri catchment is a glaciated catchment featuring rough topography with glaciers and snow-covered peaks. Hence, the elevation ranges from 3739 m to 7077 m (Fig. 4.4).

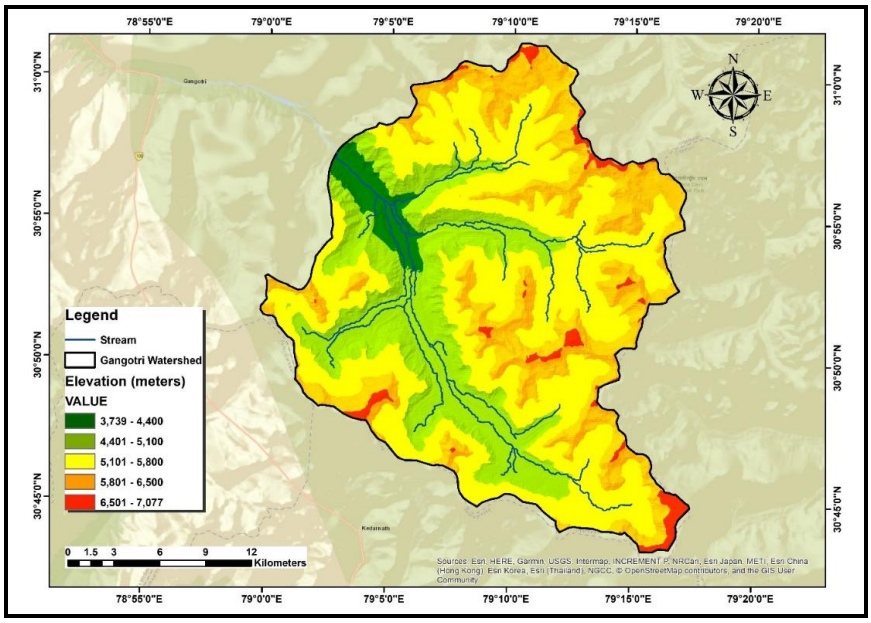

Fig. 4. 4 Map showing topographical characteristics within the Gangotri catchment

4.3 Generation of Stream Order Map

A stream order map for the study catchments has been prepared using Strahler's method, from the SRTM DEM of 1 arc sec resolution under ArcGIS 10.7 environment. The highest order in the Henval watershed was third order (Figure 4.5) whereas the Gangotri watershed was characterized by the highest stream order of four (Figure 4.6).

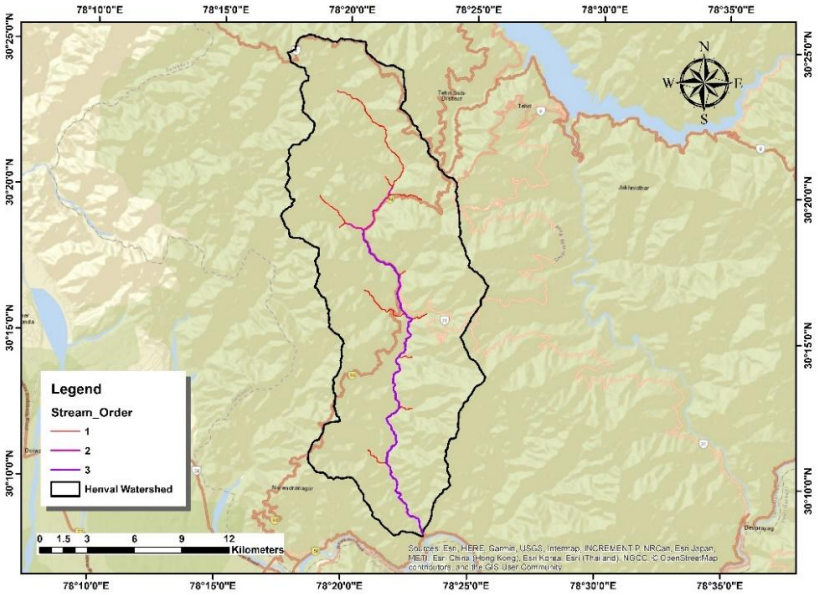

Fig. 4. 5 Stream order map of the Henval catchment

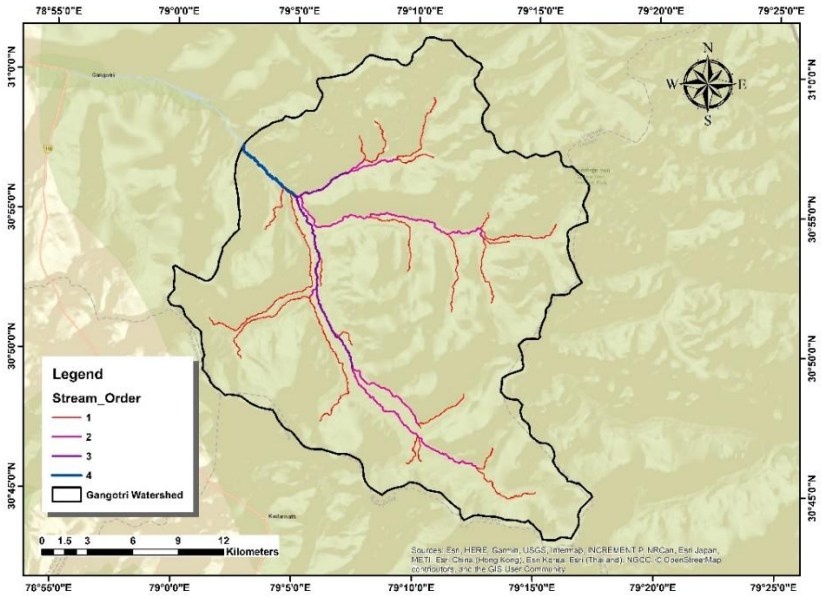

Fig. 4. 6 Stream order map of the Gangotri catchment

4.4 Variation of Recorded Variable Parameters at Henval

4.4.1 Air Temperature

The daily, monthly and annual variation of each parameter was computed for Henval site and are discussed in the subsequent sections. The variations of the daily mean value of air temperature (naturally aspirated and fan aspirated) are shown in Fig. 4.7 and the monthly mean value is shown in Fig. 4.8, which shows that air temperature is comparatively higher from May to September, which is closely linked to the increase in solar radiation. It is also found more fluctuating during March – June for all the years. The range of the daily mean air temperature is given in the Table 4.1. It can be seen from the table that there is a significant difference in the values or air temperature from the same sensor but with different types of shields. It can be noted from the that the temperature values as lower in case of fan-aspirated shiled sensor compared to the naturally aspirated sensor or the radiation shield sensor.

Table 4. 1 Ranges of the Air temperature at Henval valley

Air Temperature	Mini. Value (^{0}C)	Maxi. Value (^{0}C)	Average Value (^{0}C)
Naturally Aspirated	4.99	29.86	18.44
Fan Aspirated	4.26	29.82	17.98

4.4.2 Relative Humidity

Similar to the air temperatures, the observations for a relative humidity of air (naturally aspirated and fan aspirated) are obtained and as shown in Fig. 4.9 (daily mean RH) and Fig. 4.10 (mean monthly RH). It is found that relative humidity of air is comparatively higher in the months of July to October. The fluctuations are comparatively higher during the non-monsoon months for all the years. Interannually there is not much variation in the relative humidity, except for the year 2019 which shown some larger variation particularly in the months of May and June. The relative humidity varies from 24% to 100% in the Henval valley. Values of relative humidity from fan-aspirated sensor were found to be bit higher as compared to the values from naturally aspirated sensors.

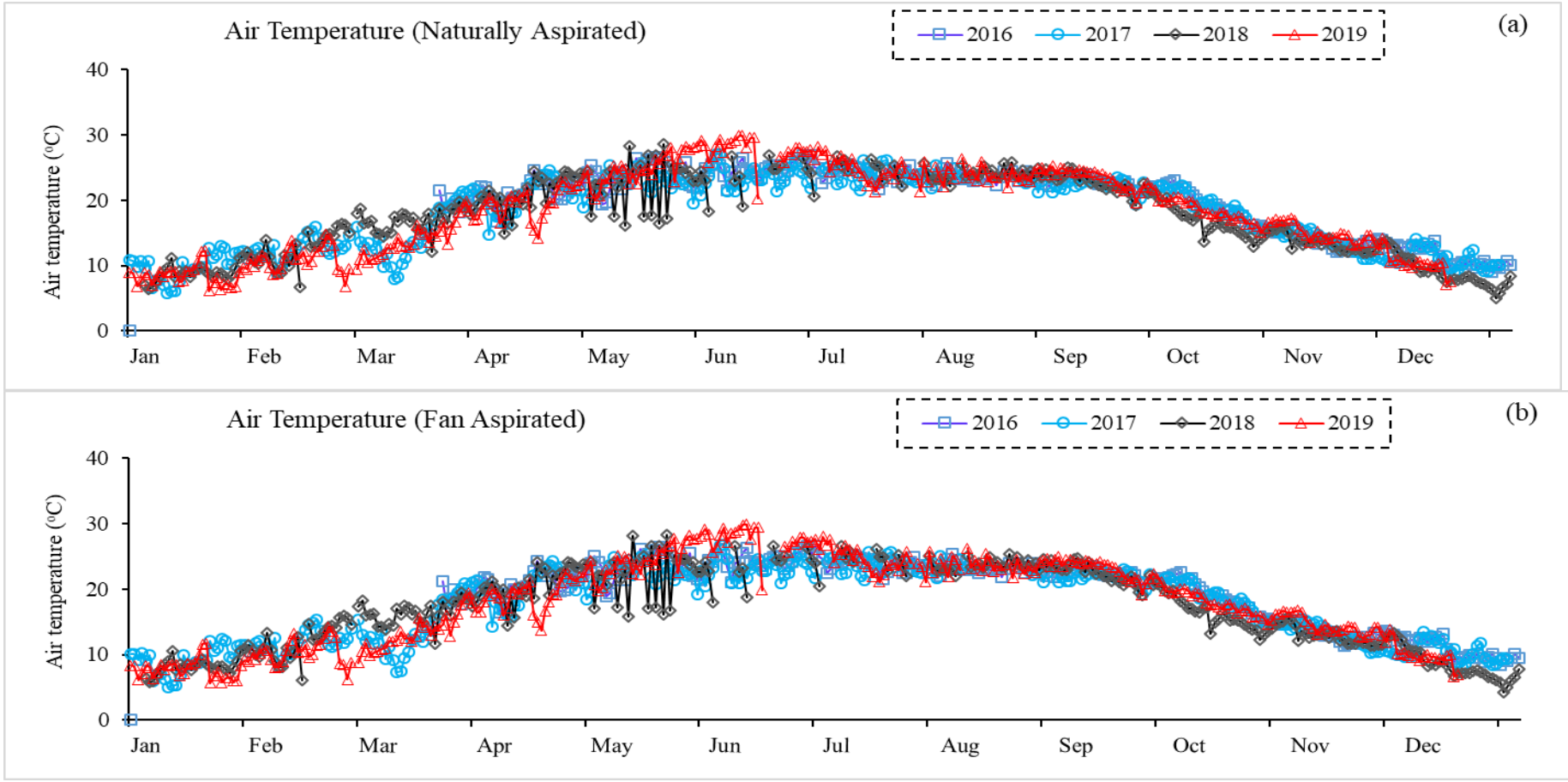

Fig. 4. 7 Variations of daily mean air temperature for naturally and fan aspirated sensors for different years

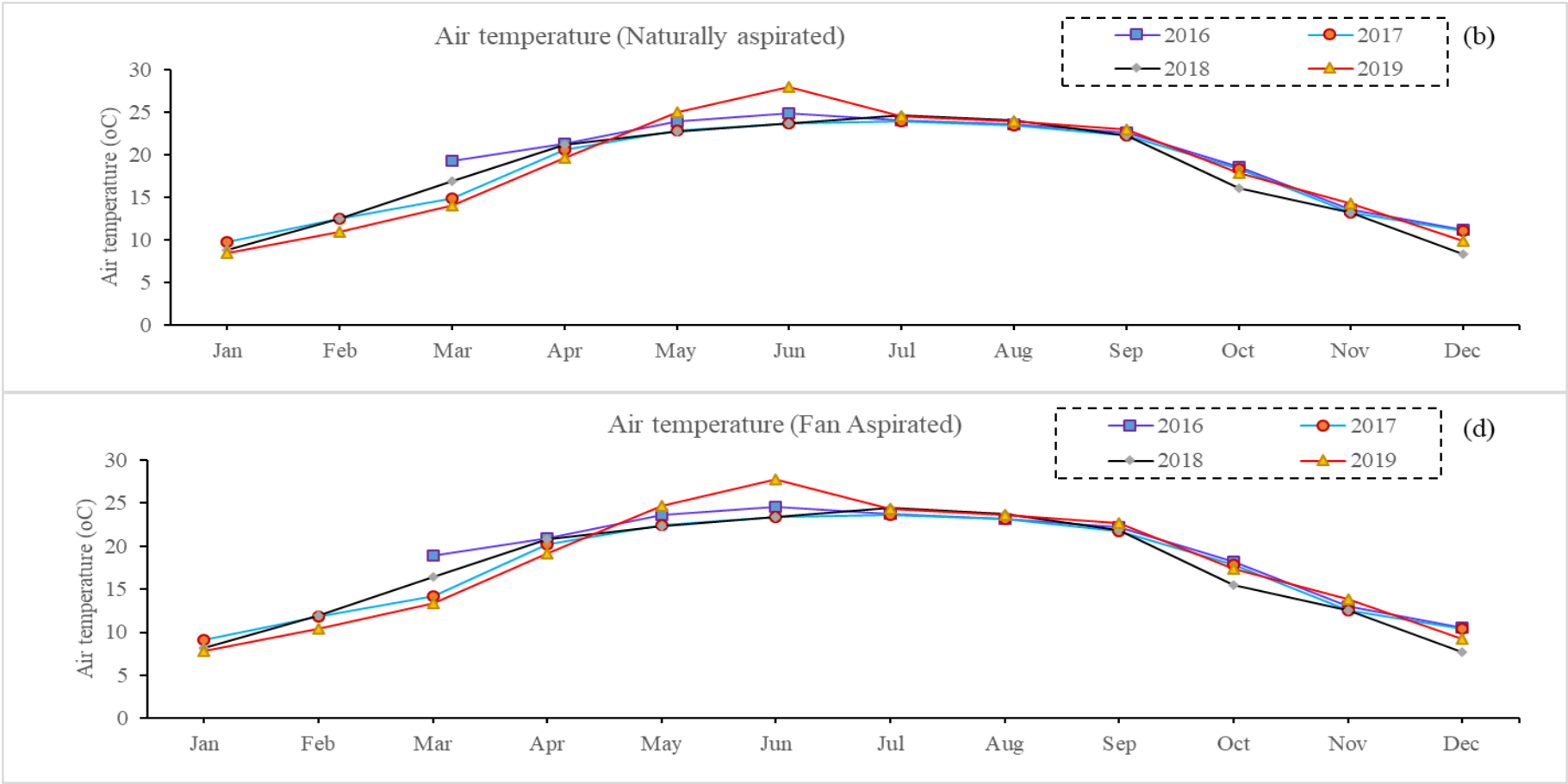

Fig. 4. 8 Variations of mean monthly air temperature for naturally and fan aspirated sensors for different years

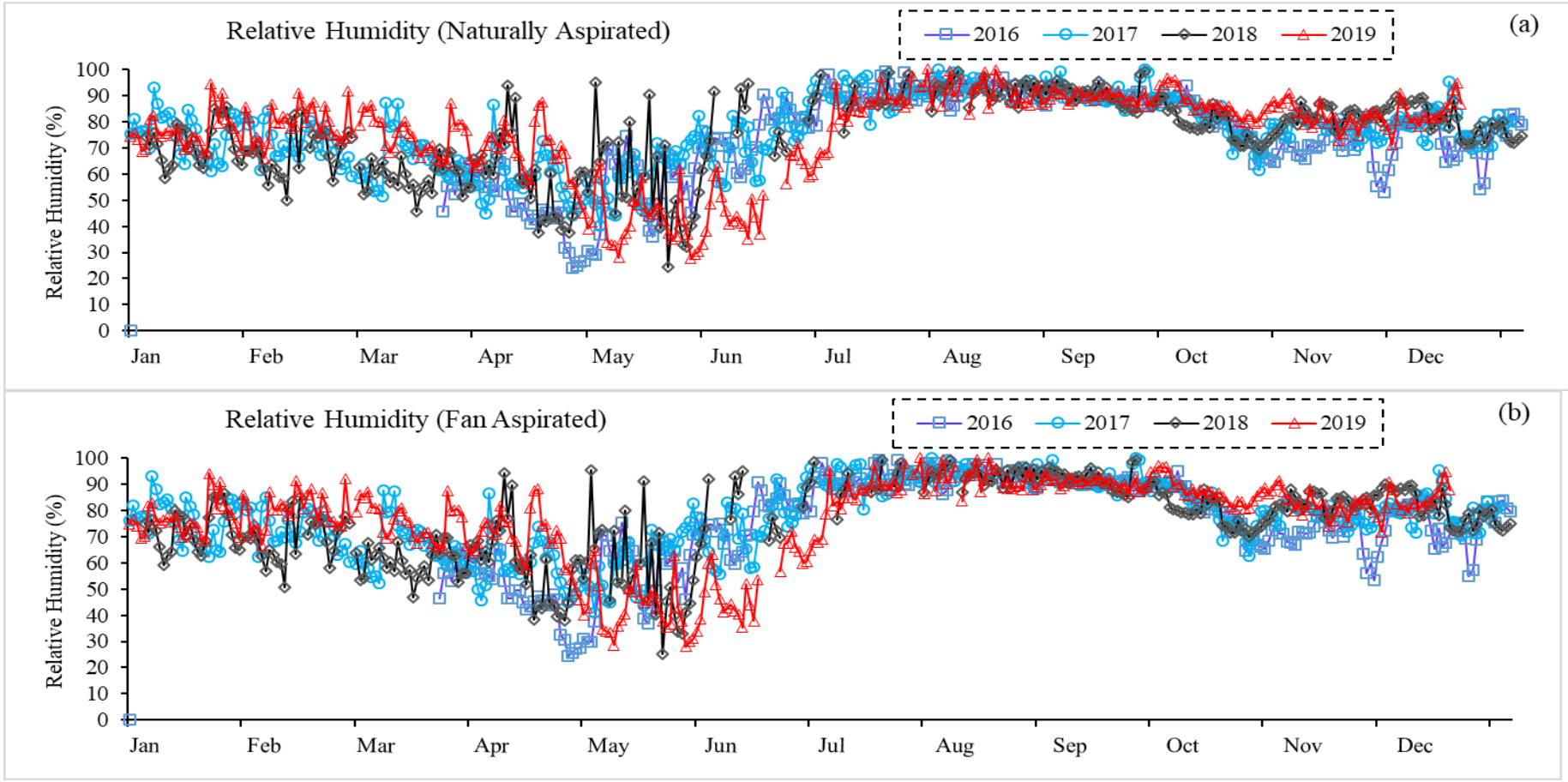

Fig. 4. 9 Variations of daily mean relative humidity for naturally and fan aspirated sensors for different years

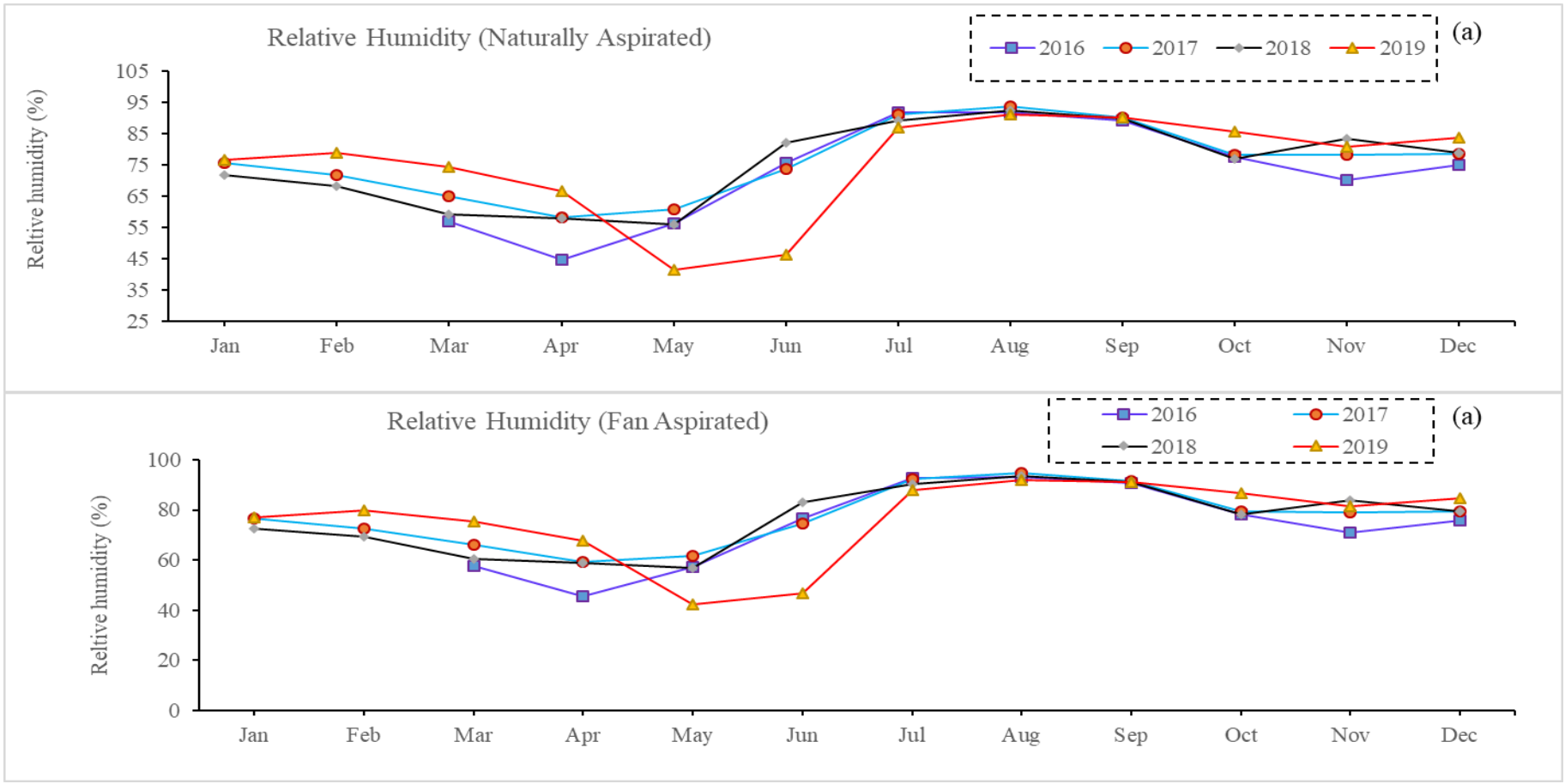

Fig. 4. 10 Variation of mean monthly relative humidity for naturally and fan aspirated sensors

4.4.3 Wind Speeed

Henval valley is located in Lesser Himalayas with an altitude of 1000m at the valley bottom and surrounded by high hills and there is south-northern opening of the valley. The geographical conditions of the valley creates unique and well defined wind profiles. There is adiabatic wind flow in the day time and catabatic wind occurs in the night. A vertical wind profiling is being attaemetd at Henval valley by putting wind sensors at different heights.

Fig 4.11 shows the variation of mean daily wind speed at different heights (0.5 m, 2 m, 4 m, 6 m and 10 m). The wind speed is observed maximum in the months of May-June whereas it is found minimum in July - September at the height is 50 cm and 2 m. The wind speed data at 4 m, 6 m and 10 m were not recorded regularly due to technical error continuously and hence difficult to analyze. The average wind speed increases with the increase in height. Mean monthly values for different years are plotted and presented in Fig. 4.12. The average wind speed at 0.2m height was found to be 0.95km/hr and 1.83km/hr at height of 2m at the Henval valley. The data analysis indicates the values of the wind speed becomes larger as the height of measurement goes up.

4.4.4 Rainfall

Rainfall is an important component of hydrological cycle and essential for any kind of hydrological studies. A tipping bucket type of raingauge has been installed at the Henval valley to capture the rainfall records. Fig. 4.13 (b) shows the observed pattern of daily rainfall which indicates the highest rainfall (higher peaks) during the monsoon season.

The monthly rainfall is also plotted for all recorded four years in Fig. 4.13 (a). Almost no rain is observed in October and November in all the years. Frequent rainfall is observed with lesser magnitudes from January to May in 2016 and 2017. Year 2017 was found to be a wet year with a total annual rainfall of 1414mm whereas, year 2018 received only 720mm of annual rainfall. Based on the four years records the average annual rainfall was estimated as 985mm. The share of the monsoonal rainfall was found to be 79% of the total annual rainfall in the catchment.

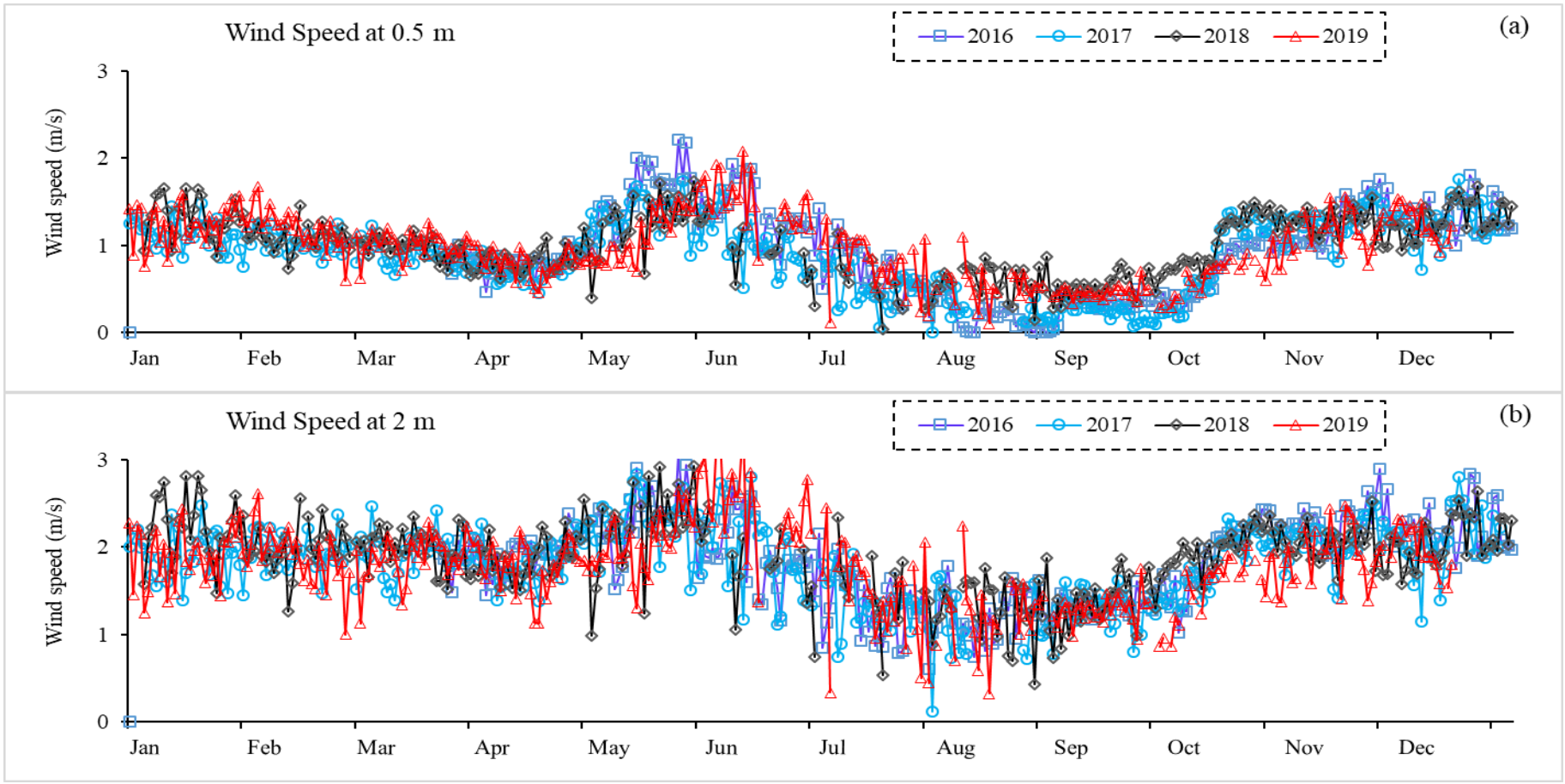

Fig. 4. 11 Variations of mean daily wind speed at 0.5m and 2m height

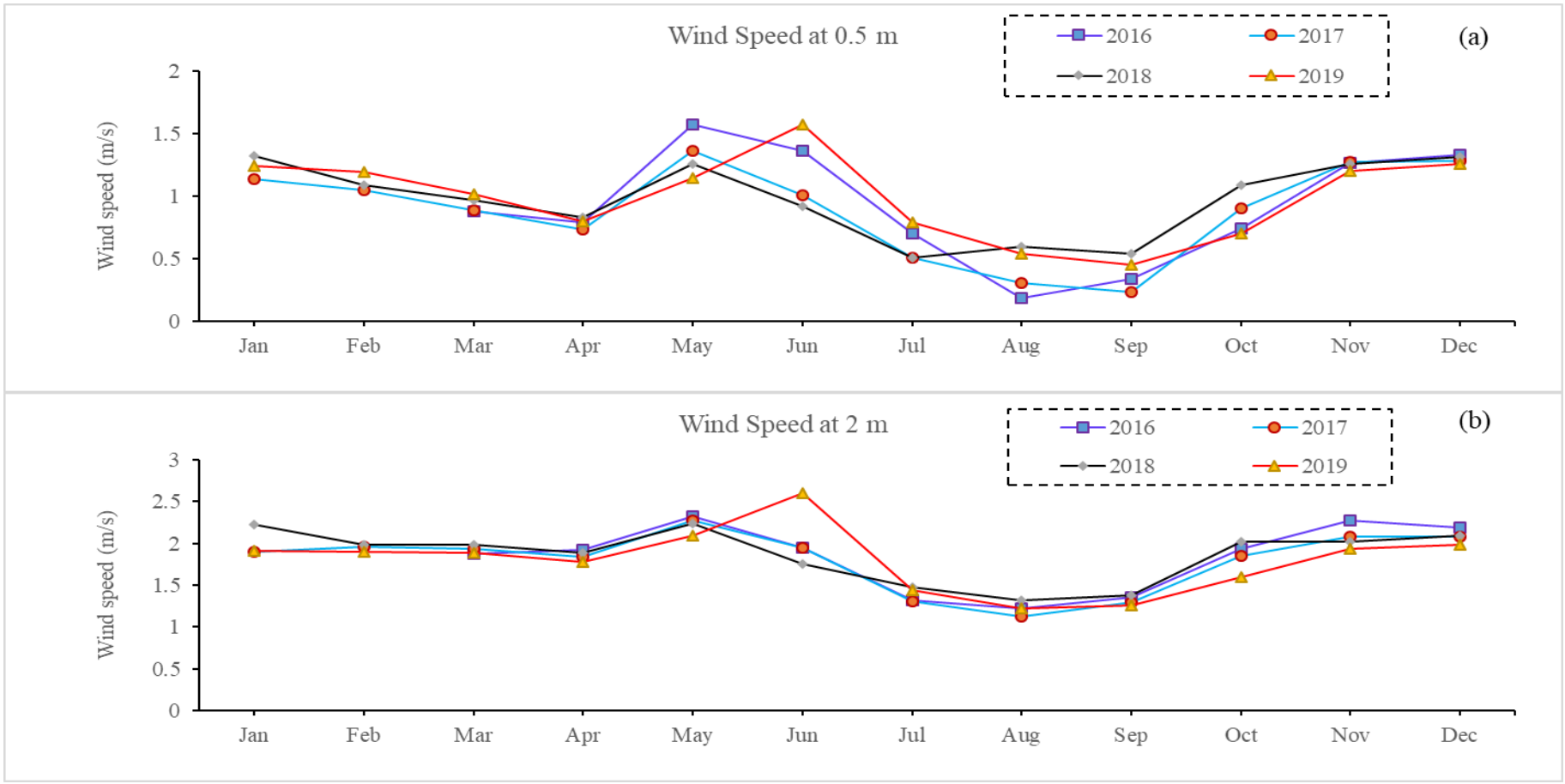

Fig. 4. 12 Variation of mean monthly wind speed at 0.5m and 2m height

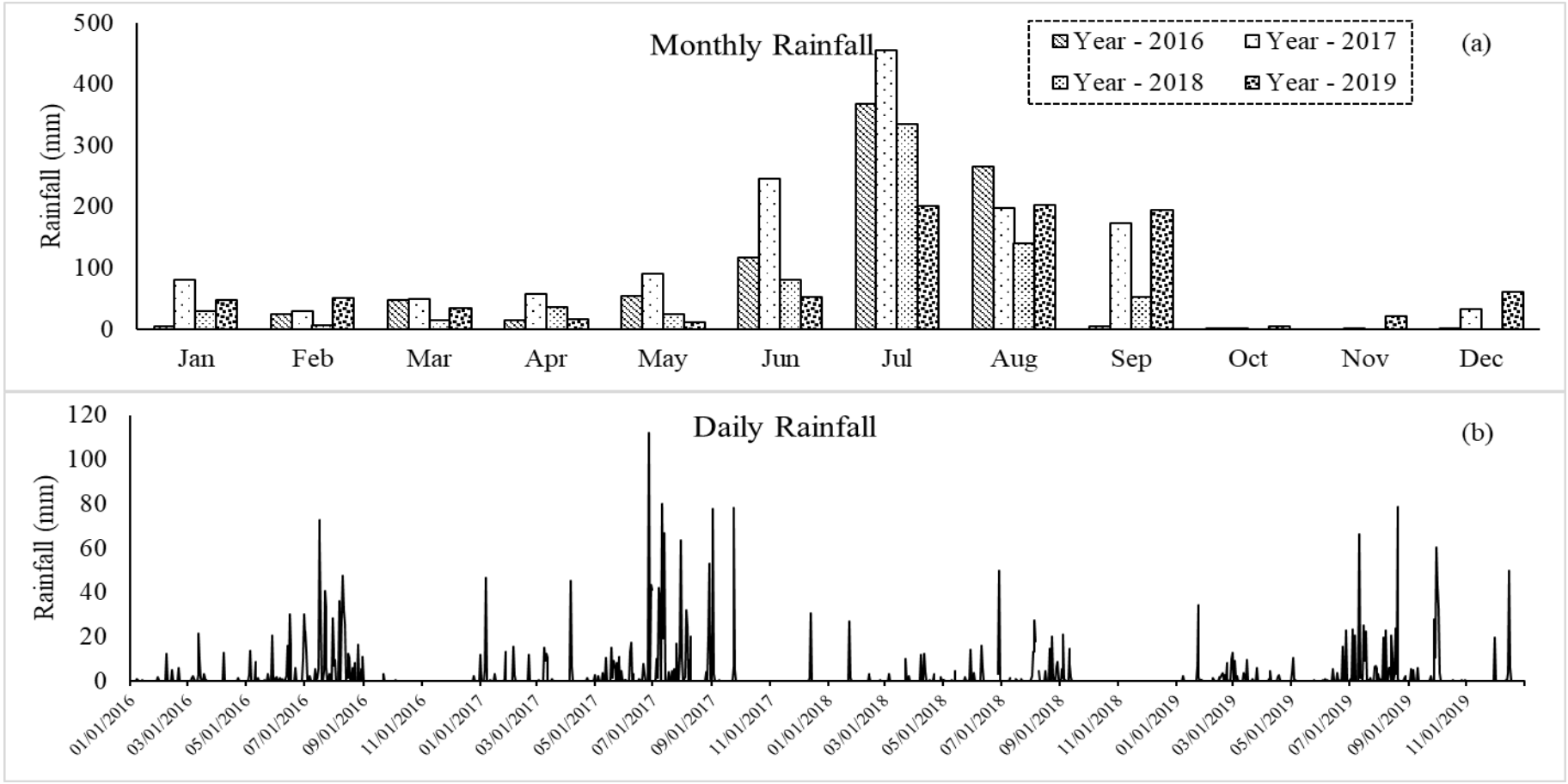

Fig. 4. 13 (a) Variations of monthly rainfall in different years and (b) Daily rainfall time series at Henval valley.

4.4.5 Soil Moisture and Soil temperature

Soil plays an important role in the water balance of a catchment. The physical properties of soil mainly soil moisture and soil temperature are critical for seed germination, plant growth and productivity of the land. The soil temperature affects plant growth indirectly by affecting water and nutrient uptake as well as root growth. At a constant moisture content, a decrease in temperature results in a decrease in water and nutrient uptake. At low temperatures, transport from the root to the shoot and vice versa is reduced. Apart from this the change in the soil moisture in terms of storage is essential for water balance equation. At Henval valley TDR probes are being used for monitoring the soil moisture and soil temperature, which also provide information about the soil electrical conductivities.

The mean daily soil moisture is recorded at different depths 6 cm, 15 cm, and 50 cm below the ground surface, as shown in Fig 4.14. The mean monthly soil moisture values are also plotted and presented in the Fig. 4.15. The results indicate that the soil moisture near the ground surface (6 cm, 15 cm and 50 cm) is highest in the months of July-September and lowest in the months of May and June. This variation of soil moisture is attributed to the occurrence of rainfall in the rainy season. The increase in soil moisture near the ground surface in non-rainy months is due to irrigation. The fluctuations in soil moisture decrease with the increase in depth due to the lesser effect of meteorological phenomena. Similar to soil moisture, electrical conductivity (EC) is also recorded at different depths (6 cm, 15 cm and 50 cm) below the ground surface.

Daily soil temperature is recorded at different depths (6 cm, 15 cm, and 50 cm) below the ground surface. Fig. 4.16 and Fig. 4.17 shows the variation of the daily and monthly soil temperature respectively. From the figures it can be observed that the soil temperature starts increasing in the month of April and reaches the maximum in the month of June- July, and starts decreasing from October onwards in all the years which is closely linked to the occurrence of rainfall events, increase in solar radiation and clear sky in summer and monsoon months. Soil permittivity increases with increasing water content in the soil.

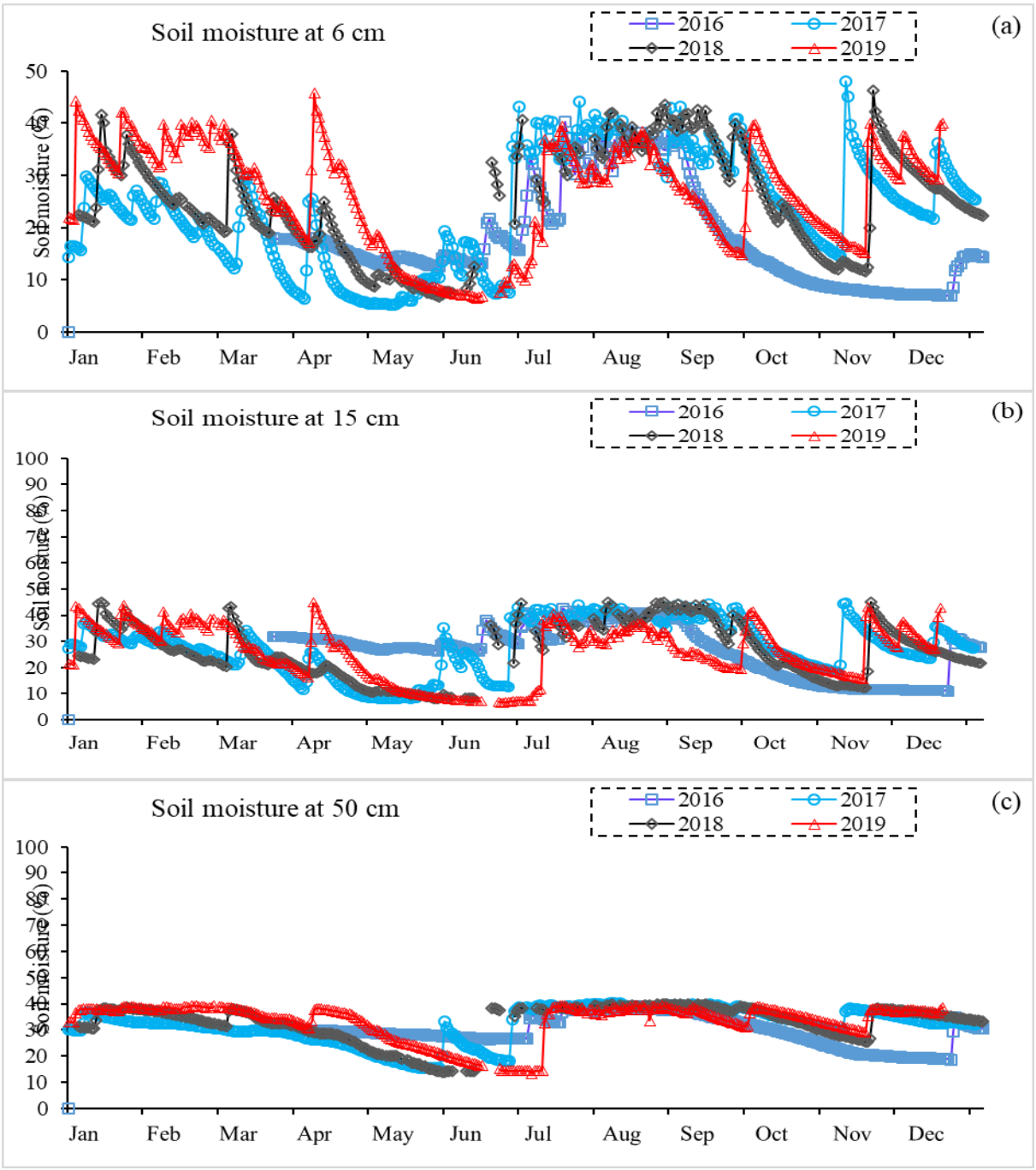

Fig. 4. 14 Variation of daily soil moisture at different depths

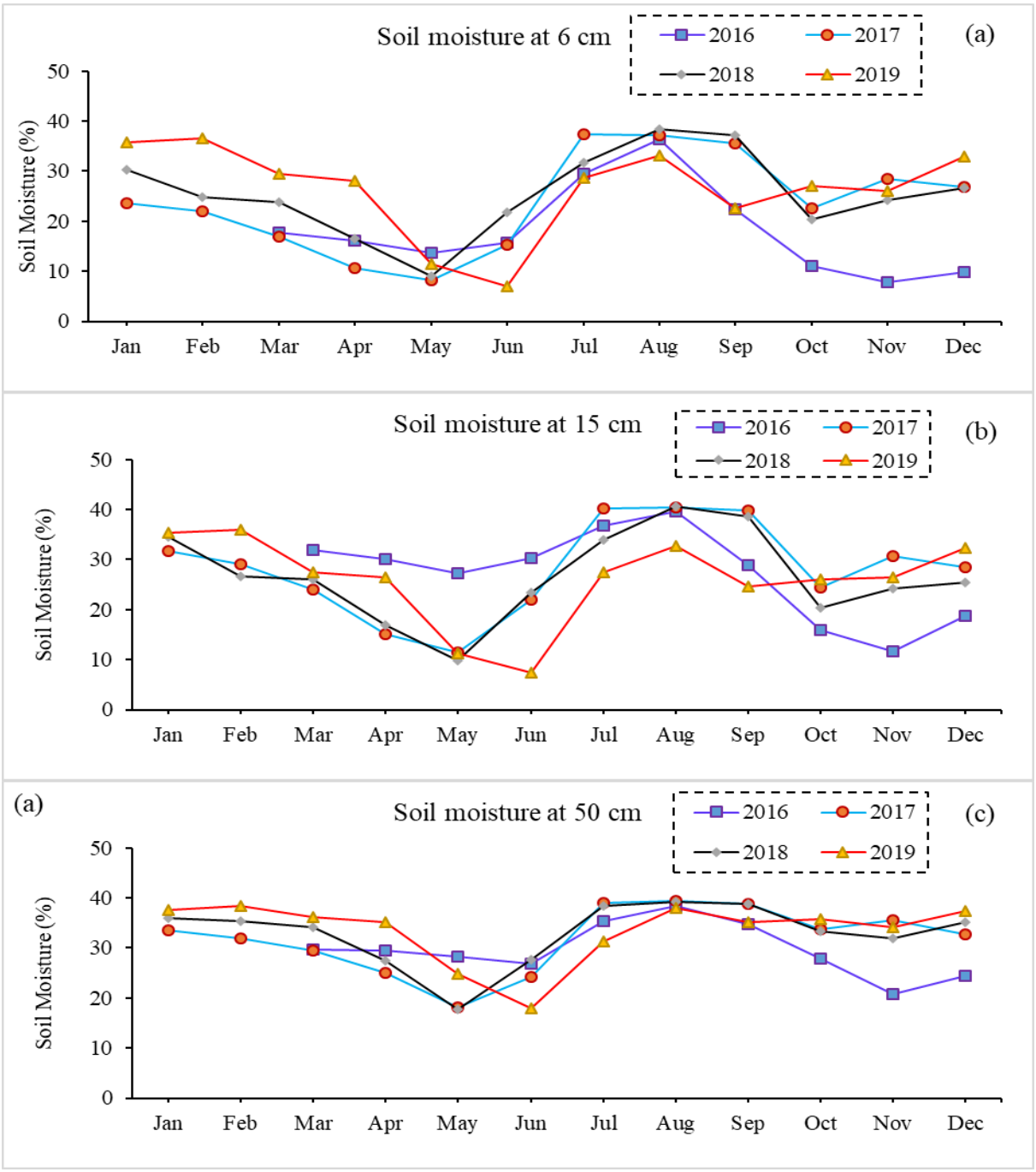

Fig. 4. 15 Variation of mean monthly soil moisture at different depths

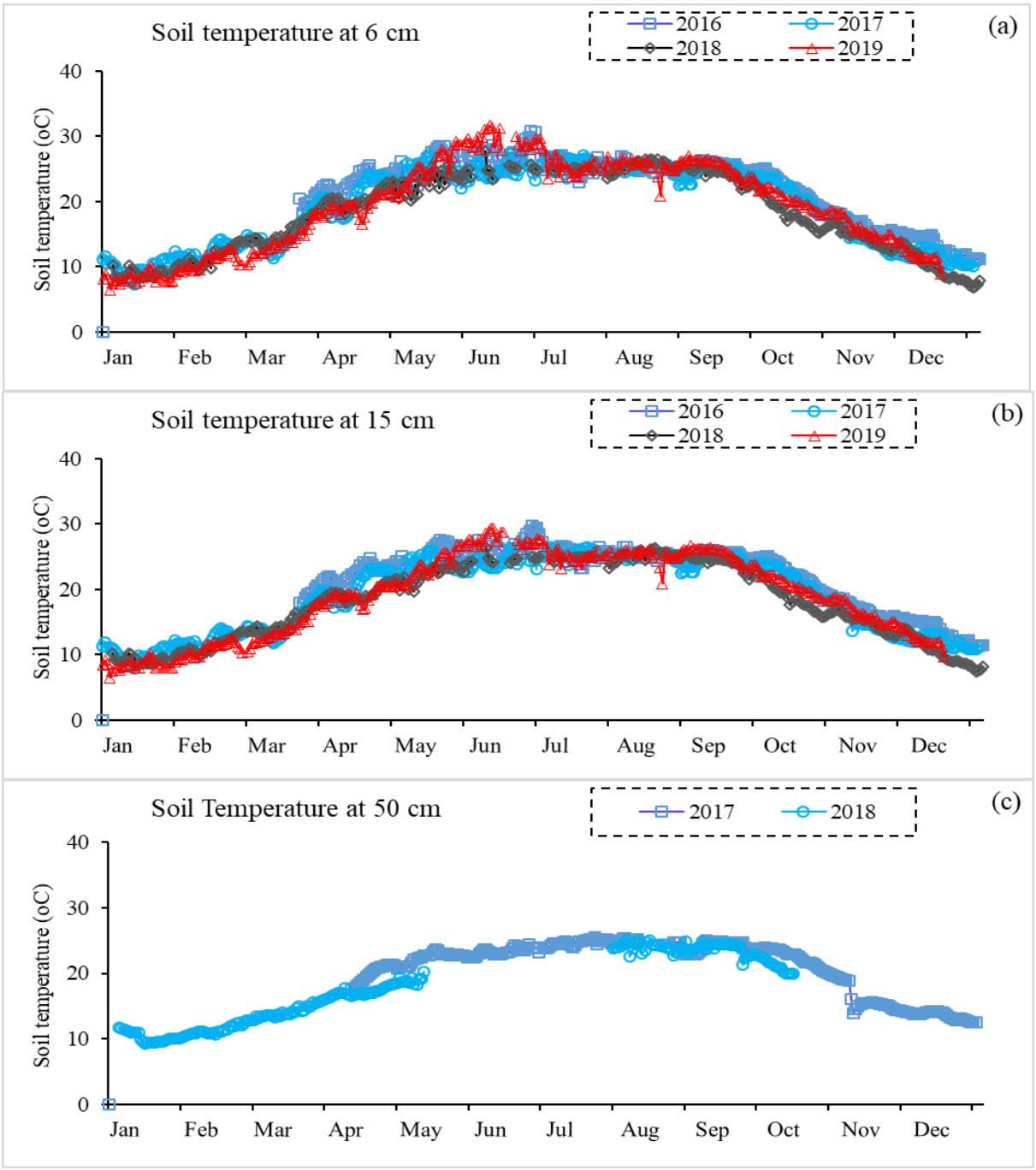

Fig. 4. 16 Variations of daily soil temperature at different depths

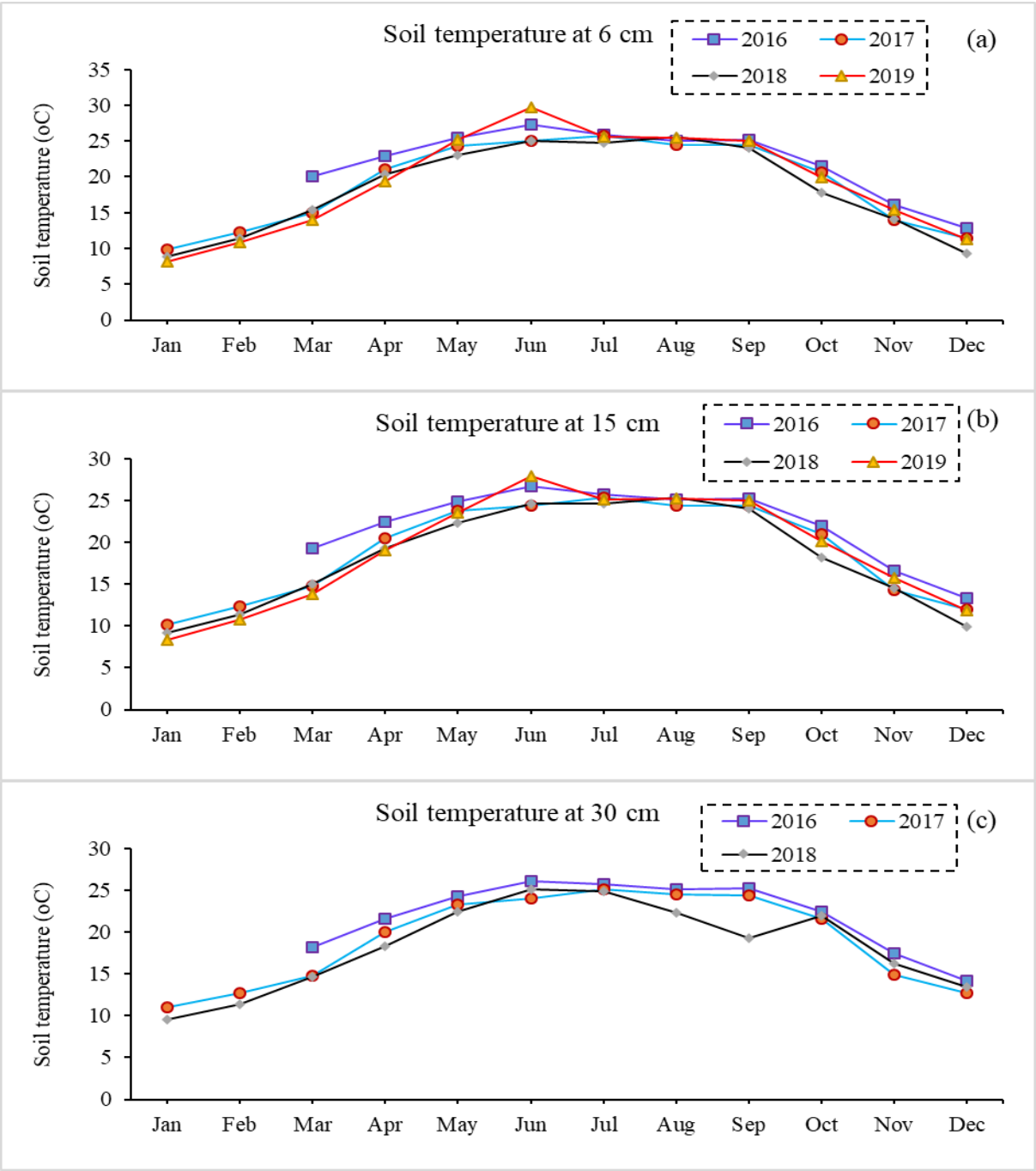

Fig. 4. 17 Variations of mean monthly soil temperature at different depths

4.4.6 Other Data

Apart from the aforesaid described variables, some other data like atmospheric pressure and solar radaitions are also being monitored at Henval valley. Fig. 4.18 shows the variation of atmospheric pressure throughout the year. Here, it follows a smooth trend for all the years, and the seasonal variation is almost negligible. The atmospheric pressure is comparatively high for the year 2016 and 2017, whereas, for the year 2018 and 2019, it is observed low.

Fig. 4.19 shows the variation of net radiation which indicates that the highest net radiation is available in the months of April-September. The increased net radiation in this period is attributed to the increased incoming solar radiation in the summer season as well as the clear sky in the rainy season. The fluctuations are also very high during this period for all the years, which may be due to cloud cover.

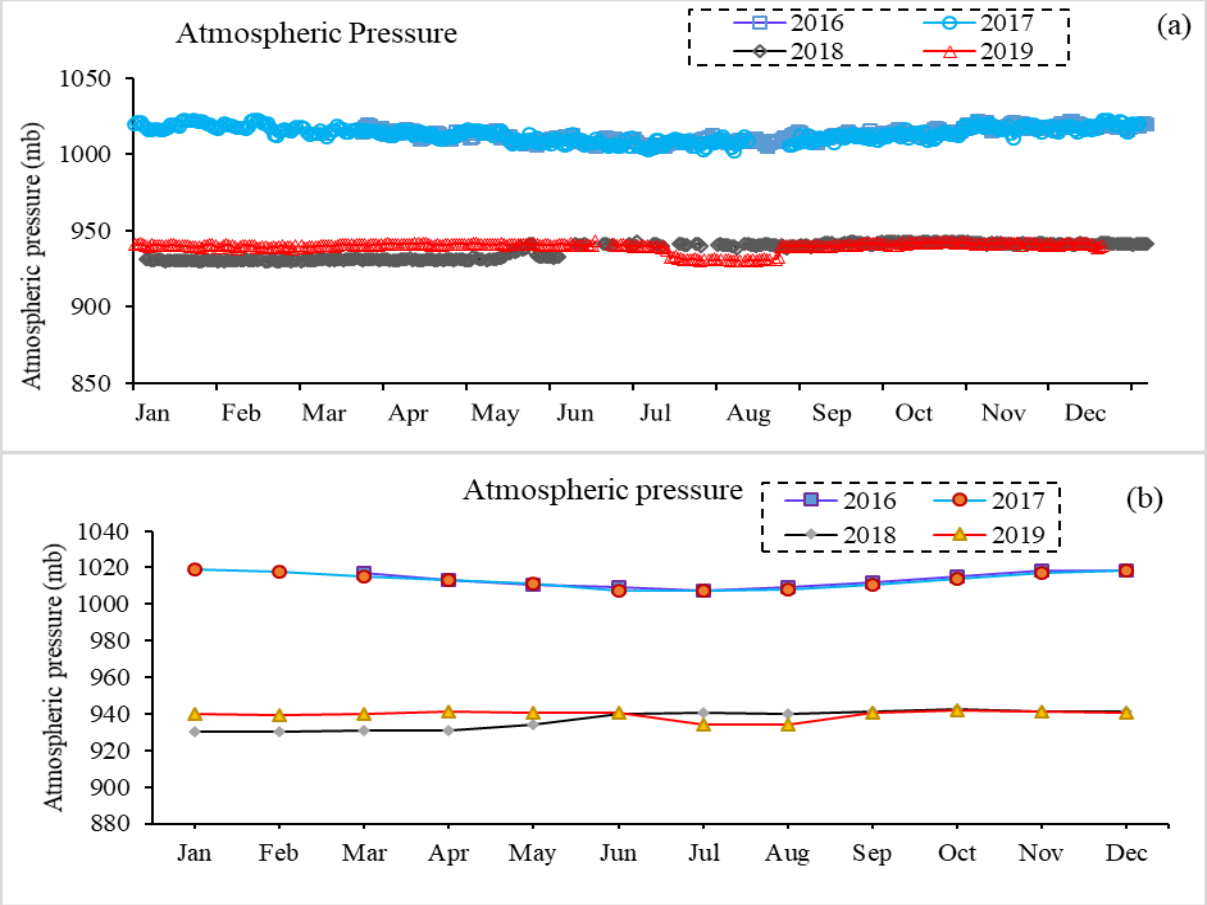

Fig. 4. 18 Variation of atmospheric pressure

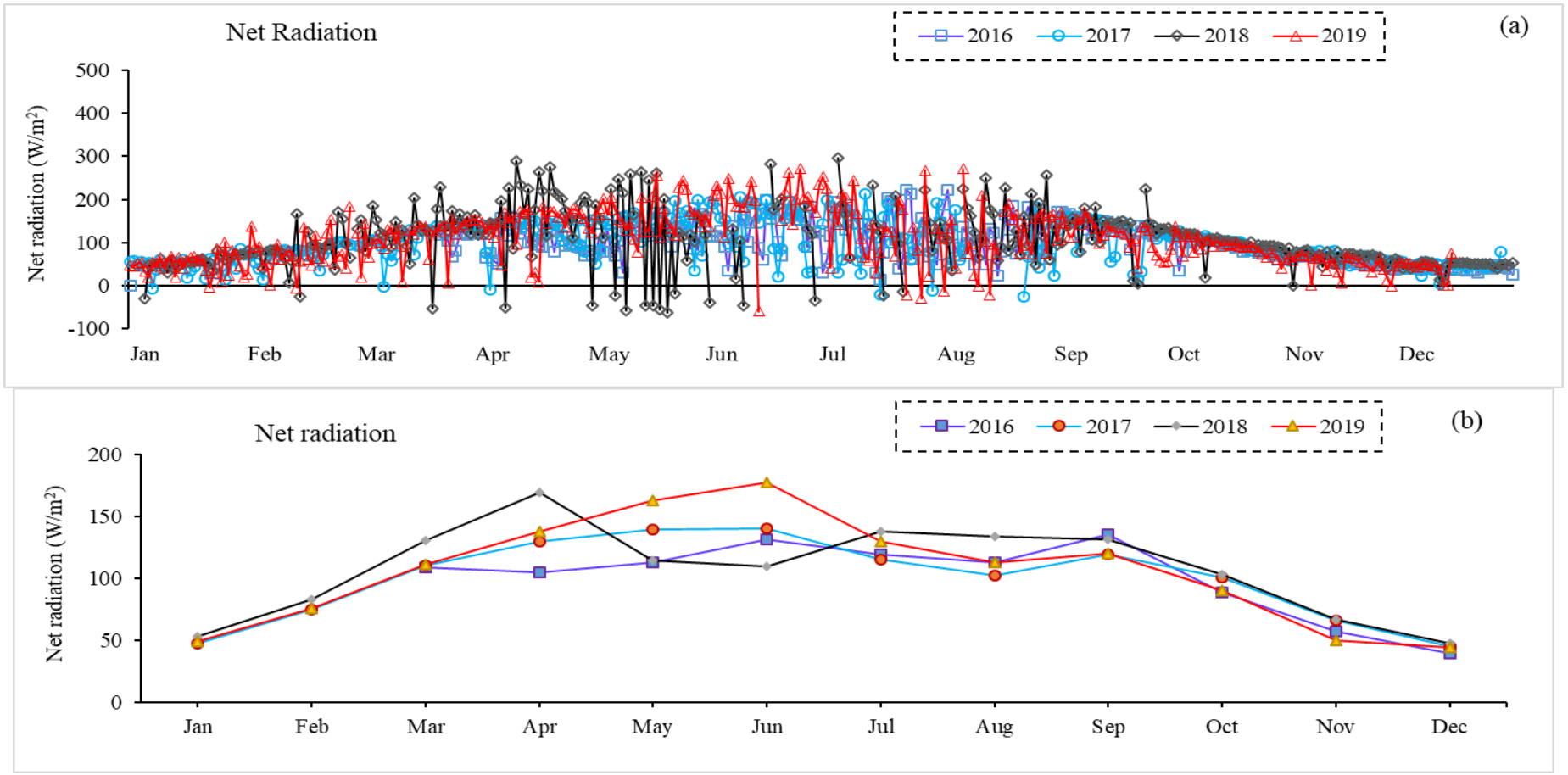

Fig. 4. 19 (a) Daily variation of net radiation and (b) mean monthly variation of net radiation

4.5 Study of Diurnal and Daily Variation in ATRH Measured by Different Sensors

The variation (diurnal and daily) in average air temperature, measured at the height of 2m from the surface by two different sensors: Sensor with Radiation Shield and Fan aspirated Shield has been studied to find a discrepancy in measurement if it exists. The temperature recorded by these sensors during 21-22 August 2019 has been plotted to see the diurnal variation in air temperature (Figure 4.20).

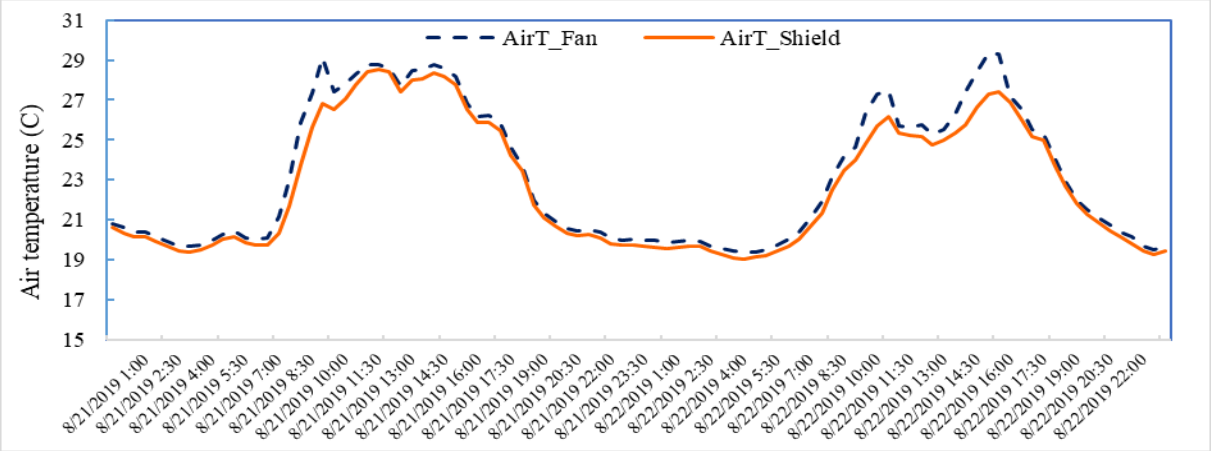

Fig. 4. 20 Diurnal variation in average air temperature measured by radiation shield and fan aspirated shield sensor at Nagani

The temperature measured by the two sensors, in general, follows the same curve and no significant difference in the magnitudes are observed. However, at peak hours, the sensor having fan aspirated shield measures a slightly higher temperature than the sensor having a radiation shield. A more or less similar pattern is also observed in case of daily variation of temperatures, recorded from these sensors (Figure 4.21). The relative humidity recorded from March 23rd, 2016 to December 31st, 2019 by these sensors is also plotted to examine its daily pattern of variation, as shown in Fig. 4.22. Similar to the temperature, no significant difference in the amount of relative humidity is found.

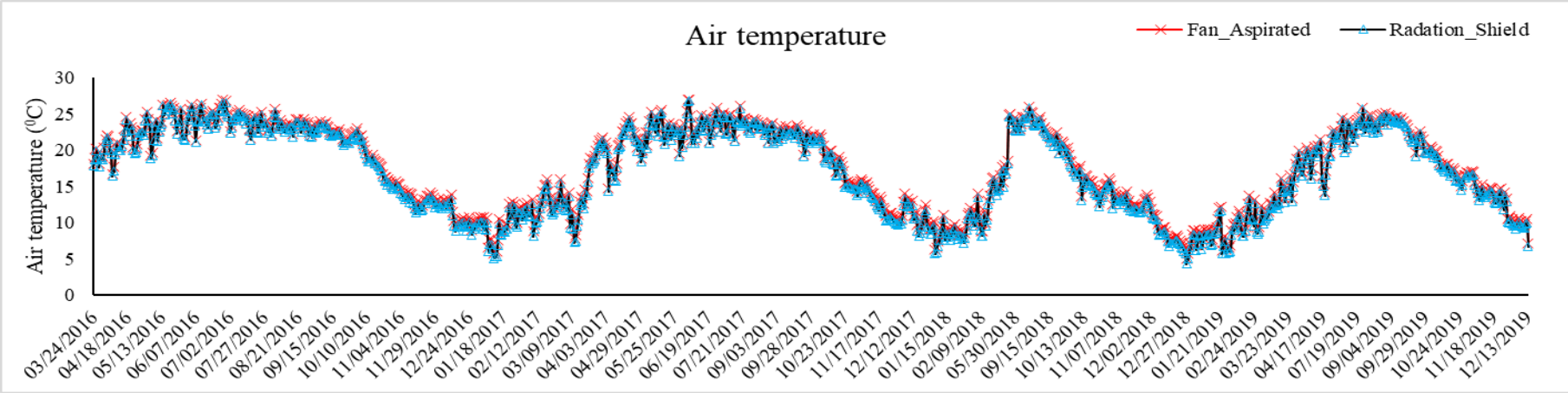

Fig. 4. 21 Daily variations in average air temperature measured by radiation shield and fan aspirated shield sensor at Nagani

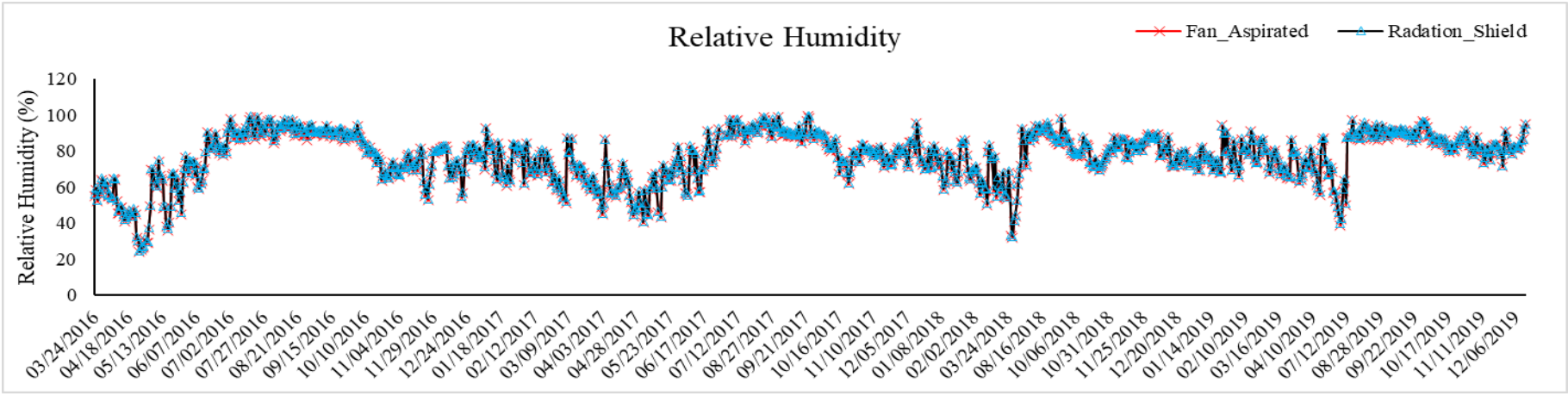

Fig. 4. 22 Daily variations in relative humidity measured by radiation shield and fan aspirated shield sensor at Nagani

4.6 Study of Diurnal and Daily Variation in Wind Speed measured at Different Heights

The effect of altitude on the speed of wind has been assessed by the sensors installed at different height from the surface respectively. A considerable variation in the pattern of wind speeds (WS_50cm WS_2m, WS_4m, WS_6m and WS_10m) are observed over time due to differences in altitude. This has been shown in Figure 4.23 (diurnal variation) and Figure 4.24(daily variation), respectively. The speed of wind measured near-surface (WS_50cm, WS_2m) is characterised by relatively low speed due to resistance imposed by the surface with respect to wind speed sensed at higher heights.

4.6 Study of Daily Variation in Different Components of Solar Radiation

The daily variation in different components of solar radiation such as Incoming Shortwave Radiation (SW_IN), Outgoing Short-Wave Radiation (SW_OUT), Long-Wave UP (LW_UP) and Long Wave down (LW_DN) has been examined to study nature of heat flux transfer mechanism between surface and atmosphere (Fig. 4.25). The highest flux has been recorded for SW_IN whose values ranges between 0 to 1132 W/m^2 whereas the values for SW_OUT has been found in the range of 0 to 202 W/m^2 over the surface of the earth. The values of LW_IN and LW_OUT are found in the middle of 310 to 621.3 W/m^2, and 244.7 to 448.2 $W/m^{2,}$ respectively.

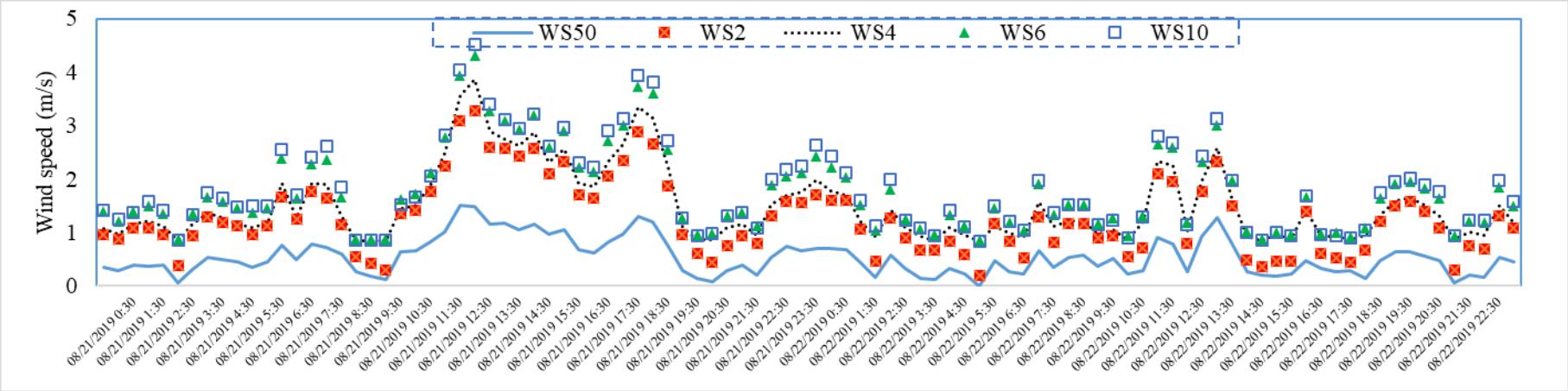

Fig. 4. 23 Diurnal variation in average wind speed measured at different heights at Nagani

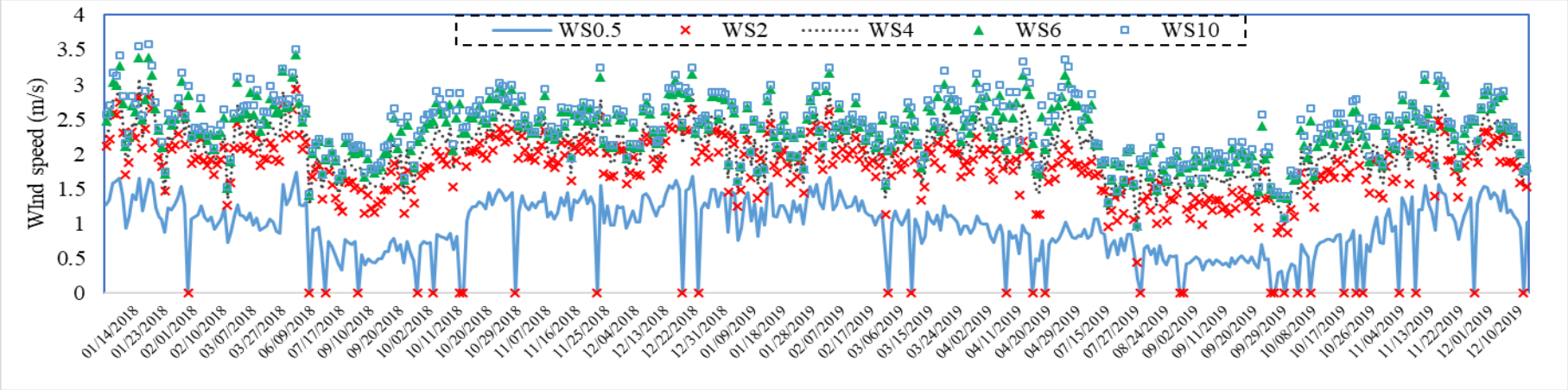

Fig. 4. 24 Daily variations in average wind speed measured at different heights at Nagani

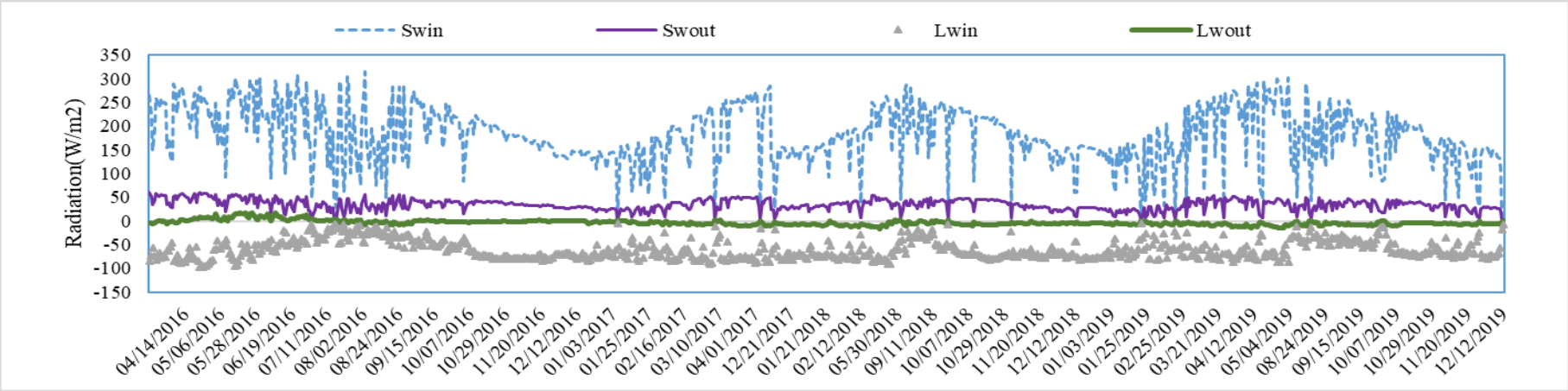

Fig. 4. 25 Daily variation in different components of solar radiation at Nagani

4.7 Comparison of Satellite Rainfall Estimates and Rain Gauge Measurements

To find an effective solution for the discrepancies in the rain gauge measurements of the Henval catchment after 2019, different satellite rainfall estimates were compared with the rain gauge measurements for the same region. The comparison study included different satellite rainfall products at varying spatial and temporal scales viz. GPM, NASA Power, CHIRPS, IMDAA. The spatial resolution of GPM, NASA POWER, CHIRPS and IMDAA are 0.1,0.5,0.05 and 0.12 degrees, respectively. Various statistical measures were adopted to analyze the results on different time scales and select the best alternative for the rain gauge observations. Statistical analysis results of the estimates w.r.t gauge measurements from 2016 January 1 to 2017 December 31 on a daily time scale are tabulated in Table 4.2.

Table 4. 2 Statistical analysis on a daily time scale for Henval

Metrics	GPM	NASA POWER	CHIRPS	IMDAA (NGFS)
NSE	-0.27	0.45	0.09	-0.09
RMSE	12.35	8.15	10.46	11.48
R^2	0.11	0.45	0.28	0.31
PBIAS	5.38	-1.60	1.89	79.65

Overall results of the statistical analysis were inferior, which could be due to the irregular distribution of rainfall events throughout the year. However, the best among all the datasets compared was the NASA POWER dataset of rainfall estimate with the highest values for NSE and R^2, 0.45 each and the lowest for RMSE and PBIAS, 8.15 and -1.6, respectively. Scatter plots of the different rainfall estimate along with their corresponding simple linear regression equation where the gauge data is an independent variable are given in Figure 4.26.

Furthermore, analysis of different rainfall estimates and rain gauge measurements has been carried out in a monthly scale using the average of sum of precipitation for each month from 2016 to 2017. Monthly variations of rainfall as per different datasets is given in Figure 4.27. Precipitation is observed to be less in the months of January to April and then gradually increasing to reach the peak in July. The precipitation is observed to decline after that and tends towards minimal to no precipitation since October corresponding to the winter season. Furthermore, rainfall estimates have shown a maximum deviation from rain gauge measurements during July followed by September.

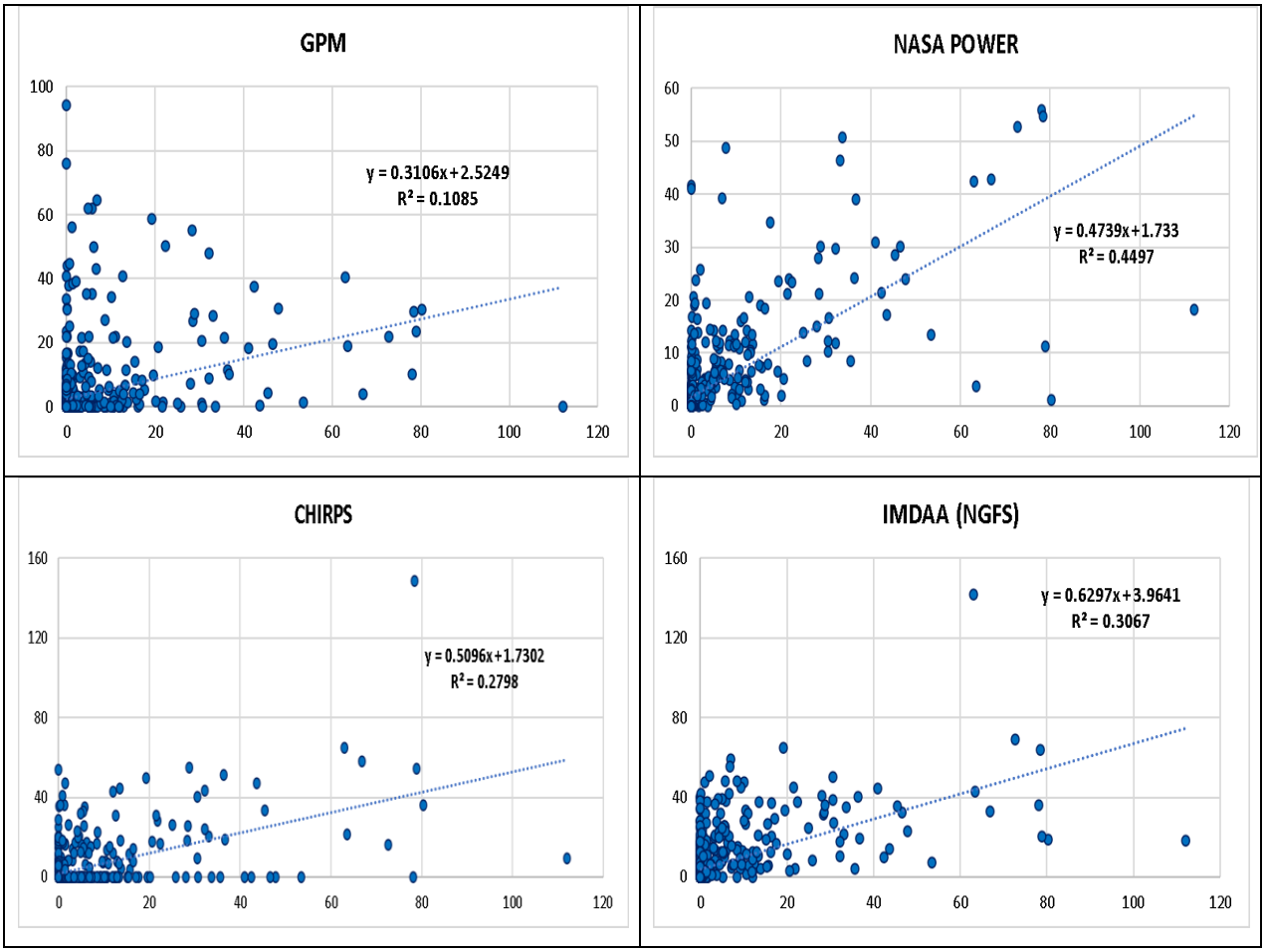

Fig. 4. 26 Comparison of different rainfall estimates on a daily scale

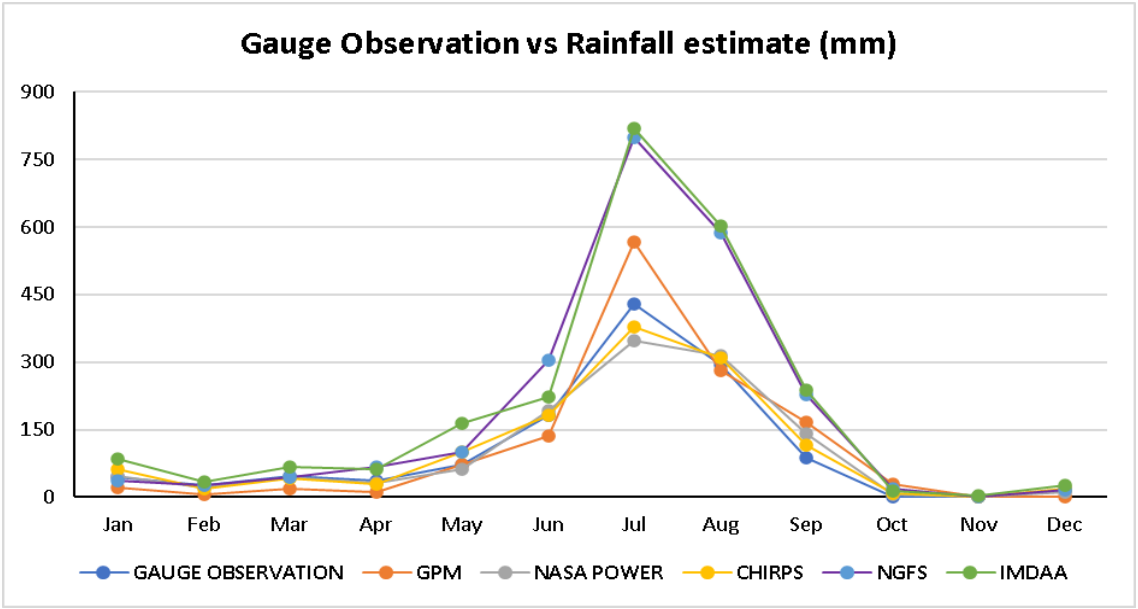

Fig. 4. 27 Monthly variations in rainfall at Henval

Statistical analysis was carried out to better interpret the correlation of rainfall estimates w.r.t rain gauge measurement on a monthly time scale and are tabulated in Table 4.3. Best statistical results were given by CHIRPS followed by NASA POWER. The CHIRPS yielded the highest NSE and R^2 values of 0.93 each whereas NASA POWER yielded 0.88 and 0.89, respectively. RMSE and PBIAS values of CHIRPS were 35.6 and 1.89 while NASA POWER resulted in 45.51 and -1.6, respectively.

Table 4. 3 Statistical analysis on a monthly time scale

Metrics	GPM	NASA POWER	CHIRPS	IMDAA (NGFS)	IMDAA
NSE	0.64	0.88	0.93	-0.52	-0.85
RMSE	80.47	45.51	35.60	164.88	181.74
R^2	0.76	0.89	0.93	0.83	0.77
BIAS	5.38	-1.60	1.89	79.65	88.56

The correlation between rainfall estimates and rain gauge measurements on a monthly scale are represented as scatter plots and given in Fig. 4.28 along with the corresponding simple linear regression equation. Since the findings from the statistical analysis of datasets on different time scales were not exactly aligned, the CHIRPS and NASA POWER datasets were further examined in detail and the results obtained are represented in Figure 4.29 and Table 4.4

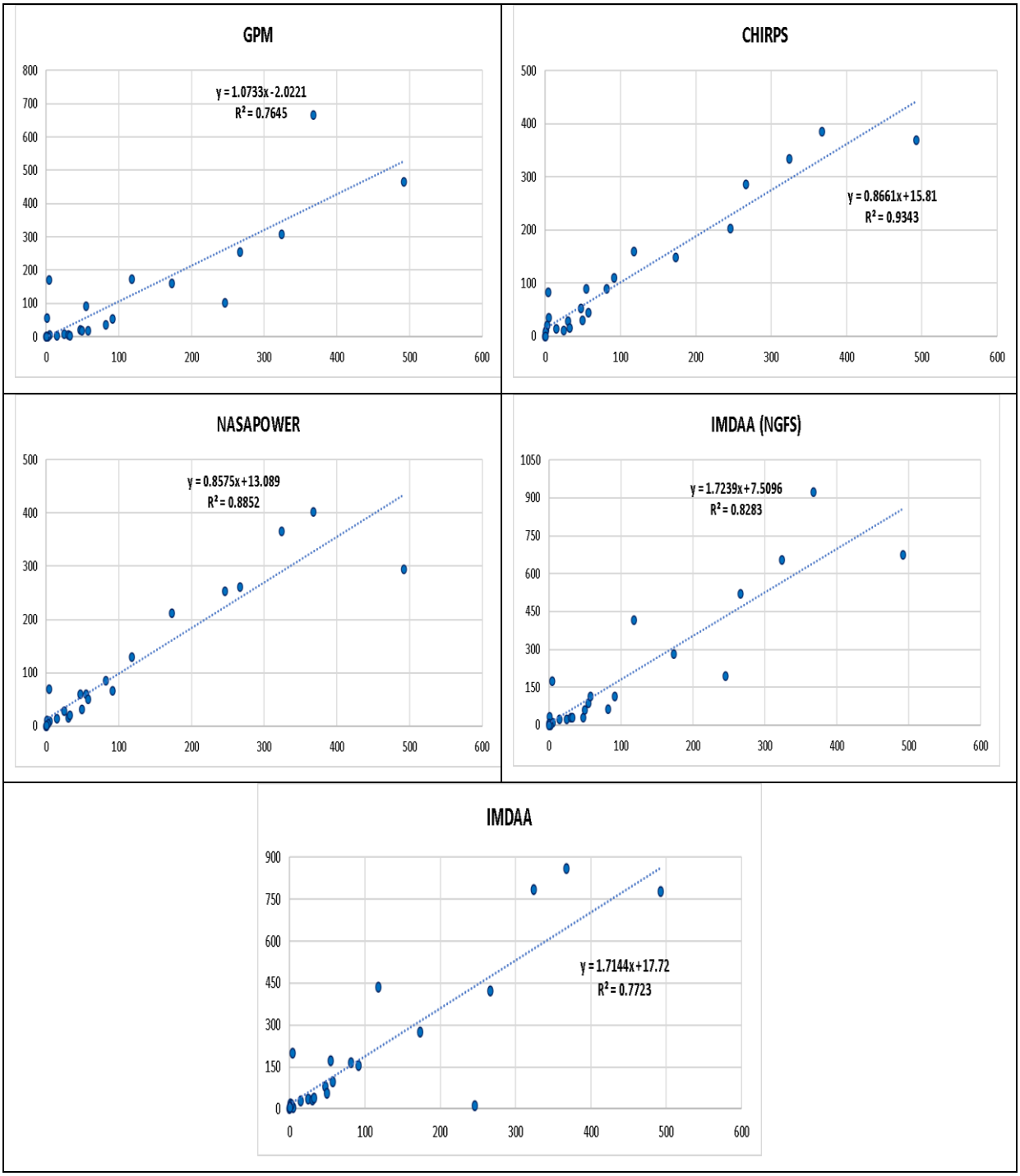

Fig. 4. 28 Comparison of different rainfall estimates on a monthly scale

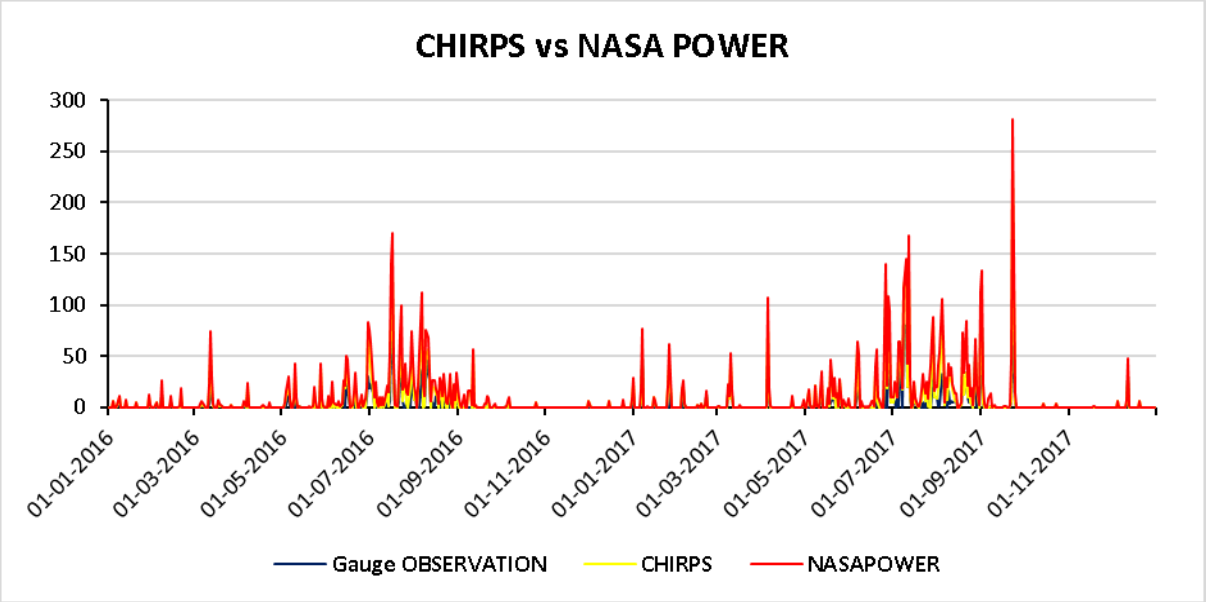

Fig. 4. 29 Precipitation time series data

Table 4. 4 Comparison of CHIRPS and NASA POWER

DATA SET			CHIRPS		NASAPOWER	
TIMESCALE			DAILY	MONTHLY	DAILY	MONTHLY
TOTAL		AVERAGE OF GUAGE	3.40	103.48	3.40	103.48
		AVERAGE	3.46	105.44	3.34	101.83
		NSE	0.09	0.93	0.45	0.88
		RMSE	10.46	35.60	8.15	45.51
		R^2	0.28	0.93	0.45	0.89
		BIAS	1.89	1.89	-1.60	-1.60
ANNUAL	2016	AVERAGE OF GUAGE	2.47	75.45	2.47	75.45
		AVERAGE	3.14	95.68	2.87	87.42
		NSE	0.01	0.93	0.67	0.96
		RMSE	8.06	30.95	4.69	22.11
		R^2	0.28	0.96	0.67	0.98
		BIAS	26.81	26.81	15.86	15.86
	2017	AVERAGE OF GUAGE	4.32	131.51	4.32	131.51
		AVERAGE	3.79	115.19	3.82	116.24
		NSE	0.11	0.93	0.36	0.83
		RMSE	12.41	39.71	10.53	60.45
		R^2	0.28	0.96	0.37	0.84
		BIAS	-12.41	-12.41	-11.61	-11.61

Overall, the NASA POWER dataset has been identified as the better-performing dataset on a daily scale, with NSE and R^2 values of 0.45 each whereas the CHIRPS dataset performed the best on a monthly scale with NSE and R^2 values of 0.93 each. RMSE values are found to be 8.15 and 35.60 respectively. Furthermore, an annual analysis of the data has been carried out.

NASA POWER datasets have performed the best on daily as well as monthly time scales for the year 2016. The corresponding values of NSE, RMSE, R^2 and BIAS were 0.67, 4.69, 0.67 and 15.86 respectively on a daily scale whereas, on a monthly scale, values obtained were 0.96, 22.11, 0.98 and 15.86 respectively. However, for the year 2017, NASA POWER performed the best on a daily scale with NSE and R^2 values of 0.36 and 0.37 respectively while the RMSE and BIAS values are 10.53 and -11.61 respectively. CHIRPS performed the best on a monthly time scale with high NSE and R^2 values of 0.93 and 0.96, respectively. The RMSE values were found as 39.71 while BIAS was -12.41.

Bias factor for the NASA POWER and CHIRPS datasets were calculated using linear scaling method and tabulated in Table 4.5. Bias correction was done to NASA POWER and CHIRPS datasets based on the gauge measurements on a monthly scale. Linear regression analysis for the bias-corrected CHIRPS and NASAPOWER datasets on a daily time scale was done and represented in Figure 4.30.

Table 4. 5 Bias correction factor for CHIRPS and NASA POWER datasets for Henval

Month	CHIRPS	NASAPOWER
January	0.69	0.93
February	1.42	1.24
March	1.16	1.06
April	1.22	1.12
May	0.73	1.15
June	1.00	0.95
July	1.14	1.23
August	0.95	0.94
September	0.77	0.63
October	0.07	0.12
November	---	0.08
December	0.96	1.45

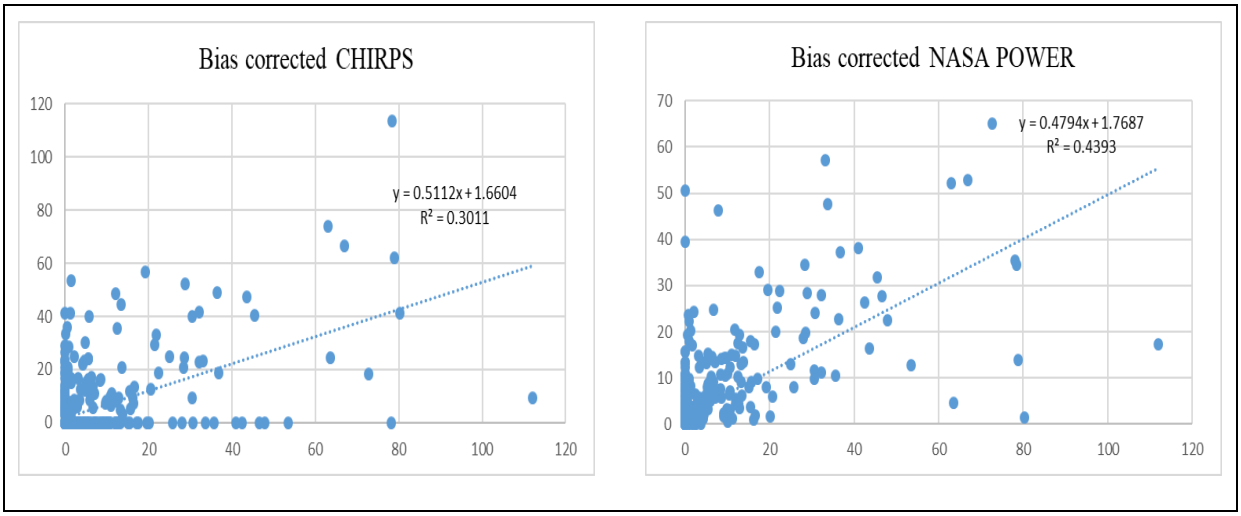

Fig. 4. 30 Bias corrected CHIRPS and NASA POWER data sets for Henval

Statistically, bias correction slightly improved the CHIRPS dataset whereas deteriorated the NASA POWER dataset. Since the original NASA POWER dataset was characterized with better statistics, the NASA-POWER dataset has been identified as a potential proxy for gauge measurements in the Henval watershed on a daily scale.

The scarcity of observed hydro-meteorological data was more acute for the glaciated Gangotri watershed as ground measurements were only available during the ablation season. Hence, a similar comparative analysis of different meterological datasets was done to identify the best meterological dataset for the Gangotri watershed to overcome the scarcity of in-situ meterological data. The datasets were selected based on the continuous availability of finer resolution data in a daily time step to meet the requirements of the glacio-hydrological modeling using SPHY. The different datasets analyzed to find out the best alternative to in-situ meterological datasets were CHIRPS, GPM IMERG, ERA5, NASA Power, IMDAA and ERA5-Ag with the spatial resolutions 0.05º, 0.1º, 0.25º, 0.5º, 0.1º and 0.1º respectively.

The statistical analysis of different precipitation datasets was done w.r.t to the available gauge data during ablation seasons (June to September) from 2016 to 2018 and 2022 to 2023 and their performance on a daily time step was tabulated in Table 4.6.

Table 4. 6 Statistical analysis on a daily time scale for Gangotri Watershed

Metrics	NASA POWER	CHIRPS	GPM IMERG	ERA5-Ag
NSE	-3.07	-18.84	-7.16	-2.62
RMSE	8.43	18.61	11.93	7.95
R²	0.18	0.16	0.28	0.21
BIAS	187.14	309.48	144.49	214.00

Though the datasets' performance was poor, the ERA5-Ag appeared to be relatively better with the highest NSE (-2.62) and lowest RMSE (7.95) metrics. However, the variability was better captured by GPM IMERG with the best R^2 (0.28) and lowest bias (144.49). The scatterplots of each dataset on a daily time scale along with their linear regression equation are represented in Figure 4.32.

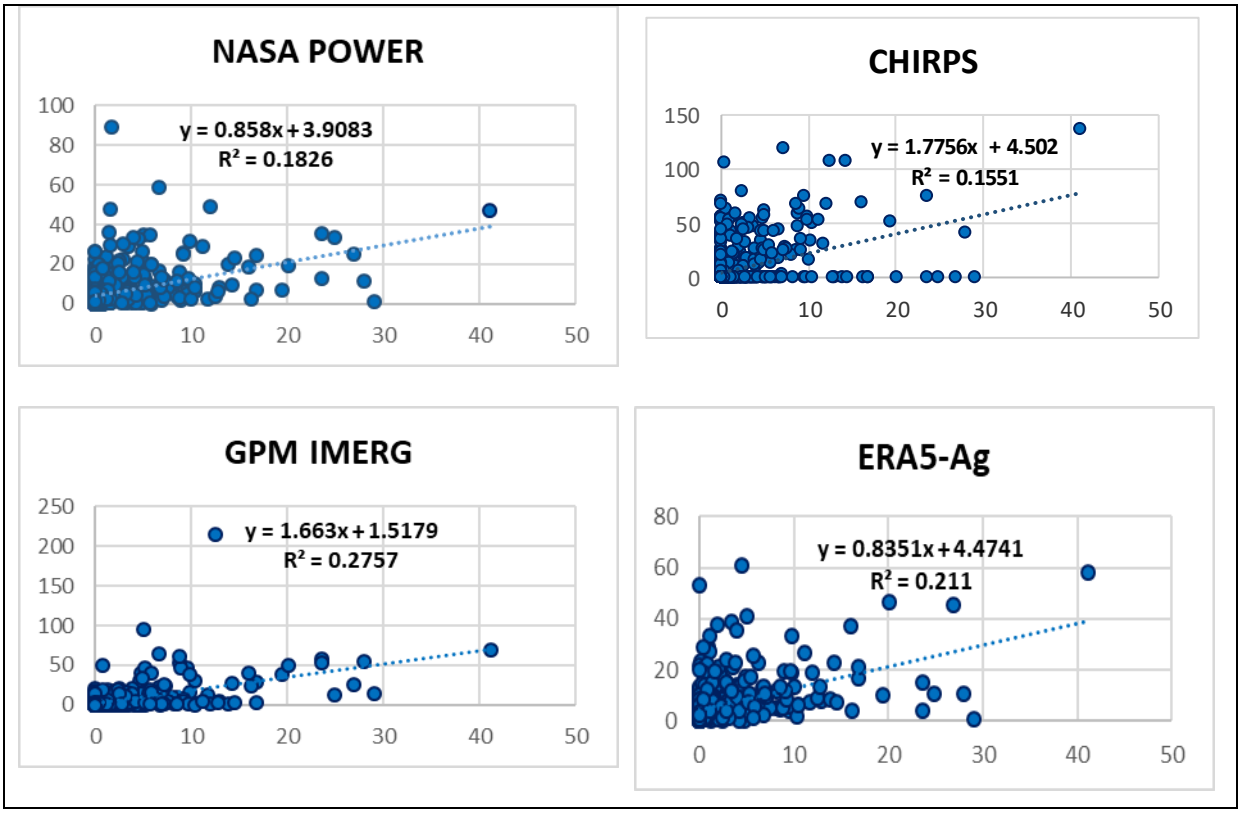

Fig. 4. 31 Comparison of different precipitation datasets on a daily scale for Gangotri Watershed

To analyze the datasets better, a comparison was done based on the average monthly precipitation of each dataset w.r.t the rain gauge measurements and are tabulated in Table 4.7.

Table 4. 7 Statistical analysis on a monthly time scale for Gangotri Watershed

Metrics	NASA POWER	CHIRPS	GPM IMERG	ERA5-Ag
NSE	-15.98	-46.22	-10.17	-21.04
RMSE	117.41	195.82	95.24	133.78
R^2	0.66	0.70	0.78	0.88
BIAS	187.14	309.48	144.49	214.00

The GPM IMERG dataset was relatively better than other datasets with the highest NSE (least negative) and lowest RMSE and PBIAS along with a strong R^2. ERA5-Ag has been identified as the second-best performer with the highest R^2 and was followed by the NASA POWER dataset with decent metrics.

Considering the better performance of GPM-IMERG data in both daily and monthly time scales, it was chosen as the potential proxy for the in-situ precipitation data, which necessitated finding the best alternative to the recorded temperature. The statistical measures considered to identify the best satellite temperature dataset are tabulated in Table 4.8. The comparison was done w.r.t. the recorded thermometer measurements for mean temperature on a daily time scale. The NASA Power dataset were found the best performer among the compared datasets with the highest (least negative) NSE, lowest RMSE, highest R^2 and least bias followed by IMDAA, ERA5 and ERA-5Ag datasets. The scatter plots of the different temperature estimates w.r.t. the gauge data is given in Fig.4.32 along with their linear regression equation.

Table 4. 8 Statistical analysis for different temperature datasets on a daily time scale in Gangotri Watershed

Metrics	NASAPOWER	ERA5	ERA5-Ag	IMDAA
NSE	-0.20	-7.40	-35.95	-4.11
RMSE	2.31	6.14	12.87	4.78
R^2	0.44	0.33	0.38	0.20
BIAS	-15.75	-54.18	-124.46	-37.93

The consistent performance by NASA Power in the individual years and overall time period under consideration were found satisfactory to be identified as the better alternative to in-situ temperature measurements in Gangotri watershed. However, due to the non-availability of in-situ data throughout the year in the Gangotri catchment, bias correction couldn't be performed and eventually the research was further proceeded with the unaltered datasets identified as the best alternative for meterological parameters.

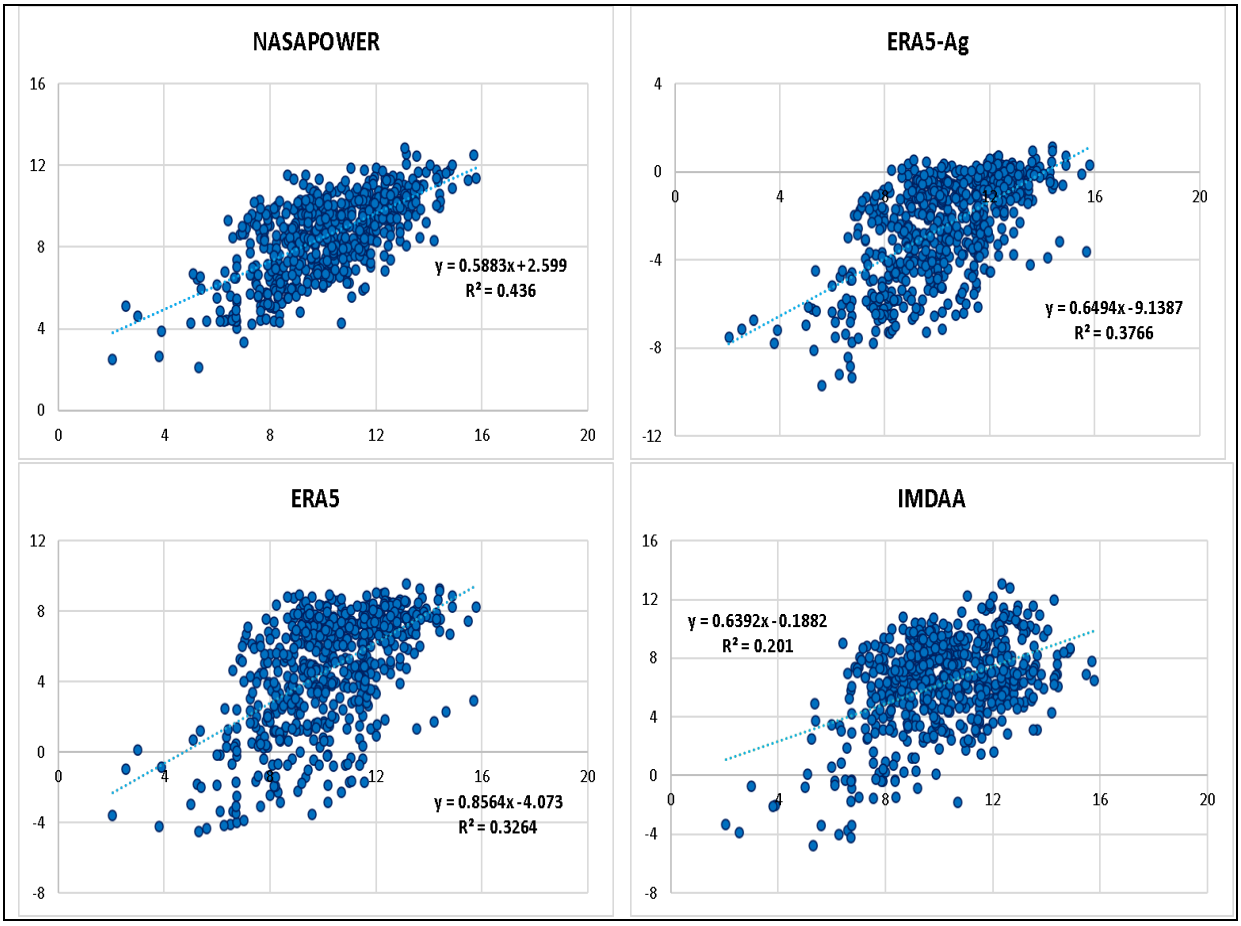

Fig. 4. 32 Comparison of different temperature datasets on a daily scale for Gangotri Watershed

Chapter 5

5.0 GLACIO HYDROLOGICAL MODELING USING SPHY MODEL

5.1 Description of SPHY model

The SPHY model is a conceptual, continuous-time, raster-based spatially distributed leaky bucket-type water balance model that can simulate the behavior of glaciers and their interaction with the hydrological system at a regional or watershed scale. It requires a large number of input parameters varying widely in space and time while transforming input into output. It is a freely available model that is useful especially in mountainous areas despite the data scarcity, complexity and variability of the region for understanding the impacts of climate change on glacier dynamics, water resources, and downstream communities (Van Vliet et al., 2012, Lutz et. al, 2014; Terink et al, 2015). The SPHY model combines best components of existing widely used simulation models viz. SRM, VIC, SWAT, SWAP, HydroS, PCR–GLOBWB, SWAP, HIMSIM. SPHY glacio-hydrological models typically integrate various components such as glacier mass balance, ice melt, snow accumulation and melt, surface runoff, groundwater flow, and streamflow routing. An overview of SPHY model is represented in the Figure 5.1.

The model is based on physical principles and incorporate data on topography, climate, land cover, digital elevation model (DEM), soil properties and other relevant factors to simulate the complex interactions between glaciers and the hydrological cycle. SPHY operates at flexible scales viz. local, regional and global, accounting for relevant terrestrial hydrological processes. The tool can be used in water resource assessment, planning, management and decision-making policies. Major concept of SPHY is mass conservation and hence, simulates the dynamic behaviour of the glaciers. Therefore, SPHY can be used for assessing the potential effects of glacier retreat on water availability, hydropower generation, agriculture, and other socio-economic aspects in regions dependent on glacier meltwater. They also aid in predicting changes in flood and drought patterns resulting from alterations in glacier contributions to river flow. SPHY also inclues lake module and erosion module enabling erosion studies. The model provides great adaptability depending on the spatial relevance of hydrological processes.

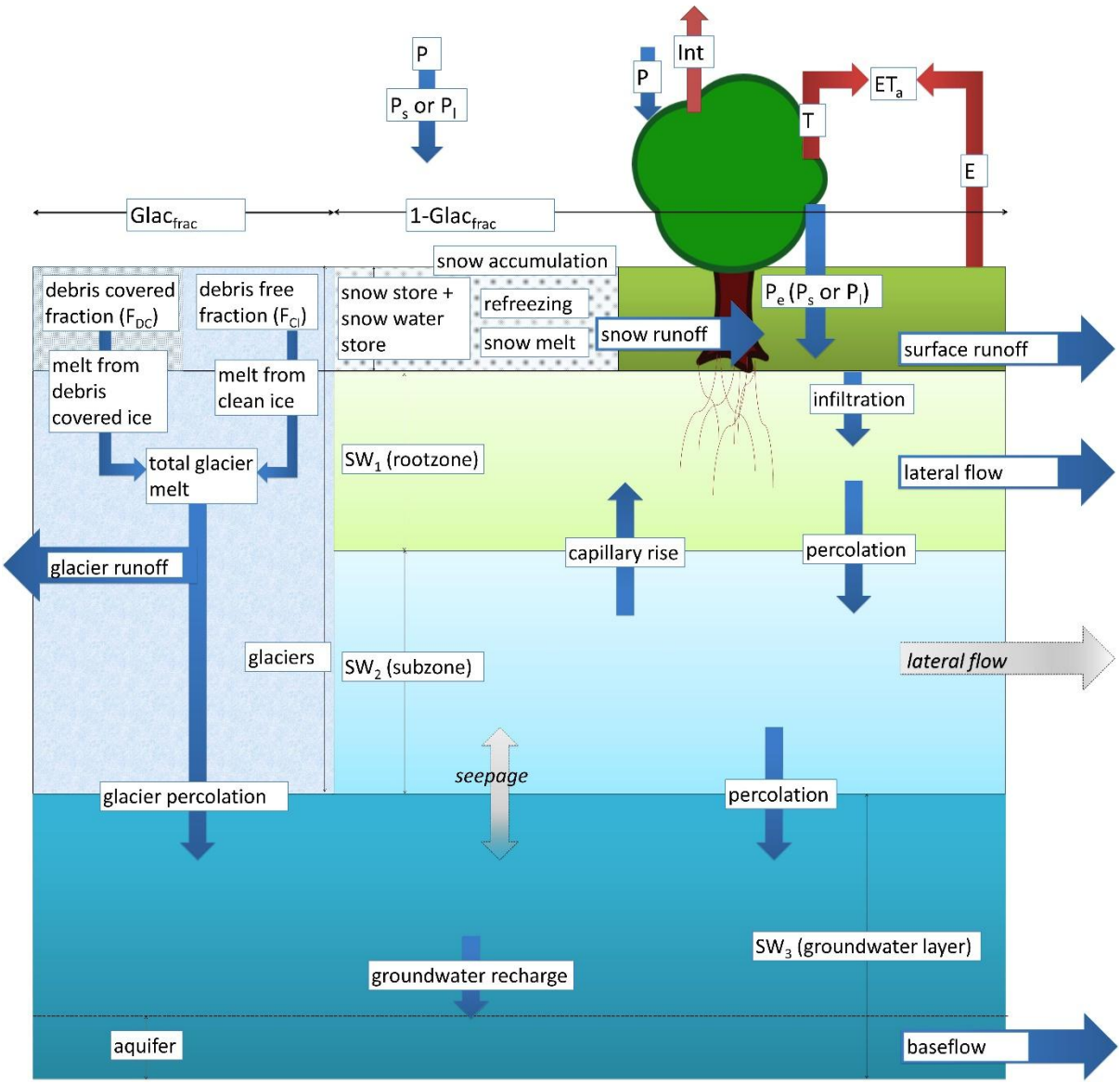

*source: sphy.readthedocs.io/en/latest/concepts.html

Fig. 5. 1 Overview of SPHY model

5.1.1 Data Needs of the SPHY model

SPHY model requires spatial data like DEM, LULC, soil, glacial cover and meteorological data. Since SPHY is grid-based model, optimal use of remote sensing data and other global data is possible. The DEM of the study area was downloaded from https:// search.earthdata.nasa.gov, where elevation data at 30 m resolution acquired through SRTM is available for the globe. The Land Use data derived using the SENTINEL image was downloaded from the ESRI land cover explorer, https://livingatlas.arcgis.com/landcoverexplorer. The image is then projected into proper

projection same as the DEM having the same datum using ArcGIS. The land use land cover maps of Henval watershed and Gangotri watershed are shown in Fig. (5.2) and Fig. (5.3) respectively. The other required inputs for glacio-hydrological modeling were prepared using the Hindu-Kush Himalaya database in the SPHY pre-processor. However, to obtain comprehensive and current data on glacial extends and their characteristics, the glacial dataset in the Hindu Kush Himalaya database in SPHY Preprocessor is updated with the latest version of the Randolph Glacier Inventory Version 7 (RGI 7.0) (RGI Consortium, 2017). The land cover map was further utilized to prepare a crop coefficient table with the corresponding crop coefficient values derived from literature.

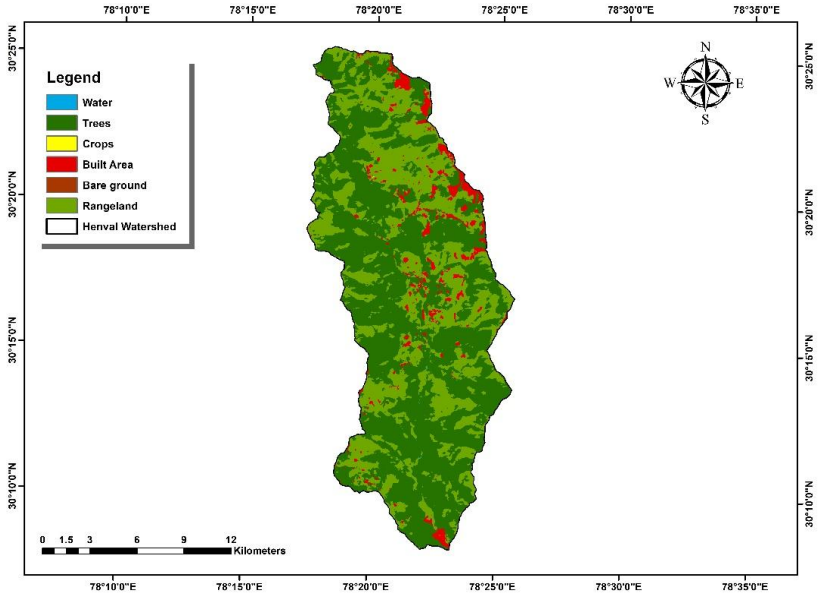

Fig. 5. 2 LULC classes map of Henval watershed

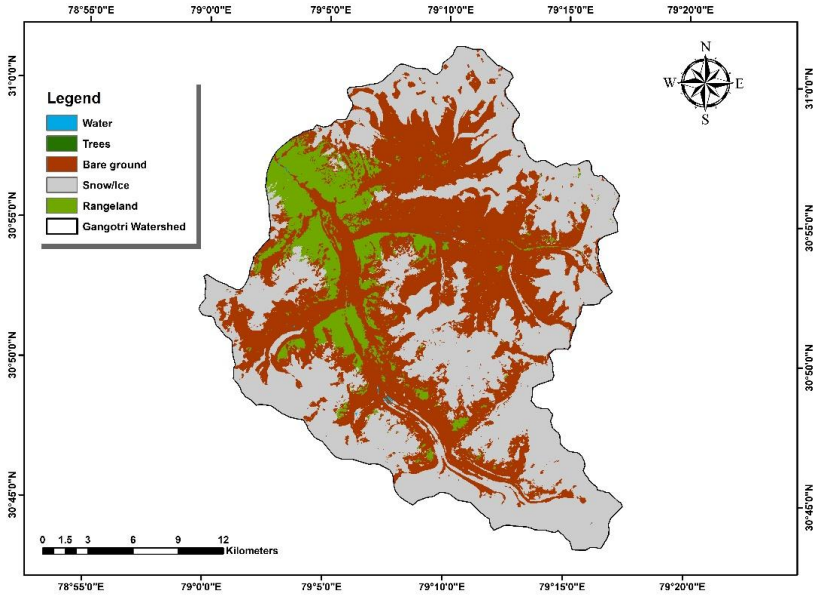

Fig. 5. 3 LULC classes map of Henval watershed

The meteorological and hydrological data required for the study at Henval watershed was procured from the AWS tower installed in Nagani village for the time being. Hence, the SPHY model was first set for the Henval sub-catchment with the outlet at Jijali-Devnagar and then, upscaled for the Henval basin with outlet at Shivapuri. The base map of the Henval sub-catchment within the Henval watershed is shown in Fig. 5.4. Thereafter, the SPHY model was set for the Gangotri watershed with the meteorological station located at Bhojbhasa and the base map is given in Fig.5.5.

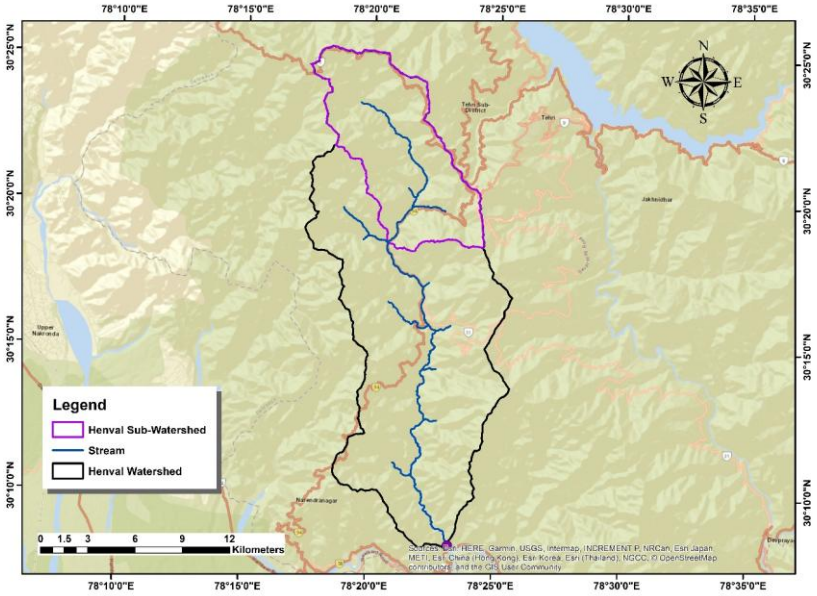

Fig. 5. 4 Base map of Henval sub-watershed

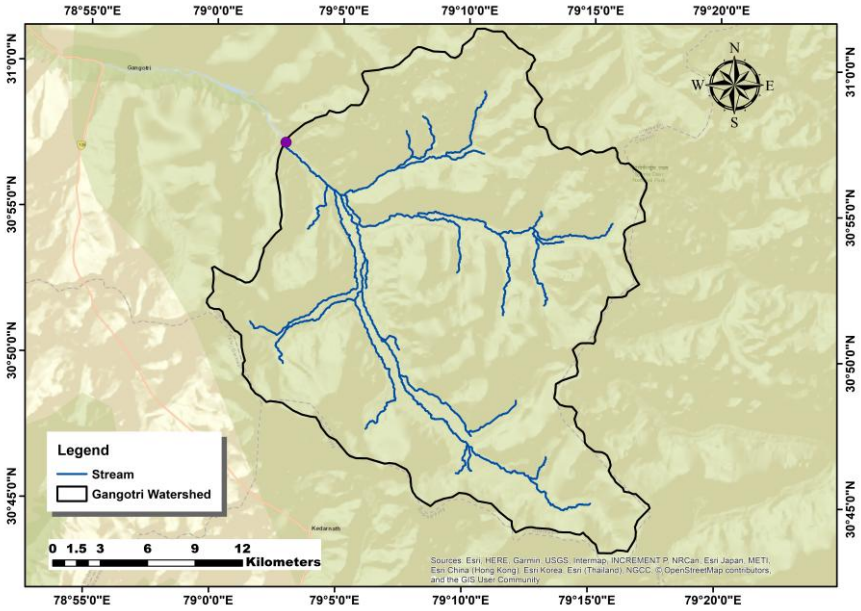

Fig. 5. 5 Base map Gangotri watershed

Precipitation and temperature in-situ datasets for Henval sub-watershed were obtained from the AWS whereas data were collected traditionally during ablation season for the Gangotri watershed. As explained in section 4.7, the in-situ meteorological data were used to find the best alternative datasets for the respective location amongst the various satellite and reanalysis datasets.

The daily discharge for the study was obtained from the broad crested compound rectangular-rectangular weir constructed at the outlet of Henval stream at Jijali-Devnagar and an automatic water level recorder installed across the Henval river at the same outlet. The cross-sectional diagram of the broad crested rectangular-rectangular weir is shown in Fig. 5.6. A compound rectangular-rectangular broad crested weir for monitoring of discharge was constructed, and its discharge can be calculated using the following equation

$$Q_t = \frac{2}{3} C_{rd1} \sqrt{2g} (2b_1) h_1^{3/2} + \frac{2}{3} C_{rd2} \sqrt{2g} b_2 h_2^{3/2}$$

$$C_{rd} = \frac{0.611 + 2.23\left(\frac{B}{b} - 1\right)^{0.7}}{1 + 3.8\left(\frac{B}{b} - 1\right)^{0.7}} + \frac{0.075 + 0.011\left(\frac{B}{b} - 1\right)^{1.46}}{1 + 4.8\left(\frac{B}{b} - 1\right)^{1.46}} \frac{h}{P}$$

Where, C_{rd}= discharge coefficient of the rectangular weir; g= gravitational acceleration; b = weir length; h = water head on the weir crest; B = channel width and P = weir height.

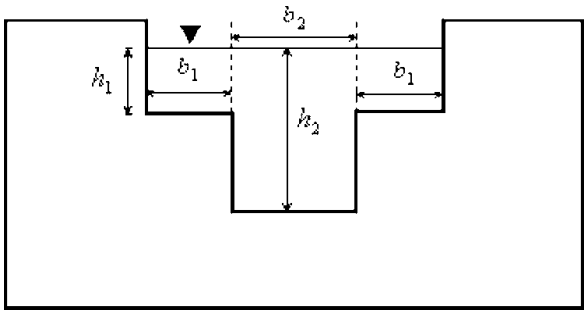

Fig. 5. 5 Cross-section of the compound rectangular-rectangular broad crested weir.

The SPHY modeling concepts for studying the hydrology of glaciated watersheds along with the relevant governing equations have been expounded in the manual.

5.1.1 Computation of Precipitation Forms

Precipitation is calculated on a daily time step at each defined grid cell capturing the spatio-temporal variability in snowfall mass balancing (Singh. Et. al, 2023). Depending on the critical temperature, SPHY models precipitation as either rain (liquid) or snow (solid) for every cell. Vegetation on the ground intercepts the precipitation and causes partial or whole evaporation (Terink et. al, 2015).

5.1.2 Calculation of Evapotranspiration

Despite the energy-based Penman-Monteith method being the sole standard method for calculating reference evapotranspiration, due to the high input data requirements SPHY model utilizes a simpler, temperature-based approach of modified Hargreaves equation to calculate reference evapotranspiration and further, calculates potential evapotranspiration using the single crop coefficient approach (Allen et al., 1998; Terink et al, 2015). Kc for each land class in the study area was derived from the literature and taken as constant throughout the simulation period.

5.1.3 Quantification of Snow Processes

Dynamic snow storage is simulated for each cell and when snow accumulates or melts, the snow storage is updated for each cell at a daily time step considering precipitation, snow melt and refreezing of rainfall and snowmelt within the snowpack. The easy approach of the Temperature Index Model with varying degree-day factors based on the empirical relationship between melt and air temperature has been used to simulate daily potential snowmelt.

DDF_S is the degree day factor for snow, which is a calibrating parameter. However, the snow storage at the end of the previous day is a limiting factor for the actual snowmelt. The snow storage from the previous day is updated to the current day with respect to the actual snowmelt and the snow accumulation of the day t. Snow accumulation accounts for both the solid precipitation and refreezing of rainfall and snow melt stored within the snowpack.

The maximum of meltwater that can freeze within the snowpack depends on the thickness of snow storage and a calibrated parameter namely water storage capacity. The water storage

capacity of the snowpack represents the capacity to refreeze the snow melt within the snowpack and is defined as the total water equivalent of snowmelt in mm that can freeze per water equivalent of snow in the snow storage in mm.

Based on the assumption in SPHY, snow melting and accumulation are limited to the grid-cell fraction designated as the non-glaciated land surface. The total snow storage comprises the snow storage along with the meltwater within it that can freeze again. However, the glacier module incorporates snow falling on glaciers. Snow runoff is generated when the air temperature surpasses the melting point and the snowpack is unable to hold any more meltwater.

5.1.4 Evaluation of Glacier Processes

Glaciers are assumed to be melting surfaces covering each glacierized grid cell completely or partially. The melting rates of clean ice and debris-covered glaciers vary necessitating separate spatial maps of both kinds of glaciers as model input. A degree-day modeling approach was adopted to differentiate the melt rates of clean and debris-covered glaciers with individual calibrated degree-day factors. The total glacial melt per grid cell is the sum of individual contributions from the debris-free glacier and debris-covered glacier with respect to the fractional glacier cover.

The glacial melt contributes to runoff as a quick direct runoff component and a slow component where it percolates to the groundwater layer, eventually becoming baseflow, which is defined by a calibrated parameter namely the glacial melt runoff factor.

5.1.5 Computing Soil Water Balance

With two upper soil storages- root zone and sub-zone layers- and third groundwater storage, the soil column structure is comparable to VIC (Liang et al., 1994, 1996) with surface runoff, lateral flow, and base flow serving as the respective drainage components. The water balance of each layer is given by:

$$SW_{1,t} = SW_{1,t-1} + Pe_t - ET_{a,t} - RO_t - LF_{1,t} - Perc_{1,t} + Cap_t$$

$$SW_{2,t} = SW_{2,t-1} + Perc_{1,t} - Perc_{2,t} - Cap_t$$

$$SW_{3,t} = SW_{3,t-1} + Gchrg_t - BF_t$$

Where, SW_t and SW_{t-1} are the soil water content on the days t and t-1, respectively, Pe_t is the effective precipitation on day t, $ET_{a,t}$ is the actual evapotranspiration on day t, RO_t is the surface runoff on day t, LF_t is the lateral flow from the soil layer on day t, $Perc_t$ is the percolation from the layer to the layer beneath on day t, Cap_t is the capillary rise to the layer from the layer below on day t, $Gchrg_t$ is the groundwater recharge consists of both glacial melt percolation and percolation to the third layer of soil on day t and BF_t is the base flow on day t. The subscript 1,2,3 represents the first layer or the root zone, the second layer or the subzone and third layer or the groundwater, respectively. All the components are in mm.

5.1.6 Estimating Actual evapotranspiration

The resulting soil moisture after surface runoff is vulnerable to evapotranspiration, depending on the soil characteristics and fractional vegetation cover. The actual evapotranspiration is assumed to rely on the stresses due to the non-optimal conditions viz. water excess and water deficit on the potential evapotranspiration captured as reduction parameters which is calculated based on Feddes equation as elaborated by Terink et al. (2015).

5.1.7 Computing Surface Runoff

A portion of the liquid precipitation infiltrates the soil, while the remaining is transformed into surface runoff. SPHY assumes surface runoff as Hewlettian runoff based on the saturation of the first soil layer.

5.1.8 Calculating Lateral Flow

The remaining moisture contributes to river discharge as base flow from the groundwater layer and lateral flow from the first soil layer. SPHY considers only that water surpasses field capacity as contributing to lateral flow and is calculated at the hill slope outlet according to Sloan and Moore. However, the catchments with a time of concentration greater than one day lag a portion of lateral flow in reaching the main channel on the same day of generation. This implies that, even in the unlikely event that no lateral flow is formed in time step t, lateral flow from earlier time steps can be generated indefinitely.

5.1.9 Quantifying Percolation

An approach similar to the SWAT model where the percolation from a layer is assumed to occur only when the water content surpasses the field capacity of that layer while the layer beneath is still unsaturated (Neitsch et al., 2009). Percolation occurs from the first to second soil layer and the second to third soil layer.

5.1.10 Computing Baseflow

The glacier melts that percolates and the water that percolates together eventually contribute to groundwater recharge. An approach similar to SWAT has been adopted to compute groundwater recharge considering the time lag caused by the depth of the groundwater table and soil characteristic. However, baseflow occurs only when the water stored in the groundwater layer exceeds a threshold and is calculated similarly to SWAT assuming a linear correlation between the rate of change in water table height and the variation in base flow. A calibrated parameter namely the baseflow recession coefficient is used to represent the baseflow response to the variations in groundwater recharge with a value ranging from 0 to 1 where higher values represent areas having rapid response to groundwater recharge.

5.1.11 Quantifying Total Routed Runoff

The total of surface runoff (RO), lateral flow from the first soil layer (LF_1), baseflow (BF), snow runoff (SRo), and glacier runoff (GRo) is the cell-specific total runoff that becomes available for routing. The surface runoff and lateral flow components are combinedly termed as rainfall runoff (RRo). All the terms are in mm.

$$QTot = RRo + SRo + GRo + BF$$

The PCRaster-supported SPHY Preprocessor QGIS plugin was used to define a river network based on DEM to route QTot through a flow direction network for retrieving river discharge. A basic flow accumulation routing scheme was performed where the accumulated amount of water that flows out of the cell into its neighboring downstream cell is calculated using the flow direction network as the sum of the specific runoff generated in the cell and the accumulated specific runoff from the upstream cells. (Terink et. al, 2015). However, a calibrated flow recession coefficient accounted for flow delay due to channel friction ranging from 0 to 1 where the lower values of Kx attribute to a fast-responding catchment.

5.2 Model Set-Up

The SPHY model was set up using the QGIS SPHY interface. SPHY pre-processor was used to delineate the watershed and create the sub-basins. The additional datasets viz. DEM, land use, rivers, slope, and soil characteristics required for the SPHY model were generated using the Hindu–Kush Himalaya database in the SPHY pre-processor. A crop coefficient table comprised of crop coefficient values of different land classes was prepared refering to the literature. Furthermore, meteorological forcing was also done in the SPHY pre-processor using the datasets identified as the best alternative to in-situ data on a daily time scale based on bilinear interpolation with a lapse rate of -0.0065 ºC/m elevation for the temperature data (Terink et. al, 2015b).

The SPHY model was run to estimate runoff for the Henval sub-watershed initially from January 2016 to December 2018. However, the SPHY run for the Gangotri watershed was done for a bit longer period from 2013 to 2019, considering the limited data availability (only for the ablation season). The outputs were available as time series and map series data.

5.3 Sensitivity Analysis, Calibration and Validation of Model

A sensitivity analysis was carried out to identify the most relevant model parameters for the study. Parametrization has been done on a quarterly and seasonal basis w.r.t. the simulated discharge of the final year of the model run. The change in hydrograph and the change in the trend of average discharge for each simulation were carefully analyzed and the observations for Henval watershed are tabulated in Table 5.1. Similarly, the observations of parameterization for the Gangotri watershed are tabulated in Table 5.2. Parameter sensitivity for annual, quarterly and seasonal averages was plotted. Parameters with the maximum difference in the average discharge corresponding to a 50% increase and a 50% decrease in the value were ranked and the most sensitive parameters were chosen. The ranking of the parameters based on their effect on a quarterly, annual, and seasonal basis for the Henval and Gangotri watersheds are represented in Table 5.3 and 5.4 respectively.

Calibration and validation were carried out based on the observed discharge from the study area on a daily time step. The approach used for calibration and validation is the minimization of error between the observed and simulated outputs. The calibration was carried out as a trial and error process by manually adjusting the model parameters relevant to the hydrological behavior of the study area. The parameters affecting the model performance were selected based on the results of sensitivity analysis. The model was calibrated for the

period of 01/01/2016 –31/12/2018 (3 years) for the Henval sub-watershed, where as in the case of the Gangotri watershed, it had to rely on the only available data (ablation season) from 2013 to 2019 (7 years). The knowledge of model concepts and river basin characteristics smoothened the process of calibration, which was otherwise a computationally demanding task. The calibration of the model was performed using the observed discharge data by adjusting the most sensitive parameters in the range as shown in Table 5.5 and 5.6, respectively for Henval and Gangotri catchments and their corresponding best fitted values of the parameters are found.

Fig. 5.6 shows the time series plot of observed and predicted runoff for the calibration period for the Henval watershed. From the time series plot, it can be seen that even though the simulated runoff is underestimated, it follows the same trend as the observed runoff. Also, the rainfall distribution aligns well with the observed and simulated runoff suggesting the model performance satisfactory.

Similarly, the simulated discharge using the calibrated parameter values of the Gangotri watershed were plotted against the observed discharge (during ablation season) as in Fig.5.7 to evaluate the performance. The statistical analysis with the most common metrics was carried out for the simulations of each watershed and results are shown in Table 5.7. The R^2 value for the calibration period was found as 0.7 to 0.75 and the NSE value ranged from 0.69 to 0.74. Hence, the model calibration was performing satisfactory in terms of its predictive skills. And the variability of the simulation w.r.t the actual observations were analysed using RMSE (1.42 to 21.94) and the Bias (-15.7 to 2.43). Since the statistical analysis gave significant results, the same parameter values were used for validation and the model was stabilized.

Table 5. 1 Sensitivity Analysis for Henval sub-watershed

a) Quarterly scale

Parameter			Alpha Gw	Root layer thickness (mm)	Sub layer thickness (mm)	Recession Coefficient	DDFS (mm/degree/day)	GW layer thickness (mm)	Saturated GW content (mm)	Initial GW storage (mm)
Default Value			0.5	500	1500	0.4	6	3000	2000	1500
Change in Discharge (%)	**Annual**	50% decrease	-0.57	-15.32	0	0	-0.02	-0.01	-0.01	0
		50% increase	0.19	9.49	0	0	0	0	0	-0.01
	JFM	50% decrease	15.7	3.91	-0.01	0	0.67	0	0	0
		50% increase	-5.14	0.48	-0.01	0	-0.01	0	0	0
	AMJ	50% decrease	3.74	-96.11	-3.3	-7.98	0	1.83	1.83	0
		50% increase	-2.2	43.78	2.11	13.72	0	0	0	1.83
	JAS	50% decrease	-0.24	-8.48	0.27	0.71	0	-0.13	-0.13	0
		50% increase	0.17	6.84	-0.15	-1.19	0	0	0	-0.13
	OND	50% decrease	-102.9	39.45	36.5	17.29	0	-57.08	-57.08	0
		50% increase	29.91	-52.48	-45.56	-62.99	0	0	0	-57.08

b) Seasonal Scale

Parameter			Alpha Gw	Root layer thickness (mm)	Sub layer thickness (mm)	Recession Coefficient	DDFS (mm/degree/day)	GW layer thickness (mm)	Saturated GW content (mm)	Initial GW storage (mm)
Default Value			0.5	500	1500	0.4	6	3000	2000	1500
Change in Discharge (%)	**ANNUAL (WATER YEAR)**	50% decrease	0.07	-15.65	-0.01	-0.01	-0.07	-0.02	-0.02	0
		50% increase	-0.02	11.58	0.03	0.03	0	0	0	-0.02
	Monsoon (JJASO)	50% decrease	-0.03	-17.3	0.02	0.01	0	-0.03	-0.03	0
		50% increase	0.01	12.92	-0.01	-0.03	0	0	0	-0.03
	Winter (NDJF)	50% decrease	1.79	-1.16	-0.62	-0.36	-0.53	0.19	0.19	0
		50% increase	-0.52	0.52	0.77	1.15	0	0	0	0.2
	Summer (MAM)	50% decrease	1.79	1.16	0.62	0.36	0.53	0.19	0.19	0
		50% increase	0.52	0.52	0.77	1.15	0	0	0	0.2

Table 5. 2 Sensitivity Analysis for Gangotri watershed

a) Quarterly Scale

Parameter			Alpha Gw	Cap rise max (mm)	DDFDG (mm/ degree/ day)	DDFG (mm/ degree/ day)	DDFS (mm/ degree/ day)	delta GW	Glac melt fraction	GW layer thickness (mm)	Initial GW storage (mm)	Saturated GW content (mm)	Recession Coefficient	Root layer thickness (mm)	Snow ini (mm)	Snow Sc	Snow wat store (mm)	Sublayer thickness (mm)	T crit
Default Value			0.2	6	6	6	4	2	0.6	3000	400	1000	0.6	500	60	0.6	60	1200	2
Change in Discharge (%)	Annual	50% decrease	0	-0.05	0.02	38.64	1.08	0	0	0	0	0	0	-0.06	0	-0.08	0	0.75	0.13
		50% increase	0	0.09	-0.02	-38.64	-0.06	0	0	0	0	0	0	0.32	-0.01	0.06	-0.01	-0.56	-0.04
	JFM	50% decrease	-2.81	0	0	47.51	4.99	-2.69	15.95	0	0	0	-10.21	0	0	-7.71	0	0	-0.58
		50% increase	-2.93	0	0	-47.51	-14.43	1.86	-15.95	0	0	0	17.46	0	0	2.38	0	0	0.77
	AMJ	50% decrease	3.3	-0.09	0.02	33.6	11.34	-0.78	4	0	0	0	-3.92	0.24	-0.01	-1.87	-0.01	1.76	-0.81
		50% increase	-1.25	0.29	-0.02	-33.6	-5.4	0.75	-4	0	0	0	20.62	0.75	0	1.23	0	-0.92	0.82
	JAS	50% decrease	0.23	-0.05	0.03	39.86	-1.83	0.06	-0.42	0	0	0	0.65	-0.18	0	0.44	0	0.48	0.41
		50% increase	0.06	0.04	-0.03	-39.86	1.47	-0.04	0.42	0	0	0	-1.49	0.19	-0.01	-0.28	-0.01	-0.47	-0.29
	OND	50% decrease	-42.77	0	0.02	46.64	0.89	5.95	-26.27	0	0	0	16.95	0.94	0.03	-0.32	0.03	0.07	-0.52
		50% increase	11.01	-0.04	-0.02	-46.64	-0.77	-6.47	26.27	0	0	0	-160.64	0.42	0.05	0.18	0.05	-0.02	0.27

b) Seasonal Scale

Parameter			Alpha Gw	Cap rise max (mm)	DDFDG (mm/ degree/ day)	DDFG (mm/ degree/ day)	DDFS (mm/ degree/ day)	Delta GW	Glac melt fraction	GW layer thickness (mm)	Initial GW storage (mm)	Saturated GW content (mm)	Recession Coefficient	Root layer thickness (mm)	Snow ini (mm)	Snow Sc	Snow wat store (mm)	Sublayer thickness (mm)	T crit
Default Value			0.2	6	6	6	4	2	0.6	3000	400	1000	0.6	500	60	0.6	60	1200	2
Change in Discharge (%)	ANNUAL (WATER YEAR)	50 % dec.	0.04	-0.03	0.03	39.37	1.07	-0.02	0.11	0	0	0	-0.12	-0.22	0	-0.2	0	1	0.27
		50 % inc.	-0.03	0.1	-0.03	-39.37	-0.4	0.02	-0.11	0	0	0	0.43	0.35	-0.02	0.07	-0.02	-0.66	-0.13
	Monsoon (JJASO)	50 % dec.	-0.16	-0.03	0.03	39.62	-0.28	0.05	-0.26	0	0	0	0.25	-0.23	0	0.37	0	1.07	0.3
		50 % inc.	0.09	0.1	-0.03	-39.62	0.71	-0.06	0.26	0	0	0	-1.22	0.38	-0.02	-0.19	-0.02	-0.7	-0.19
	Winter (NDJF)	50 % dec.	-69.26	0.02	0	39.45	12.14	2.14	-15.29	0	0	0	22.73	0.02	-0.01	-4.4	-0.01	0.02	-0.27
		50 % inc.	3.95	0.01	0	-39.45	-11.65	-2.22	15.29	0	0	0	-199.93	-0.06	0.02	2.76	0.02	-0.01	-0.14
	Summer (MAM)	50 % dec.	4.02	-0.01	0.01	36.16	18.36	-1.02	5.25	0	0	0	-5.36	-0.06	0	-7.54	0	0.05	-0.19
		50 % inc.	-1.64	0.02	-0.01	-36.16	-14.62	0.99	-5.25	0	0	0	25.89	0	0	3.4	0	-0.07	0.73

Table 5. 3 Parameter ranking for Henval watershed

Parameters	Alpha Gw	Root layer thickness	Sub layer thickness	Recession coefficient	DDFS	Delta GW	GW layer thickness	Saturated GW content	Initial GW storage
Annual	2*	1	---	---	3**	3**	---	---	---
JFM	1	2	---	---	3*	4*	---	---	---
AMJ	3	1	4	2	---	5**	---	---	---
JAS	3*	1	3*	2	---	4**	---	---	---
OND	1	2	3	4	---	5	---	---	---
Monsoon (JJASO)	3**	1	4**	2**	---	5**	---	---	---
Winter (NDJF)	3*	1	4*	5*	2*	6**	---	---	---
Summer (MAM)	1	2	4	3	5*	6**	---	---	---
ANNUAL (WATER_YEAR)	2**	1	4**	5**	3**	---	---	---	---

Major influence *Minor influence **Negligible

Table 5. 4 Parameter ranking for Gangotri watershed

Parameter	Alpha Gw	Cap rise max (mm)	DDFDG (mm/ degree/ day)	DDFG (mm/ degree/ day)	DDFS (mm/ degree/ day)	Delta GW	Glac melt fraction	GW layer thickness (mm)	Initial GW storage (mm)	Saturated GW content (mm)	Recession Coefficient	Root layer thickness (mm)	Snow ini (mm)	Snow Sc	Snow wat store (mm)	Sub layer thickness (mm)	T crit
Annual	---	6*	8**	1	3	---	---	---	---	---	---	4*	---	7*	---	2	5*
JFM	8*	---	---	1	4	6	2	---	---	---	3	---	---	5	---	---	7
AMJ	5	11*	12**	1	3	9	4	---	---	---	2	10*	---	6	---	7	8
JAS	9*	11**	12**	1	2	10**	5*	---	---	---	3	8*	13**	6*	13**	4*	7*
OND	3	12**	11**	2	6	5	4	---	---	---	1	8*	13**	9*	13**	10**	7*
Monsoon (JJASO)	9*	10*	12**	1	4*	11*	7*	---	---	---	3	5*	13**	6*	13**	2	8*
Winter (NDJF)	3	---	---	2	5	7	4	---	---	---	1	9**	11**	6	11**	10**	8*
Summer (MAM)	6	11**	12**	1	2	7	5	---	---	---	3	10**	---	4	---	9*	8*
Annual (WATER YEAR)	10**	9*	11**	1	3	12**	8*	---	---	---	5*	4*	13**	7*	13**	2	6*

Major influence *Minor influence **Negligible

Table 5. 5 Parameter values used for calibrating model for Henval sub-watershed

Rank	Major parameters	Parameter description	Unit	Range as per literature	Calibrated Value
1	Rootlayer thickness	Thickness of rootzone	mm	50 - 1000	500
2	Alpha GW	Baseflow recession coefficient	---	0.01 – 1.0	0.03
3	Recession Coefficient	Routing recession coefficient	---	0.01 – 0.99	0.9
4	Sublayer thickness	Thickness of subsoil	mm	300 - 3000	1000
5	DeltaGW	Groundwater recharge delay time	day	1 - 180	1

Table 5. 6 Parameter values used for calibrating model for Gangotri watershed

Rank	Major parameters	Parameter description	Unit	Range as per literature	Values fitted during calibration
1	DDFG	Degree Day Factor for debris-free glaciers	mm/degree/day	2-10	2.75
2	DDFS	Degree day factor of snow	mm/degree/day	2 - 9	2
3	Recession Coefficient	Routing recession coefficient	---	0.01 – 0.99	0.85
4	Sublayer thickness	Thickness of subsoil	mm	300 - 3000	1100
5	Alpha GW	Baseflow recession coefficient	---	0.01 – 1.0	0.2
6	Glac ROF	Glacial melt runoff factor	---	0 - 1	0.8
7	Delta GW	Groundwater recharge delay time	day	Positive integer	1
8	Snow_SC	Water storage capacity of Snow	mm mm−1	0 to 1	0.5
9	Tcrit	Critical Temperature	Degree celsius	-5 to 8	2.5

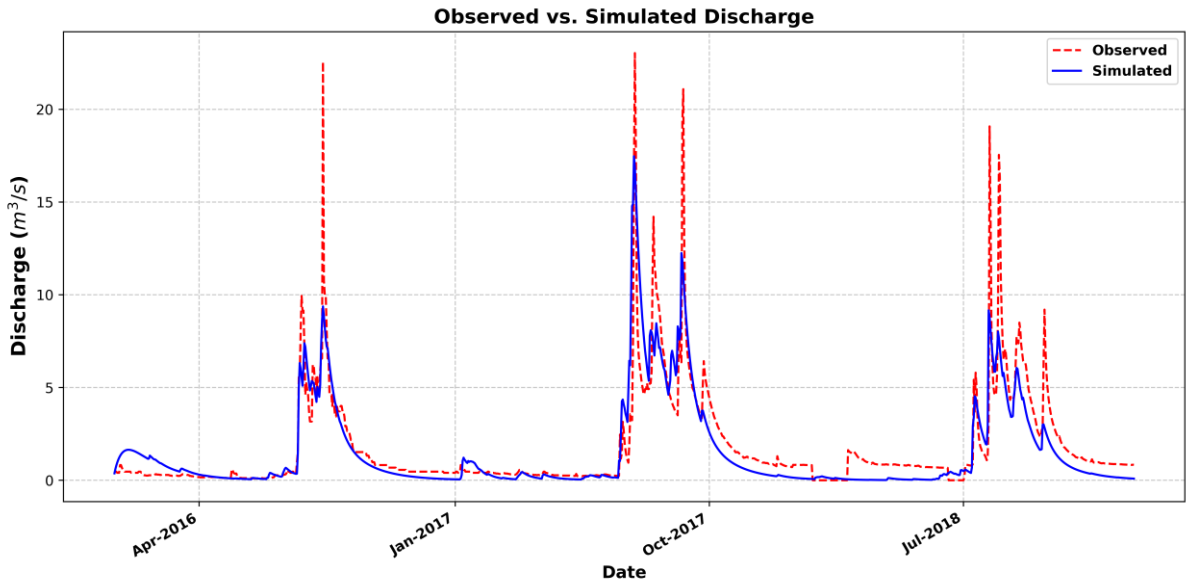

Fig. 5. 6 Time series plot of observed and simulated runoff during the calibration period in Henval watershed

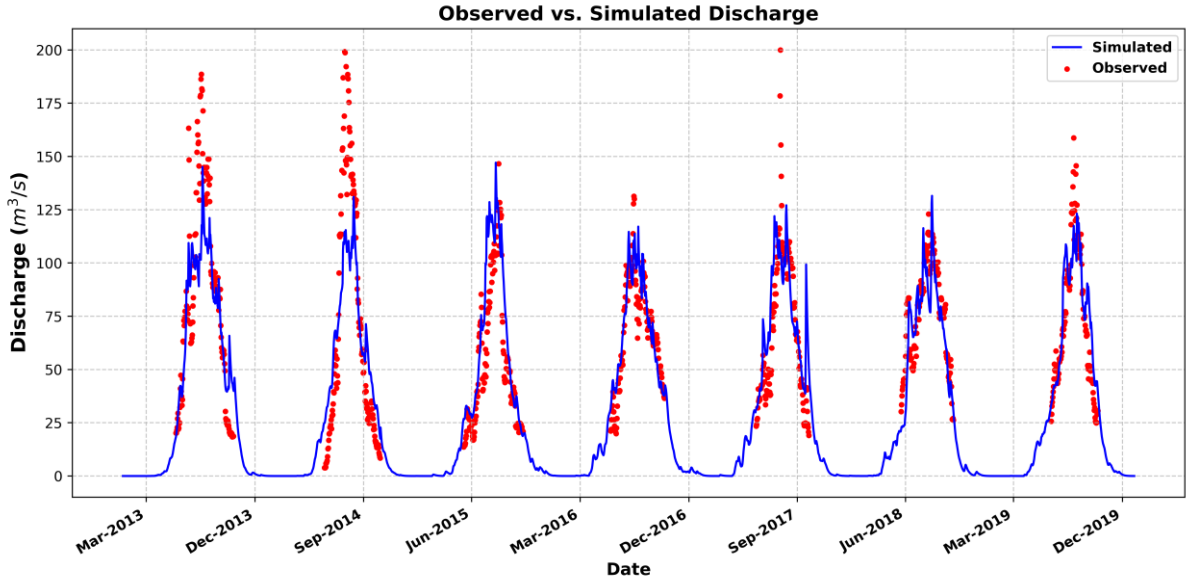

Fig. 5. 7 Time series plot of observed (ablation season) and simulated runoff during the calibration period in Gangotri watershed

Table 5. 7 Statistics for the calibrated models

Indicators	Range	Best Value	Henval	Gangotri
NSE	(- ∞ to 1)	1	0.74	0.69
RMSE	(0 to ∞)	0	1.4	21.94
R2	(0 to 1)	1	0.75	0.7
Bias	(- ∞ to ∞)	0	-15.7	2.43

5.4 Quantification of Total Routed Runoff

The stabilized model after calibration and validation was statistically analyzed using different measures to evaluate the predictability and variability of the simulations and the results are tabulated in Table 5.8. The established models slightly improved their statistical performance from that of during calibration. The simulations for the Henval watershed were initially done for the period from 01/01/2016 to 31/12/2021 for the smaller sub watershed with the outlet at Jijali and the Fig. 5.8 shows the time series SPHY discharge output . Once found satisfactory, the model was then upscaled to the larger Henval watershed with the outlet at Shivapuri with the same parameter values for an extended period from 1/1/2010 to 31/12/2023. The output discharge obtained is illustrated in Fig. 5.9. The contribution of each of the runoff components were derived and represented as Fig. 5.10. The non-glaciated Henval watershed were having only two major runoff components – baseflow and rainfall induced runoff. The Rainfall induced runoff contributes 83% to the total discharge in the watershed indicating the heavy dependency of the watershed on the rainfall especially during monsoon season for a thriving ecosystem and groundwater recharge. The visible fluctuations in the discharge over the year points out the changes in the rainfall regime in the region.

Table 5. 8 Statistics for the established models

Indicators	Range	Best Value	Henval	Gangotri
NSE	(- ∞ to 1)	1	0.74	0.69
RMSE	(0 to ∞)	0	1.4	21.32
R2	(0 to 1)	1	0.75	0.69
Bias	(- ∞ to ∞)	0	-15.7	1.08

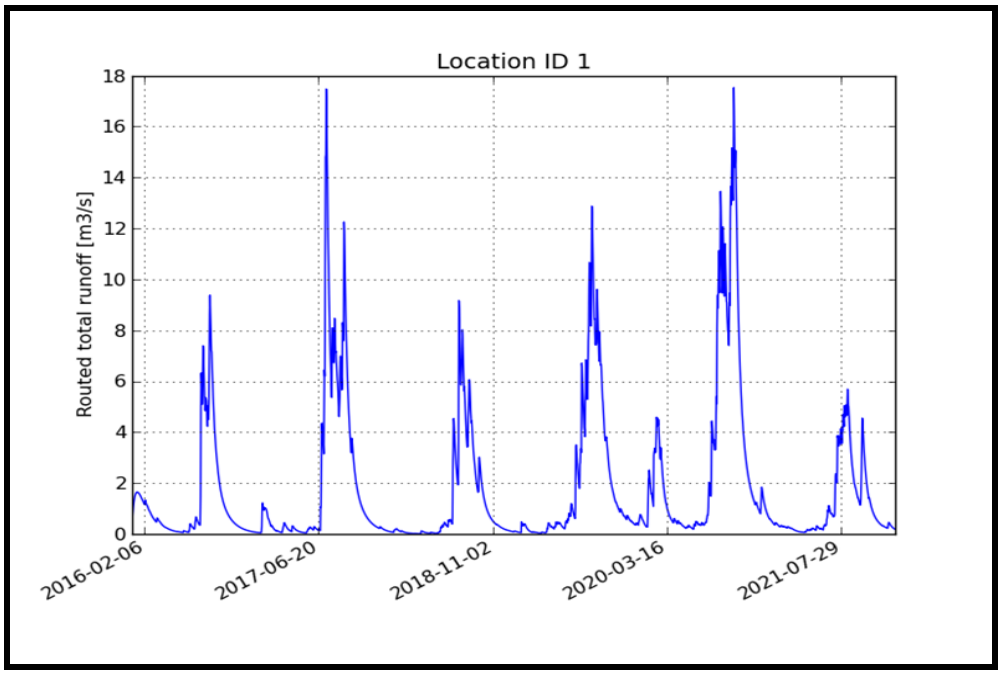

Fig. 5. 8 Time series SPHY output for the Henval sub-watershed

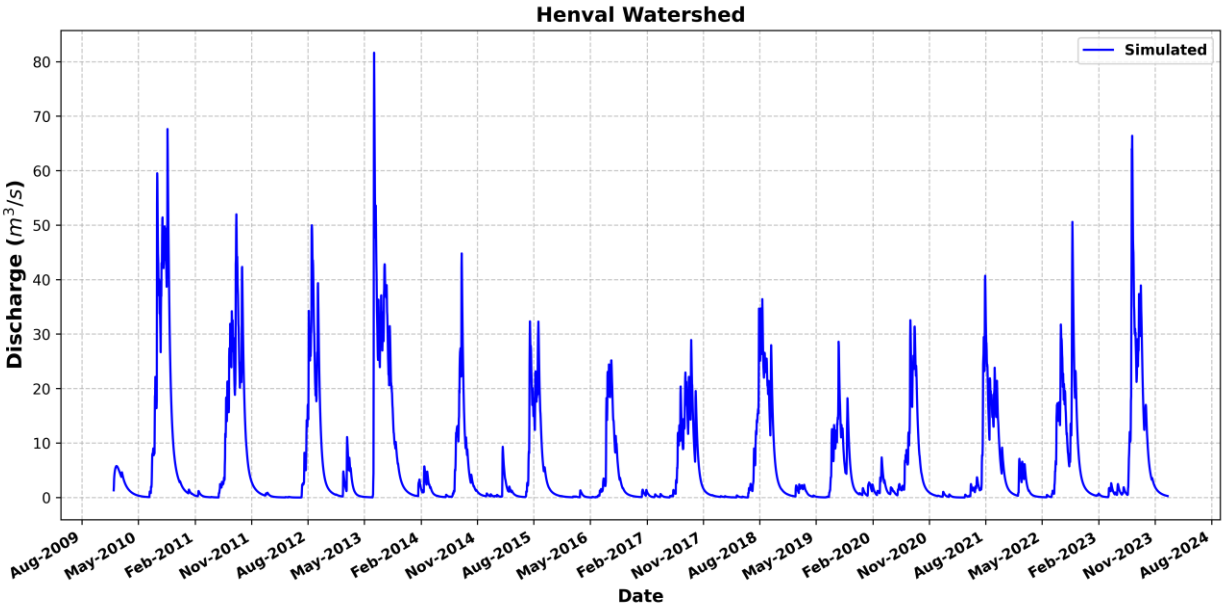

Fig. 5. 9 Time series SPHY output for the Henval watershed

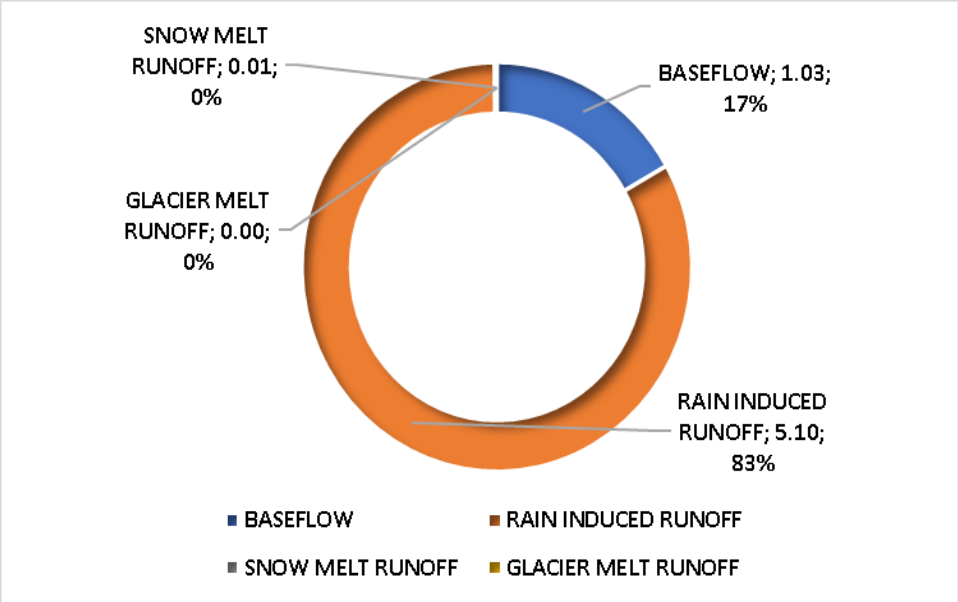

Fig. 5. 10 Relative contributions of different runoff components for the Henval watershed (m^3/s; %)

In the case of the glaciated Gangotri watershed with the outlet at Bhojwasa, the model was established and simulations were done from 01/01/2010 to 31/12/2023 and the simulated discharge is represented in Fig. 5.11. The contributors to the discharge were separated and the cryospheric components found to play a dominant role in the water availability of the region. Fig. 5.12 represents the relative contributions by each of the runoff components where glacial melt runoff was found to be the significant component responsible for more than half of the discharge (54%) at the outlet. Snowmelt runoff contributes another 22% to the region's water availability. The dominance of cryospheric components in contributing to the basin water availiability indicates the significance of rising temperatures in the region especially in the context of global climate change.

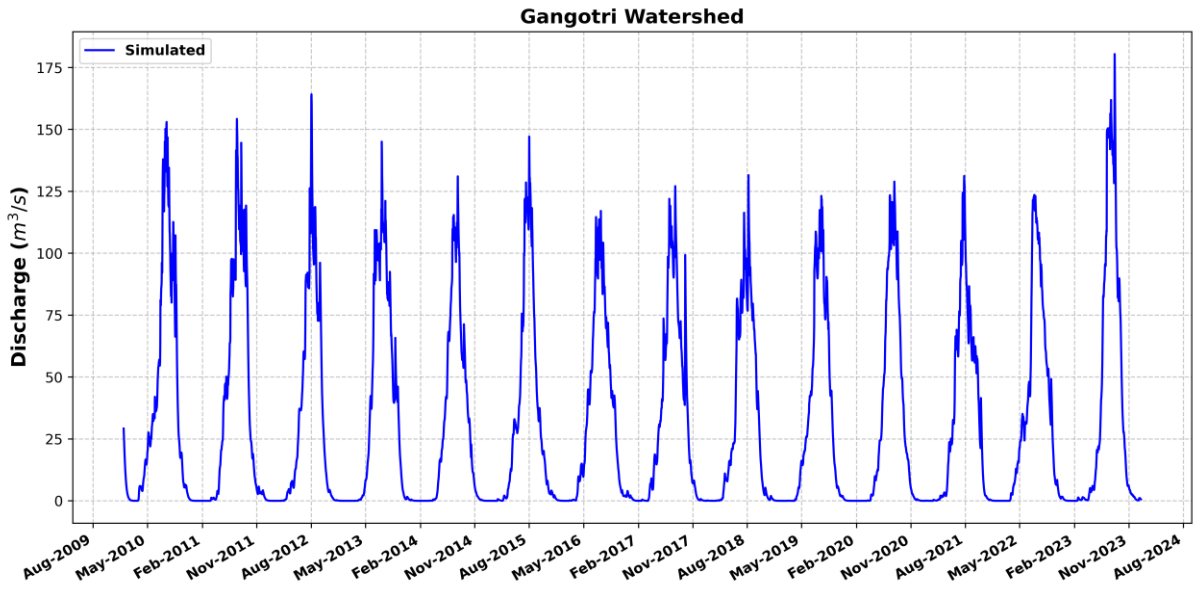

Fig. 5. 11 Time series SPHY output for the Gangotri watershed

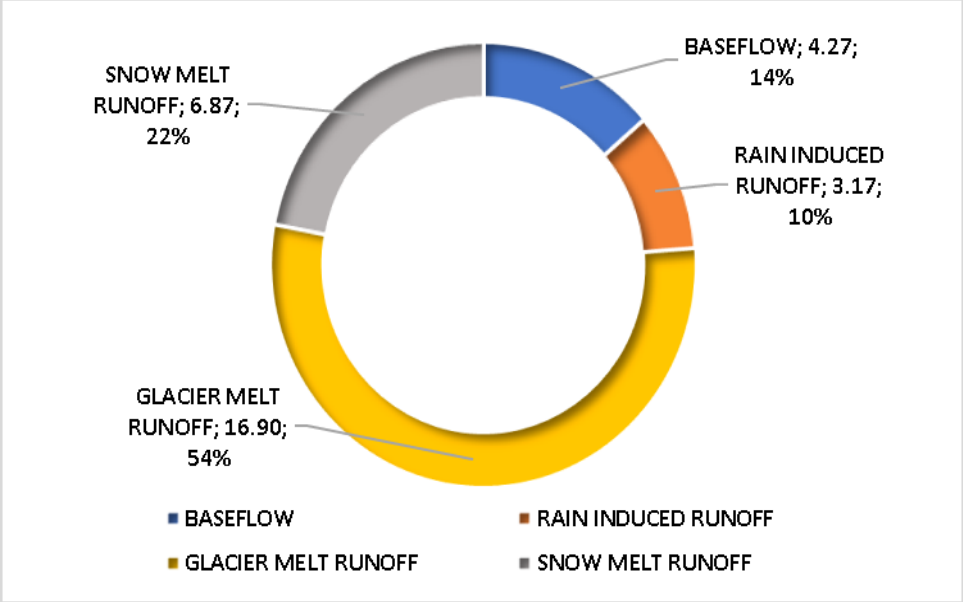

Fig. 5. 12 Relative contributions of different runoff components for the Gangotri watershed (m^3/s; %)

5.5 Water Balance of the Watershed

Water Balance is defined as the numerical calculation accounting for the inputs to, outputs from, and changes in the volume of water in the various components (e.g. reservoir, river, aquifer) of the hydrological cycle, within a specified hydrological unit (e.g. river basin) and during a specified time unit (e.g. month/year), occurring both naturally and as a result of the

human-induced water abstractions and returns. Water in the catchment is always balanced and its components are influenced by the morphology of the watershed, climatic conditions, soil characteristics and land use land cover. It is simply based on the concept of change in the storage of water. It helps in the development of River Basin Management Plans by providing a coherent framework nto cross-evaluate the information on drivers, pressures and impacts on water quantity and provides a sound basis for the quantitative management of water resources.

Estimation of the water balance components is a complicated task and can be achieved either using water balance models or hydrological models which have been developed at various time scales. The hydrologic processes are very complex and an understanding of the watershed model is essential. There exist numerous physically based distributed hydrological models and among them, SPHY is one of the widely used open source models in glacierized regions. Since the current research aimed to understand the hydrological processes and analyze the hydrological response of the glaciated and non-glaciated watersheds in North West Himalya, SPHY model was chosen for both the kind of watersheds.

The most important hydrologic processes are surface runoff, lateral flow, baseflow and evapotranspiration and the cryospheric processes are Snow melt and Glacial melt. In this study SPHY model is used to evaluate water balance components in a glaciated as well as non-glaciated watershed in the Upper Ganga Basin and the respective models were calibrated. The calibrated parameters were used for validation as well. Once stabilized, the model was established for a duration of 14 years from 1/1/2010 to 31/12/2023. The SPHY model was found working satisfactorily for both the watersheds despite their unique nature and challenges indicating the versatility of the SPHY model. This suggests the model could be used for simulating the hydrological response of the other watersheds in North West Himalaya. When supplemented with geospatial techniques and better datasets by integrating the in-situ data and satellite data in the data scarce Himalayan region, the model can be a very helpful tool to understand the hydrological processes and simulate the hydrological response of the watersheds in the region. In the context of the rising challenges due to the climate change, it is critical to understand the response of the Himalayan watersheds to the variations in the meteorological parameters due to their -either glaciated or non-glaciated watersheds- very dependent nature on temperature and precipitation regime for region's water availability. The integration of glacio-hydrologic models like SPHY, climate models and

longer historical datasets can effectively help us to be resilient in the face of climate change with better adaptation techniques and policies, given the hydrological and ecological importance of the Himalayan watersheds.

Chapter 6

6.0 SUMMARY AND CONCLUSION

6.1 General

The study titled **"Monitoring and Assessment of Mountain Ecosystem and Services in North-West Himalaya (Phase-II): Monitoring and Modeling of Hydrological Processes in Glaciated and Non-Glaciated Watersheds of North-West Himalaya"** represents the second phase of a broader initiative aimed at understanding the dynamic hydrological processes of the Himalayan region. Led by the Indian Institute of Remote Sensing (IIRS), Dehradun, and funded by the Indian Space Research Organisation (ISRO), this collaborative project builds upon the foundational work carried out in Phase I, which focused on establishing hydro-meteorological observatories in strategically selected watersheds across Himachal Pradesh and Uttarakhand.

In Phase II, the study emphasizes an integrated approach to monitoring, data assimilation, and hydrological modeling, with specific attention to both glaciated and non-glaciated watersheds. Two major catchments—Henval (a non-glaciated watershed) and Gangotri (a glaciated watershed)—served as primary experimental sites for the deployment of advanced instruments and modeling efforts. These watersheds were chosen to represent the heterogeneity in topographic, climatic, and hydrological conditions across the North-West Himalayas, enabling the research team to compare and contrast runoff generation mechanisms under differing cryospheric influences.

6.2 Field Instrumentation and Data Monitoring

A critical outcome of this project was the successful installation of advanced hydrometeorological instrumentation in the Henval and Gangotri catchments. These observatories were designed to continuously record essential variables such as precipitation, air and soil temperature, relative humidity, wind speed, radiation, snow depth, and stream discharge. The instrumentation enabled researchers to capture fine-resolution temporal and spatial variations, which are critical for understanding eco-hydrological feedbacks in mountainous terrain.

These continuous in-situ datasets not only enhance the ground truthing of satellite observations but also fill essential data gaps in Himalayan hydrology—particularly in high-

altitude, remote locations where data availability is sparse or inconsistent. In particular, the long-term monitoring enabled by this infrastructure provides a robust foundation for future hydrological assessments and climate impact analyses.

6.3 Remote Sensing Integration and Data Analysis

Given the complex terrain and inaccessibility of high-altitude Himalayan watersheds, remote sensing plays a pivotal role in augmenting field-based observations. As part of this study, multi-source satellite datasets were integrated for monitoring snow cover, glacier dynamics, surface water availability, sediment load, and meteorological conditions.

To address inconsistencies and limitations in rain gauge data—especially after 2019 in the Henval watershed—a comparative evaluation of various satellite-based precipitation products was undertaken. The performance of different datasets, including GPM, CHIRPS, NASA POWER, and IMDAA, was assessed at both daily and monthly temporal resolutions.

The results demonstrated that NASA POWER provided the best daily-scale estimates (NSE = 0.45, R^2 = 0.45), while CHIRPS performed optimally at the monthly scale (NSE = 0.93, R^2 = 0.93). This indicates the feasibility of utilizing remotely sensed precipitation data to supplement or substitute ground-based measurements, particularly in data-scarce, high-altitude regions like Gangotri. Furthermore, NASA POWER datasets were found to be reliable for estimating temperature, reinforcing their applicability for glacio-hydrological modeling in the Himalayan environment.

6.4 Hydrological Modeling Using the SPHY Model

A major thrust of this study involved the application of the **Spatial Processes in HYdrology (SPHY)** model to simulate and analyze watershed hydrology. The SPHY model, a spatially distributed, raster-based, leaky bucket-type water balance model, is well-suited for regions with complex terrain and diverse land cover—including glaciated zones.

The SPHY model was set up using QGIS for both the Henval and Gangotri watersheds. The process involved watershed delineation, sub-basin creation, land cover and soil classification, meteorological input preparation, and snow/glacier modeling. Key model parameters were identified and refined through sensitivity analysis. Seasonal and quarterly calibration of parameters was conducted using observed discharge data from the final model year.

Calibration and validation exercises revealed satisfactory agreement between observed and simulated runoff values, particularly during the ablation season. This demonstrates the

model's robustness in capturing the seasonal dynamics of snow and glacier melt in high-altitude watersheds. In the Gangotri watershed, model simulations successfully reproduced runoff dynamics, indicating effective parameterization of glacio-hydrological processes. Likewise, in the Henval watershed, the model accurately simulated discharge generation primarily influenced by rainfall and subsurface flow components.

A significant contribution of this modeling exercise is the estimation of runoff partitioning into various components—such as snowmelt, glacier melt, rainfall runoff, and baseflow—which provides valuable insights into the water balance and dominant hydrological drivers in each watershed. Such understanding is critical for predicting changes under future climate scenarios and for managing water resources sustainably.

6.5 Comparative Insights from Glaciated and Non-Glaciated Catchments

By focusing on both glaciated (Gangotri) and non-glaciated (Henval) watersheds, the study offers a comparative perspective on hydrological functioning across different Himalayan systems. In Gangotri, glacier melt plays a significant role in sustaining baseflow during the dry season, while in Henval, rainfall and subsurface flow dominate the hydrological response. These contrasting behaviors highlight the importance of tailored management and modeling approaches for different catchment types.

Furthermore, the findings underscore the increasing vulnerability of glacier-fed systems to climate change. Changes in glacier mass balance, snowline elevation, and melt rates can substantially alter streamflow regimes, with implications for downstream water availability, agricultural practices, and disaster management.

6.6 Implications and Future Directions

The outcomes of this study hold significant relevance for hydrological research, water resource planning, and climate adaptation strategies in the Himalayan region. Several key implications emerge:

- **Model Applicability**: The SPHY model's satisfactory performance in both glaciated and non-glaciated watersheds demonstrates its potential as a versatile tool for hydrological modeling in diverse mountain environments. The model can be extended to other ungauged or data-scarce basins in the region.
- **Data Integration**: The combination of ground-based observations with remote sensing products improves the reliability of hydrological simulations, especially

where in-situ data is lacking or inconsistent. This integrated approach is particularly valuable in the Himalayas, where terrain and logistical challenges limit field data collection.

- **Climate Change Adaptation**: The ability to simulate the impact of snow and glacier melt on streamflow is vital for anticipating the hydrological consequences of climate change. Improved understanding of melt dynamics can inform water storage, flood management, and irrigation planning.
- **Upscaling and Policy Relevance**: The methods and models developed in this study can be scaled to the basin level, aiding regional water management authorities and policymakers in developing evidence-based strategies for water security and disaster mitigation.
- **Capacity Building and Infrastructure**: The establishment of long-term hydrometeorological observatories has created a valuable infrastructure for ongoing research. It also contributes to capacity building through training, data sharing, and collaborative studies across institutions.

6.7 Conclusion

This study marks a significant step toward understanding and modeling the complex hydrological processes of the North-West Himalayas, particularly in the context of climate-sensitive glaciated and non-glaciated systems. Through a combination of field instrumentation, remote sensing, and advanced modeling, the research provides actionable insights into the dynamics of mountain hydrology.

The successful application of the SPHY model, supplemented by satellite data, demonstrates a promising framework for simulating watershed behavior under current and future climatic conditions. The project's outcomes not only deepen scientific knowledge but also support informed decision-making for sustainable water resource management in the Himalayan region.

Moving forward, continued monitoring, model refinement, and expansion to additional watersheds will further strengthen the region’s hydrological resilience and enhance our ability to address emerging challenges related to water security, ecosystem services, and climate adaptation in mountain environments.

7.0 REFERENCES

Allen RG, Pereira LS, Raes D, Smith M. 1998. Crop evapotranspiration: guidelines for computing crop water requirements. Irrigation and Drainage Paper No. 56. Rome (Italy): Food and Agriculture Organization of the United Nations.

Bhutiyani, M. R., Kale, V. S. and Pawar, N. J.: Climate change and the precipitation variations in the northwestern Himalaya: 1866-2006, Int. Jour. Climatol., 30,535-548 doi: 10.1002/joc.1920,2010.

Bhutiyani, M. R., Kale,V. S. and Pawar, N. J.: Long-term trends in maximum, minimum and mean annual air temperatures across the Northwestern Himalaya during the twentieth century, Climatic Change, 85,159-177, doi: 10.1007/s10584-006-9196-1, 2007.

Fatima, E. et al. (2020) Future water availability from the western Karakoram under representative concentration pathways as simulated by CORDEX South Asia. Theoretical and Applied Climatology, 141: 1093-1108.

Future Water. (n.d). Hydrological models and SPHY. Retrieved April 16, 2023, from https://www.futurewater.eu/tools/hydrological-models-sphy/

J. J Mcdonnell, M Sivapalan, K Vache, S Dunn, G Grant, R Haggerty, C Hinz, R Hooper, J Kirchner, M. L Roderick, J Selker, M Weiler. (2007). Moving beyond Heterogeneity and Process Complexity: A new Vision for Watershed Hydrology. Water Resources Research

J. W Kirchner. (2006) Getting the Right Answers for the Right Reasons: Linking Measurements, Analyses, and Models to Advance the Science of Hydrology. Water Resources Research

Lutz, A. F., Immerzeel, W. W., Shrestha, A. B., and Bierkens, M. F. P. (2014). Consistent increase in High Asia's runoff due to increasing glacier melt and precipitation, Nature Climate Change, 4, 587– 592, doi:10.1038/nclimate2237.

M Sivapalan, Pattern. (2005) Process and Function: Elements of a Unified Theory of Hydrology at the Catchment Scale. In: Anderson MG (ed.) Encyclopedia of Hydrological Science. John Wiley & Sons

NASA Shuttle Radar Topography Mission (SRTM) (2013). Shuttle Radar Topography Mission (SRTM) Global.

Neitsch, S. L., Arnold, J. G., Kiniry, J. R., & Williams, J. R. (2009). 1.1 Overview of soil and water assessment tool (SWAT) model. Tier B, 8, 3-23.

Penman, H.L., 1948. Natural evaporation from open water, bare soil and grass. Proc. R. Soc. London Ser. A., 193: 120--145.

Rowan, A.V., Duncan, J.Q., Gibson, M.J., Glasser, N.F., Westoby, M.J., Irvine-Fynn, T.D.L., Porter, P.R., and Hambrey, M.J. (2017). The sustainability of water resources in High Mountain Asia in the context of recent and future glacier change. Article in Geological Society London Special Publications, DOI: 10.1144/SP462.12

Simoni, S., Padoan, S., Nadeau, D.F., Diebold, M., Porporato, A., Barrenetxea, G., Ingelrest, F., Vetterli, M. and Parlange, M.B. (2011). Hydrologic response of an alpine watershed: Application of a meteorological wireless sensor network to understand streamflow generation. Water Resources Research, 47, W10524, doi:10.1029/2011WR010730, 2011.

Singh, V. P.: 1989, Hydrologic Systems, Vol. II, Watershed Modelling, Prentice-Hall, Inc.

Singh, V., Jain, S. K., Nagale, D. S., & Singh, J. (2023). Glacier changes and their impacts on the melt runoff in high and moderate elevation ranges of the Himalayan Upper Ganges Basin. Hydrological Processes, 37(5), e14897.

Terink, W., A.F. Lutz, G.W.H. Simons, W.W. Immerzeel, P. Droogers. 2015. SPHY v2.0: Spatial Processes in HYdrology. Geoscientific Model Development, 8, 2009-2034, doi:10.5194/gmd-8-2009-2015.

Terink, W., A.F. Lutz, W.W. Immerzeel. 2015b. SPHY: Spatial Processes in HYdrology. Graphical User Interfaces (GUIs). FutureWater report 143

Thayyen, R. J., &Dimri, A. P. (2014). Factors controlling Slope Environmental Lapse Rate (SELR) of temperature in the monsoon and cold-arid glacio-hydrological regimes of the Himalaya. The Cryosphere Discussions, 8(6), 5645-5686, doi:10.5194/tcd-8-5645-2014.

Van Vliet, M. T., Franssen, W. H., Yearsley, J. R., Ludwig, F., Haddeland, I., Lettenmaier, D. P., & Kabat, P. (2012). Global river discharge and water temperature under climate change. *Global Environmental Change*, 22(2), 168-177.

Wei-ZuGu, Jiu-Fu Liu, Jia-Ju Lu and Jay Frentress (2013). Current Challenges in Experimental Watershed Hydrology, Current Perspectives in Contaminant Hydrology and Water Resources Sustainability, Dr. Paul Bradley (Ed.), ISBN: 978-953-51-1046-0.

*****